A Structural Study of the Dogpaw Gold Deposit in the Rowan-Kakagi Greenstone Belt, Western Superior Province, Northwestern Ontario

by

Alexander Krapf-Jones

A thesis
presented to the University of Waterloo
in fulfillment of the
thesis requirement for the degree of
Master of Science
in
Earth Sciences

Waterloo, Ontario, Canada, 2021

AUTHOR'S DECLARATION

This thesis consists of material all of which I authored or co-authored: see Statement of Contributions included in the thesis. This is a true copy of the thesis, including any required final revisions, as accepted by my examiners.

I understand that my thesis may be made electronically available to the public.

STATEMENT OF CONTRIBUTIONS

This thesis is my own work. The following contributor, Dr. Chris Yakymchuck, performed the U-Pb analysis, provided results (Table A.1, A.2, A.3, A.4, A.5, A.6) and content for figures (Figures 3.23, 3.24, Fig. 3.26).

Abstract

The Dogpaw deposit is a structurally controlled gold deposit hosted in the Neoarchean, Rowan-Kakagi greenstone belt of the Western Wabigoon of the Superior Province. The study area is located approximately 80 kilometers south-southeast of Kenora, Ontario, in the historic Kenora-Fort Frances mining district. The Rowan-Kakagi greenstone belt consists of two metavolcanic terranes separated by the crustal-scale, Pipestone-Cameron fault zone: 1) the Kakagi Lake volcanic terrane, which hosts the Dogpaw gold deposit, and 2) the Rowan Lake volcanic terrane. Volcanism in the Kakagi Lake volcanic terrane is interpreted to have started with the deposition of the Katimiagamak Lake and Snake Bay mafic volcanics (2.73-2.72 Ga) followed by the emplacement of several mafic and felsic intrusions, including the Kakagi sills (2.72-2.71 Ga), and ending with the deposition of intermediate pyroclastic rocks of the Kakagi Lake Group at 2.71 Ga.

The Pipestone-Cameron fault zone is one of several prominent structural features of the Rowan-Kakagi greenstone belt. The structural geology of the greenstone belt has largely gone underexplored, however bedrock mapping along the trend of the Pipestone-Cameron fault zone in the Dogpaw-Flint Lake map area has revealed a network of faults which consists of a major, dominantly dextral, east-southeast striking deformation zone and a network of secondary faults with compatible kinematics. These shear zones that constitute the Pipestone-Cameron fault zone are characterized by a mappable gradation in strain intensity, abundant kinematic indicators, and a core of ankerite-sericite foliation.

A number of reported gold occurrences in the Rowan-Kakagi greenstone belt are spatially associated with the Pipestone-Cameron fault zone. Gold mineralization at several of these

occurrences consist of quartz and iron carbonate rich ore veins hosted in brittle-ductile and ductile shear zones. At the Dogpaw deposit the bulk of gold mineralization is expressed at surface as lodes of quartz-pyrite breccia veins and sheeted, quartz-carbonate veins hosted in a network of ductile to brittle-ductile, conjugate shear zones which occur at the upper succession of a layered mafic to ultramafic sill. These conjugate shear zones developed due to broadly, north-south directed compression during deformation and their distribution is controlled by the primary, textural heterogeneity of the hosting rock. These gold-hosting structures where subsequently overprinted by a subsidiary structure of the Pipestone-Cameron fault zone, the Dalby Bay shear zone, deforming the early geometry of the deposits and presenting a challenge for previous workers when attempting to delineate mineralization at the property. The Dalby Bay shear zone is interpreted as a secondary deformation zone of the Pipestone-Cameron fault zone based on compatible kinematics and identical style of deformation.

Four samples were collected for LA-ICP-MS U-Pb analysis at the Dogpaw deposit. Weighted mean $^{207}Pb/^{206}Pb$ zircon ages were yielded from two samples collected from late-tectonic, quartz-feldspar porphyry dykes. These dykes crosscut both veins of high-grade gold and are themselves deformed within the boundaries of the Dalby Bay shear zone. Results from the analysis of sampled dykes provide a minimum age constraint on the timing of gold mineralization at the Dogpaw deposit at approximately 2696 to 2694 Ma. Results from the analysis of a sample collected from the hosting intrusion provides a maximum timing on gold mineralization at 2717 Ma. These geochronology results, coupled with the U/Pb dating and mapping by previous workers, provides new constraints on gold mineralization, deformation and igneous activity in the Rowan-Kakagi greenstone belt.

Acknowledgements

I would like to thank my supervisor, Dr. Shoufa Lin, for our many discussions and his continued mentoring, support and encouragement throughout this project. I would also like to acknowledge my committee members: Dr. Chris Yakymchuk, for both his contributions to this thesis and support; and Dr. Brian Kendall for introducing the world of radiogenic isotopes to me. I would like to thank all three committee members for providing course material that both provided the fundamental knowledge to complete this research project and helped develop a healthy, critical mind to the science.

I would like to thank the Ontario Geological Survey for both the direct contributions to this thesis and the opportunities I received to develop as a geologist while a member of their field mapping crews. I would like to thank Steven R. Meade of the Ontario Geological Survey for leading, organizing and providing support during three field seasons, no small feat. I would also like to thank Jacob Wroblewski, Carson Kinney, Tommy Clark and Ryan Norris for their support throughout the field mapping seasons. A special thanks to Carson Kinney for his hard work and discussions during the 2016 field season and contribution to the analysis of samples collected at the Dogpaw deposit.

I would like to acknowledge the love and support of my family, Helen Krapf-Jones, David Jones and Nicholas Krapf-Jones, throughout my academic career. A special thanks and acknowledgement to my friends Qihang Wu and Katia Jellicoe for their many discussions about geology and many laughs. I would like to thank my friends and fellow grad students at the University of Waterloo and the staff and faculty of the Earth and Environmental Science Department. Most importantly, I would like to thank my best friend and partner of many wonderful years, Clara Xiong. The best petrography lab partner I ever had.

It would be impossible to truly acknowledge every person and all your contributions, big and small. When things got difficult, it was the kindness, encouragement and laughs of so many great people in my life that kept me going. Thank you all.

Dedication

This thesis is dedicated to my grandmother, Marta Krapf

“To the Family!”

Table of Contents

List of Figures

List of Tables

Chapter 1
Introduction

1.1 Introductory Statement

This M.Sc. thesis research project is focused on a historic gold occurrence, the Dogpaw gold deposit. The deposit is hosted by the Neoarchean rocks of the Rowan-Kakagi greenstone belt in the Western Wabigoon subprovince of the Superior Province in Ontario (Fig. 1.1, 1.2, 1.3). The main objective of this project was to provide a modern and comprehensive study on the structural geology and gold mineralization at the deposit and place these observations in a larger regional structural framework. In Chapter 1 the background geology and overall objectives of the thesis are introduced. Chapter 2 provides structural data and field observations on the major belt-scale fault, the Pipestone-Cameron fault zone, providing a larger structural framework for the subsequent chapter. This is followed by Chapter 3 which focuses on the structural geology, gold mineralization and timing constraints at the Dogpaw deposit. Finally, Chapter 4 summaries the conclusions of the thesis and provides recommendations for future exploration and development at the deposit and the larger map area.

This study began as a collaborative mapping project between the Ontario Geological Survey and the Department of Earth and Environmental Science at the University of Waterloo. Field work was conducted in coordination and collaboration with the regional-scale bedrock mapping project led by Professional Geoscientist, Steven R. Meade of the Ontario Geological Survey (Meade 2015, 2016, 2017).

1.2 The Superior Province

The Superior Province provides a unique window into the crustal history of the Archean. The interior and margins of the subprovinces that constitute the Superior record and preserve Archean magmatism, sedimentation, metamorphism, tectonics, and post-cratonization events, the mechanisms and timing of which are still being explored. The crustal and tectonic evolution of the Superior Province and subprovinces has experienced significant reinterpretation as a result of regional scale, multidisciplinary projects in the last few decades (e.g., NATMAP, Lithoprobe transects) (Percival et al., 2006; Percival et al., 2012). One of the objectives of these craton-scale projects was to address ongoing questions about Archean magmatic, tectonic and mineralizing events in the Superior Province. Our current understanding of these processes is largely the result of the province-to-province synthesis of both recent and historic geological, geochemical, structural and radiogenic isotope data from the Superior Province (Percival et al., 2012).

Models for the assembly of the western Superior Province, as outlined in Percival et al. (2006), recognize several Neoarchean accretionary events which generally ‘young’ from north to south and are marked by episodes of early deformation, regional metamorphism, gold introduction and a later phase of regional deformation. However, debate remains concerning whether these fundamental processes in the Archean functioned analogously to modern tectonic processes or were unique during the early history of the Earth. The western Superior Province has received its fair share of attention, with debate concerning the ‘nature’ or style of tectonics during the Archean being well rooted in early work. These debates arose during an effort to explain common characteristics inherent in what appear to be distinct subprovinces of the Superior. These observations include a consistent younging of supracrustal rocks from north to

south and the linear forms of greenstone-intrusive terranes. Integrated studies in the Superior Province began to produce a body of data that suggested that modern 'style' plate tectonics were active in the Late Archean (de Wit, 1998). This debate is still very much alive with some authors proposing the synchronous operation of both vertical and horizontal mechanisms in the Neoarchean (eg. Lin and Beakhouse, 2013). While others, such as Bédard (2006), have proposed models for the establishment of Archean continental crust and its early architecture with horizontal processes being a relatively minor mechanism. As the breadth of tools available to the modern Precambrian geologists continues to improve, any resolution to these questions concerning the geological processes in the Archean will still likely hinge on integrated studies founded on rigorous field work.

1.3 The Western Wabigoon

The Western Wabigoon is considered an extensively studied subprovince of the Superior and continues to provide Precambrian workers with unique insights into Archean processes. This is partly due to the excellent quality of bedrock exposure, particularly an abundance of shoreline outcrops, and a long history of geological mapping (Lawson, 1888) and mineral exploration (Beard and Garratt, 1976). This has consequently led to the rise of further questions concerning its tectonic history and gold endowment.

The Western Wabigoon subprovince is characterized by almost equal portions Neoarchean metavolcanics and syn-volcanic, tonalitic batholith complexes as well as minor metasedimentary deposits (Figs. 1.1, 1.2). To the north of the Western Wabigoon is the Winnipeg River terrane, a plutonic terrane dominated by tonalite-trondhjemite-granodiorite (TTG) suites and a preserved Meso- to Paleoarchean crustal history (Melnyk et al., 2006). To

south of the Western Wabigoon subprovince is the Quetico subprovince, a largely metasedimentary terrane with a complex deformation history punctuated by plutonic activity (Percival et al., 2006). The metamorphic grade of the Western Wabigoon subprovince is dominantly greenschist, however higher-grade zones are found along intrusive contacts of some coeval batholiths and along subprovince boundaries (Beakhouse et al., 1996).

Unlike the crustal history of its neighboring terranes, the majority of supracrustal rocks of the Western Wabigoon subprovince are believed to have evolved over a relatively short time span, an approximately 50 – 70 Ma interval in the Neoarchean. The Western Wabigoon is believed to have first formed sometime between 2.77-2.72 Ga following the breakup of the Winnipeg River terrane and accreted to the Winnipeg River – Marmion composite terrane between 2.71 Ga and 2.70 Ga during the Central Superior orogeny (Percival et al., 2006).

Relative to the polydeformed supracrustal rocks found along its boundaries, for example the Savant-Sturgeon greenstone belt at the south-west facing boundary between the Western Wabigoon and Winnipeg River terrane (Sanborn-Barrie and Skulski, 2006), the internal structural architecture of the Western Wabigoon largely consists of first-order crustal-scale faults and folds that can be traced for hundreds of kilometers (Fig. 1.2). Understanding how these structures evolved is important as they control the bedrock map pattern in the Western Wabigoon and are common features of other subdivisions of the Superior Province. These major, crustal-scale structures likely first developed in response to broadly north-south compression during the accretion of the subprovince to the Winnipeg River – Marmion composite terrane boundary between 2.71 and 2.70 Ga (Percival et al., 2006). It has also been suggested that some of these

folds developed as synclinal keels during doming of the greenstone rocks as a response to the emplacement of large syn-volcanic batholiths (Beakhouse et al., 1996).

A number of major crustal-scale faults transect the greenstone rocks of the Western Wabigoon subprovince (Fig. 1.2). These are believed to be long lived structures and can record a complex tectonic history. These include the over 100km long Wabigoon fault located along the northern boundary of the Western Wabigoon, the broadly dextral Quetico fault at the southern boundary (Mackasey et al., 1974), and the Pipestone-Cameron fault zone. The structural geology of these faults has been addressed at varying levels, while for others, such as the Pipestone-Cameron fault zone, the kinematics and style of deformation is relatively unknown (Blackburn, 1980; Edwards and Stauffer, 1999).

The Western Wabigoon subprovince has a long history of mapping, exploration, and study. At the time of this research project there are over 100 documented academic studies (B.Sc., M.Sc. and Ph.D.), industry and government reports at some level concerned with the crustal history and mineral endowment of the subprovince. Consequently, this has created an excellent foundation for future projects in the Western Wabigoon, with many questions remaining concerning the tectonic history of the volcanic-intrusive terranes that constitute the subprovince and the genesis of mineral resources hosted within its boundaries. The Rowan-Kakagi greenstone belt is a typical example, where available data on lithostratrigraphy, geochemistry and geochronology are available however the structural geology has remained largely underexplored and a modern synthesis of available data is lacking. Although purely speculative, the lack of apparent mineral endowment in the Western Wabigoon subprovince relative to the more prolific Archean terranes, such as the Abibiti subprovince of the Superior

Province, may be due to the relatively fewer integrated, modern, multidisciplinary studies focused on the Western Wabigoon. This project focuses on a sliver of the greater Western Wabigoon subprovince and aims to contribute to the growing body of work on the Archean geology of Superior Province and its gold endowment.

1.4 Orogenic Gold Deposits in Ontario

There is a general consensus that orogenic gold deposits, or structurally controlled lode gold deposits, were localized in structural features during the later stages of deformation and regional metamorphism of their hosting subprovinces, and that mineralization was broadly synchronous with late felsic magmatism (Colvine et al., 1988; Percival et al., 2006). Earlier workers, such as Colvine et al. (1984, 1988) summarized the characteristics of lode gold deposits in Ontario. These observations include that most deposits are predominantly found in the greenstone rocks of greenstone-intrusive belts and have a strong spatial association with crustal-scale fault systems and syn- to late-tectonic plutons (Colvine et al., 1988). Since this work, greenstone-hosted lode gold deposits have been recognized as an important subset of gold deposits (Dube and Gosselin, 2007). This has subsequently led to a large body of work focused on the structural geology and timing of these types of deposits. The strong spatial association with regional-scale faults, which are often long-lived structures, suggests a structural relationship between deposit-scale auriferous structures and these regional faults. Therefore, understanding the evolution of these structures is important when, for example, looking for prospective sites of gold mineralization outside of a known deposit or delineating a known deposit at depth. These gold-bearing structures can be reactivated or completely transposed by subsequent phases of deformation following a mineralizing event(s), as in the current model for some of the gold

occurrence in the Rowan-Kakagi greenstone belt (see Melling, 1986, 1988). For example, mesoscopic scale folds or the zone of intersection of planar structures may be areas of relatively instantaneous stress release, acting as a favorable path for gold bearing fluids in a stressed country rock. Additionally, the important role of competency contrasts inherent in a hosting rock, aiding in both the localizing of strain and development of these gold-bearing structures, has been demonstrated at a number of gold occurrences in Ontario (Colvine et al., 1988).

Current models for the genesis of orogenic gold deposits are the result of detailed work in some of the most well-studied and prolific gold-hosting Archean terranes, such as the Abitibi-Wawa subprovince in Ontario (Colvine et al., 1988) or the Kalgoorlie terrane of western Australia (Groves et al., 2018). These models have been applied to other terranes with similar crustal histories to compare gold deposits around the world. While debate remains concerning the fluid source and timing of gold mineralizing events, orogenic gold deposits are linked to the tectonic history of their hosting rocks and so studying the structural geology of an occurrence and the larger greenstone belt is key to both developing that occurrence and elucidating information that may aid in further exploration. In the case of the Western Wabigoon subprovince, and in particular the Rowan-Kakagi greenstone belt, the bedrock geology has been well-mapped however the regional structural geology is relatively less understood.

1.5 The Rowan-Kakagi Greenstone Belt

The Rowan-Kakagi greenstone belt is one of several greenstone-intrusive terranes that are collectively referred to as the Savant Lake – Crow Lake belt. The most recent geological map compilation of the Rowan Lake and Kakagi Lake areas is by Johns (2007) at a scale of 1:50 000. The area around the Dogpaw and Dubenski properties was mapped by Davies and Morin (1976)

at a scale of 1 inch to 0.5 miles. The evolution of the Rowan-Kakagi greenstone belt is outlined by Davis and Edwards (1982, 1986) who conducted field mapping and high precision U-Pb geochronology in the Kakagi Lake volcanic terrane. Their findings are summarized below, and approximate geochronological sampling locations are shown in Figure 1.3.

The Rowan-Kakagi greenstone belt consists of two metavolcanic terranes: 1) the Kakagi Lake volcanic terrane and 2) the Rowan Lake volcanic terrane. The two terranes are separated by the crustal scale, northwest-trending Pipestone-Cameron fault zone (PCFZ).

The Dogpaw deposit is hosted in the Kakagi Lake volcanic terrane. Volcanism in the area is interpreted to have started at 2731 +4.0/-2.9 Ma with the deposition of the Katimigamak and Snake Bay volcanics (Davis and Edwards, 1986). A U-Pb age was yielded from a pegmatitic section of a gabbro from the Katimigamak Formation which Davis and Edwards (1986) reported as been emplaced contemporaneously with the deposition of the hosting Katimigamak Lake and Snake Bay volcanics. The Katimiagamak Lake and Snake Bay volcanics are overlain by intermediate pyroclastic rocks of the Kakagi Lake Group volcanics. A felsic tuff at the top of the Kakagi Lake Group volcanic succession yielded a U-Pb age of 2711 +1.3/-1.2 Ma (Davis and Edwards, 1986).

The Kakagi Lake Group volcanics are intruded by the belt-scale, layered, mafic to ultramafic intrusions, referred to as the Kakagi sills. A pegmatitic section from a Kakagi sill at the base of the Kakagi Lake Group volcanics yielded a U-Pb age of 2724.8 +2.5/-2.3 Ma. The contact relationship between the Kakagi sills and the country rocks suggest these kilometer-wide layered intrusions were emplaced not long after the deposition of the Kakagi Lake Group volcanics (Davis and Edwards, 1986). Basalts of the Katimiagamak Lake and Snake Bay

volcanics are intruded by the Aulneau Batholith and the Sabaskong Batholith. A tonalite phase and a grandiorite phase of the Aulneau Batholith yielded U-Pb ages of 2716 +4.9/-2.8 Ma and 2709 +3.9/-1.5 Ma, respectively (Davis and Edwards, 1986). A sample taken from the Sabaskong Batholith returned an age of 2724.4 +1.9/-1.8 Ma (Davis and Edwards, 1982).

The Rowan Lake volcanic terrane is located northeast of the PCFZ; its internal structural architecture is characterized by the northeast-southwest trending Shingwak anticline and the Monte Cristo shear zone. The Rowan Lake volcanic terrane is dominated by mafic flows that display well-preserved primary structures north of the Shingwak anticline. The Rowan Lake volcanics are intruded by the Nolan Lake stock, a syn-tectonic granitoid intrusion (Lewis and Woolgar 2011).

Several belt-scale folds and faults control the bedrock map pattern in the Rowan-Kakagi greenstone belt. This includes the Kakagi Lake syncline and the Pipestone-Cameron fault zone found within the map area of this project. While the structural geology of the Rowan-Kakagi has gone underexplored relative to other greenstone belts of the Western Wabigoon, other workers, such as Edwards and Stauffer (1999), compared lithologies and structures between the Pipestone Lake area, 20 kilometers to the southeast, and the Rowan-Kakagi Lake area. They concluded that these belt-scale folds and faults originated during early phases of deformation (D1-D2), the result of accretionary tectonism at the subprovince's boundaries, and that other metavolcanics-intrusive terranes of the Western Wabigoon subprovince experienced a similar early tectonic history.

The Pipestone-Cameron fault zone is a prominent, broadly northwest trending regional fault zone separating the Kakagi and Rowan Lake volcanic terranes. To date there has been no successful correlation of volcanics across the fault and the sense and degree of displacement is

unknown. Inferred movement along the Pipestone-Cameron fault zone is largely based on qualitative data, such as the lack of the calc-alkaline pyroclastic rocks on the northeast side of the fault versus the southwest side, suggests northeast side up, vertical displacement (Blackburn, 1980). The apparent offset of lithologies and arcuate form of belt-scale folds proximal to this deformation zone suggests there was a component of dextral, strike-slip movement (Fig. 1.2, 2.1). Additionally, there has been no known systematic study of the regional fault and so much about the fault is speculative. This is addressed in more detail in Chapter 2.

1.5.1 The Dogpaw-Flint Lake Map Area, Access and Exposures

The Dogpaw-Flint Lake map area falls within the Flint Lake study area defined by Meade (2017) and is centered on the trenched exposures at the Dogpaw gold deposit (Fig. 1.3). Both shoreline and roadside exposure in the study area are of excellent quality. Supracrustal rocks in the study area include volcanics and sedimentary rocks of both the Kakagi and Rowan Lake terranes and 3 layered sills of the Kakagi sills. The study area also includes a well exposed section, approximately 10 kilometers, of the Pipestone-Cameron fault zone along the shorelines of Dogpaw, Flint and Caviar Lake. Bedrock exposures of the Kakagi Lake Group volcanics can also be accessed between kilometer 7 and kilometer 14 along the Cameron Lake road off Highway 71 south of the community of Sioux Narrows, Ontario. Numerous logging roads branch off from the Cameron Lake road and access in the area is largely controlled by seasonal logging. Dogpaw, Flint and Caviar Lake are interconnected and shoreline outcrops of both the Kakagi and Rowan Lake terranes can be accessed by boat from a launch at Whitefish Bay off highway 71 south of Sioux Narrows, Ontario.

Several mineral occurrences, including the Dogpaw gold deposit, are found in the Dogpaw-Flint Lake map area (Fig. 1.3). Many of these historic gold occurrences have numerous trenched exposures with mineralization expressed at surface. Over several decades the Dogpaw deposit has been examined by a number of mineral exploration companies. The deposit has numerous mechanically striped outcrops that provide accessible exposures of key structural relationships. Field work carried out in the summer of 2016 and 2017 included mapping and sampling of several trenched exposures around the Dogpaw deposit. The trenches were gridded and mapped at a scale of 1:200, or at 1:50 where important structural relationships were observed. Reconnaissance mapping in the area around the deposits was conducted to characterize the regional geological setting of the deposits, including key shoreline exposures of the Pipestone-Cameron fault zone in Dogaw-Flint Lake map area. Mapping of the Kakagi sill and Kakagi Lake Group volcanics was also carried out to help characterize these important lithological units.

1.6 Gold Deposit History and Previous Work

This study focused on the Dogpaw gold deposit (Fig. 1.3). Due to a near century of mineral exploration, the Rowan-Kakagi greenstone belt hosts dozens of known gold occurrences which have received varying levels of study and development. A full history of these occurrences is given in detail by Ball (2014). A summarized history of exploration at the Dogpaw deposit and other developed gold occurrences in the Rowan-Kakagi greenstone belt are provided in Appendix C. In the Rowan-Kakagi greenstone belt claim ownership of many of these deposits has been sporadic and industry data can be either difficult to find or incomplete.

The current model for gold mineralization in the Rowan-Kakagi Lake area is largely the result of the work by D. R. Melling (Melling and Watkinson, 1985, 1986; Melling, 1986; Melling, 1988; Melling, 1989). These studies on the Cameron Lake deposit (Occurrence 3, Fig. 1.3) and deposits in its vicinity provided the first evidence for a structural control on gold mineralization in the Rowan-Kakagi area. Since then exploration efforts has focused on localities along the trend of the Pipestone-Cameron fault zone. There are several key characteristics of gold mineralization in the Rowan-Kakagi greenstone belt that are commonly reported between different gold occurrences. The following is a summary of information from (Ball, 2014; Drabble et al., 2015; Melling, 1988, 1989). It is not an exhaustive summary and differences do occur at each deposit.

Ball (2014) reported that anomalous gold values at several historic gold occurrences are hosted in discrete shear zones that display both ductile-brittle and brittle deformation mechanisms. These shear zones are typically found in proximity to or at the contacts between volcanics and mafic to ultramafic intrusions. The geometry of the ore body appears to have been modified by a later stage of brittle-ductile deformation and re-activation of the hosting shear zones. Gold concentrations are highest in zones of extensional quartz veins and quartz vein breccia. There is a strong correlation with sulfide content, primarily pyrite, commonly reported between to 10-15% approximate volume %, being favorable targets for mineralization. There is a common proximal quartz-ankerite-sericite-pyrite alteration assemblage that commonly envelopes the highest gold concentration.

1.7 Geoscience Gaps and Project Objectives

As outlined in the previous sections the Rowan-Kakagi greenstone belt has experienced a long history of gold exploration and geological mapping. Some early workers in the belt suggested that gold occurrences were synchronous to their hosting deformation zones and speculated that their final geometries were related to the tectonic history of the Pipestone-Cameron fault zone (Melling 1989). The importance of the pre-existing anisotropies in the hosting rock was also noted by these workers, for example at the Cameron Lake gold deposit where the plunge of the ore body is parallel to the intersection of a set of bedding controlled shear zones. Since Melling's work in the 1980's of the Cameron Lake gold deposit a structurally related genetic model for gold mineralization has been used by industry on other gold occurrences in the Rowan-Kakagi greenstone belt, however this model has largely gone undeveloped since.

While it is tempting to draw parallels to other Archean lode gold deposits in Ontario a structural relationship between gold hosting structures in the Rowan-Kakagi greenstone belt and the Pipestone-Cameron fault zone has not been demonstrated. Shear zones and faults that transect gold occurrences in the belt have been speculatively correlated to the regional fault zone, but a relationship has not been demonstrated. This is likely due to the lack of study focused on the Pipestone-Cameron fault zone, whose kinematics and style of deformation are largely unknown, while efforts by industry have been focused on developing past occurrences. It may also likely be due to the lack of a systematic study that correlates geology across the respective property lines of different gold occurrences. How these structures developed, how they may have been altered and deformed by subsequent tectonic and magmatic events and the relative timing

of gold mineralization are important for developing any model for gold mineralization in a study area. These points are addressed at the Dogpaw deposit in this thesis.

Finally, a constraint on the timing of gold introduction and deposit hosting structures has yet to be attempted. Gold mineralization in other greenstone belts of Ontario is believed to have occurred syn to late in the deformation history of the hosting belts and broadly synchronous with late magmatic activity (Colvine et al., 1988) (Beakhouse 2007). Continued study of these late-tectonic intrusion, such as the Nolan Lake stock, Stephen Lake pluton and additional radiogenic isotope studies will likely further aid in understanding the crustal history, gold mineralization and future exploration efforts by industry in the Western Wabigoon.

With these geological gaps in mind the first goal of this thesis was to provide a modern study on the structural geology of the Dogpaw deposit through property and regional-scale geological mapping, characterizing the mineralization at the deposit, and help constrain the timing of gold mineralization via field relationships and U-Pb geochronology. The second goal was to study and delineate the Pipestone-Cameron fault zone and any subsidiary deformation zones within the larger, Dogpaw-Flint Lake map area. To achieve these goals, the objectives of this thesis included:

1) A detailed study on the structural geology, gold mineralization and timing relationships at the historic Dogpaw deposit.
2) A regional-scale structural study of the Pipestone-Cameron fault zone in proximity to the Dogpaw deposit in the Dogpaw-Flint Lake map area.
3) Comparing and relating deposit-scale structural relationships at the Dogpaw deposit with the regional structural geology of the Pipestone-Cameron fault zone in the Dogpaw-Flint Lake map area.
4) Absolute and relative ages of gold mineralization at the Dogpaw gold deposit.

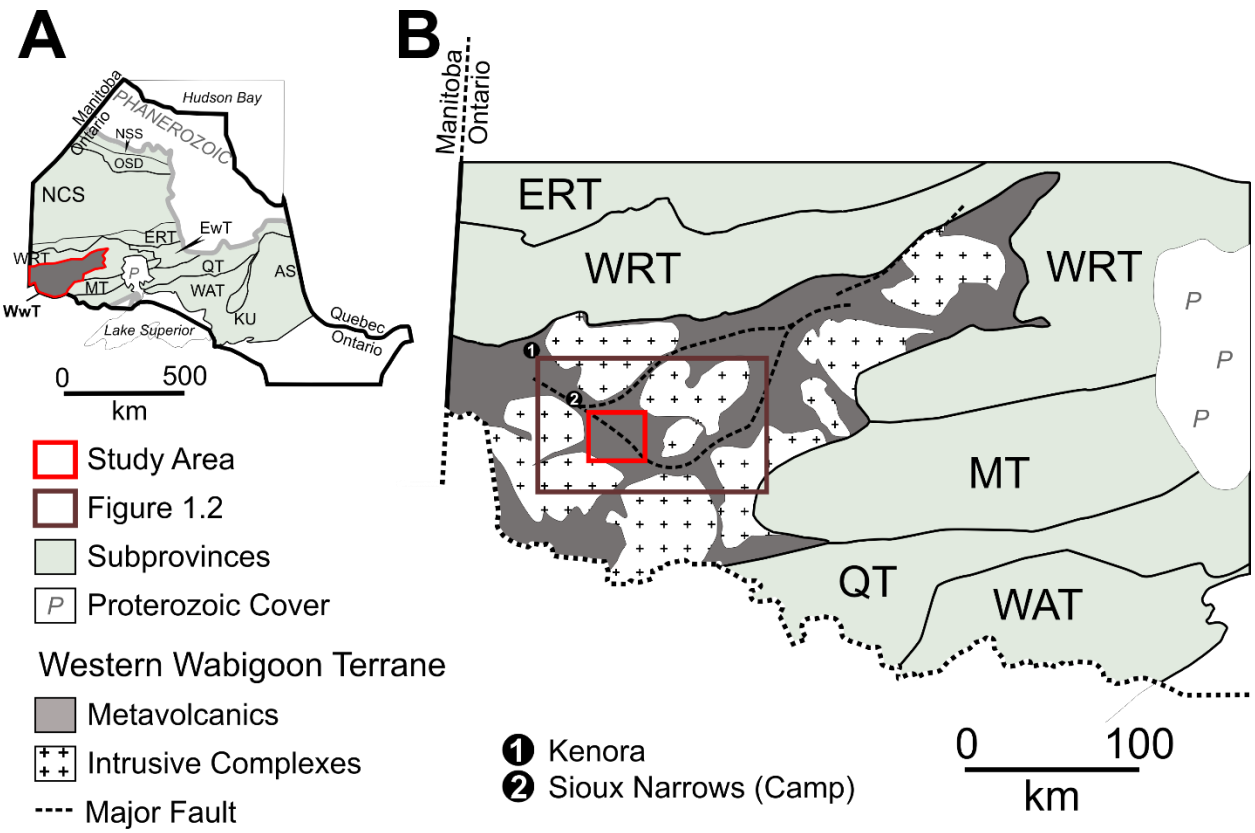

Figure 1.1: A) Simplified map of the Superior Province in Ontario, Canada (*modified* after Percival et al., 2006). Subprovinces of the Superior Province are labelled and the Western Wabigoon is highlighted in red; Abbreviations: NSS, Northern Superior superterrane; OSD, Oxford-Stull Domain; NCS, Northern Caribou superterrane; ERT, English River terrane; WRT, Winnipeg River terrane; WwT, Western Wabigoon terrane; EwT, Eastern Wabigoon terrane; MT, Marmion terrane; QT, Quetico terrane; WAT, Wawa-Abitibi terrane; KU, Kapuskasking uplift. B) Simplified map of the Western Wabigoon subprovince and bounding subprovinces of the Superior Province in Ontario (*modified* after Percival et al., 2012). The approximate location of the Kenora and Sioux Narrows (camp) are displayed and boundaries of Figure 1.2 and Figure 1.3 are outlined.

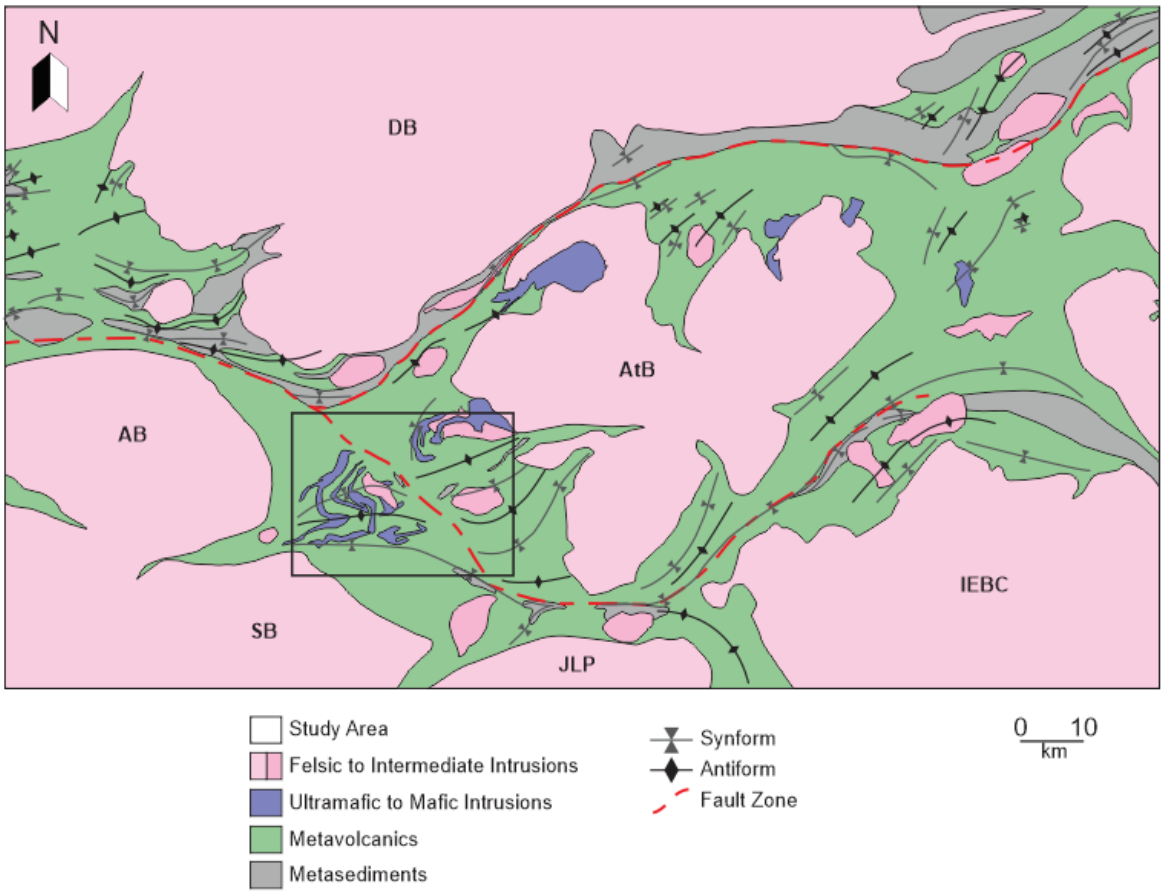

Figure 1.2: Simplified map of the central Western Wabigoon subprovince as outlined in Figure 1.1. *Modified* and redrawn from Davies and Pryslak (1963) with the location of crustal-scale faults from Ontario Geological Survey Map 2576 (Ontario Geological Survey 1992). The map focuses on the structure features of greenstone belts found in the central Western Wabigoon. The regional study area defined by Meade (2016) is outlined. Abbreviations: AB, Aulneua Batholith; AtB, Atikwa Batholith; DB, Dryberry Batholith; IEBC, Irene–Eltrut Lakes Batholithic Complex; JLP, Jackfish Lake Pluton; SB, Sabaskong Batholith.

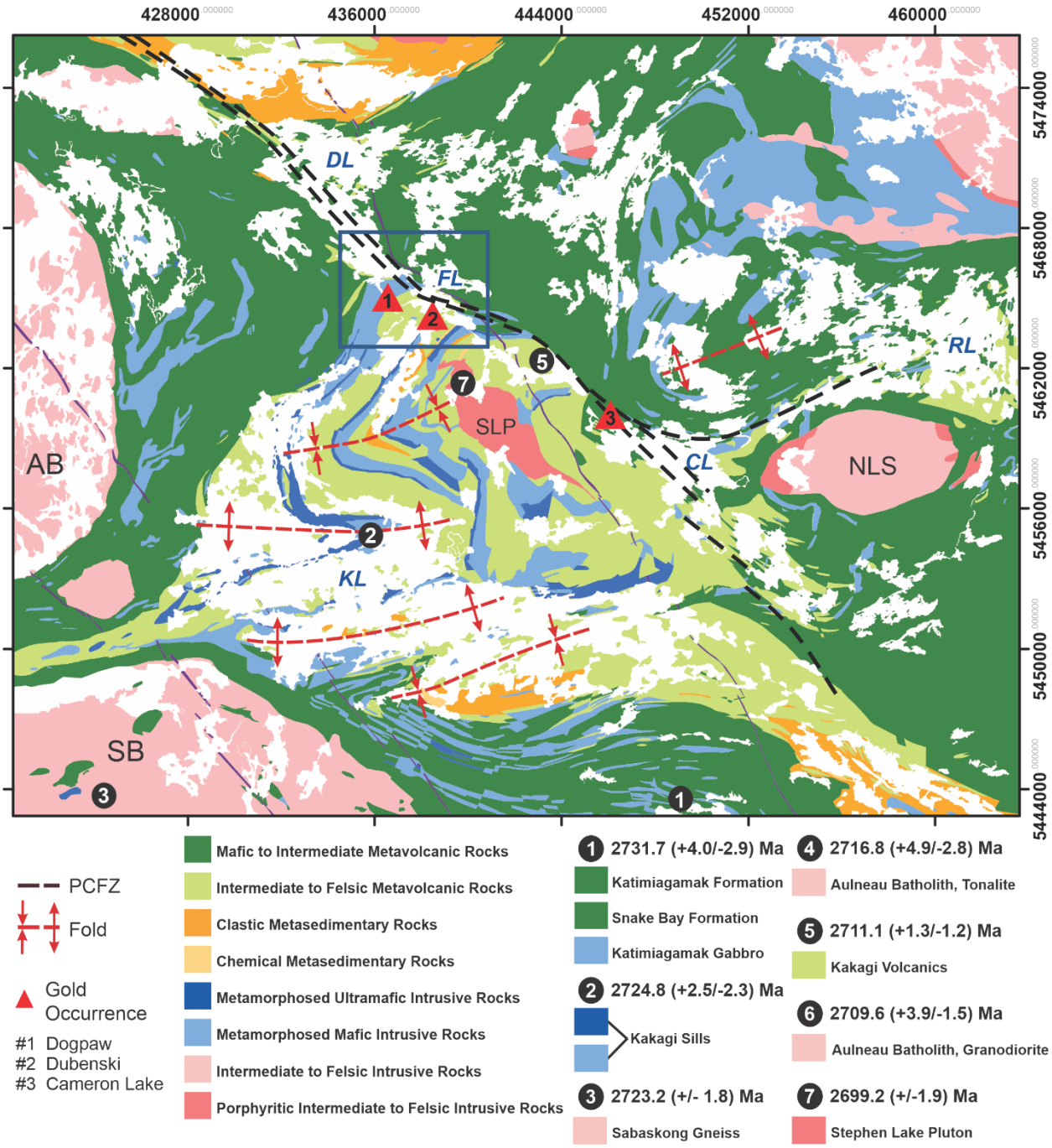

Figure 1.3: A simplified geological map of the Rowan-Kakagi greenstone belt (*modified from* Johns 2007). Sample locations from Davis and Edwards (1986) are numbered from 1-7 with sample locations 4 and 6 from the interior of the Aulneau batholith. Abbreviations: AB, Aulneau Batholith; AtB, Atikwa Batholith; CL, Cameron Lake; DL, Dogpaw Lake, FL, Flint Lake; NLS, Nolan Lake stock; KL, Kakagi Lake; RL, Rowan Lake; SB, Sabaskong Batholith; SLP, Stephen Lake pluton; Universal Transverse Mercator (UTM) coordinates are provided using North American Datum 1983 (NAD83) in Zone 15.

Chapter 2
Structural Geology of the Pipestone-Cameron Fault Zone, Dogpaw-Flint Lake Area, Rowan-Kakagi Greenstone Belt, Western Superior Province, Ontario

2.1 Introduction

The Pipestone-Cameron fault zone is a prominent, broadly northwest-trending network of brittle-ductile faults that separates the Kakagi Lake and Rowan Lake volcanic terranes. The structure has been noted by several previous workers in the Rowan-Kakagi greenstone belt (eg., Ball 2014; Melling 1989; Davies and Edwards 1986) and has been speculated as a major control on the distribution of gold occurrences, including the Dogpaw deposit (Fig. 2.1). A number of major shear zones, some of which host gold occurrences, have been interpreted as splays of the Pipestone-Cameron fault zone. This includes the Cameron Lake shear zone, the interpreted hosting structure of the Cameron Lake deposit (Ball 2014). At the Dogpaw deposit, the Dalby Bay shear zone, a suspected splay of the Pipestone-Cameron fault zone, transects the deposit and variably overprints earlier gold-bearing structures. To provide a regional structural framework for the observations at the Dogpaw deposit and better constrain the Pipestone-Cameron fault zone, shoreline mapping at a scale of 1: 20 000 and inland mapping at a scale of 1:5 000 was conducted in the Dogpaw-Flint Lake map area. Results from this work suggest that the Dalby Bay shear zone is a second-order structure of the Pipestone-Cameron fault zone, with structural features identical to other suspected splays and compatible kinematics.

2.2 Structural Geology

The Pipestone-Cameron fault zone has been interpreted to extend for tens of kilometers in the Rowan-Kakagi greenstone belt (Fig. 2.1). During the 2017 field season in the Dogpaw-Flint Lake map area, several shear zones were mapped, and trends delineated along strike with structural observations and measurements collected along several suspected splays, including the Dalby Bay shear zone (Fig. 2.2). In the northern half of the map area around Dogpaw and Flint Lake, there is an abundance of shoreline bedrock exposures and the profile of several shear zones are well exposed. These shear zones strike east-southeast and their structural features suggest a dextral sense of movement. In the southern half of the map area around Cedartree Lake, shoreline exposures are equally abundant, however there are relatively fewer shear zones. These structures strike east-northeast and have a sinistral sense of movement. Shear zone boundaries and S-C foliation were used to interpret the along-strike trend of these shear zones and the trend of the larger Pipestone-Cameron fault zone.

2.2.1 East-southeast Trending Shear Zones, Dogpaw and Flint Lake

Several dextral, east-southeast trending shear zones are found in the northern half of the map area. These structures are characterized by a marginal domain of gradational strain followed by a well-defined central domain of higher strain. The structural features that result from this gradation in strain vary depending on the lithology deformed and relative position to the apparent center.

At the interpreted boundary of these shear zones and the relatively massive country rock there is a dominantly pure strain component exemplified by the elongation and flattening of primary features, sometimes accompanied by a weak foliation. This includes exposures of

deformed pillow basalts (Fig. 2.3 A and B) and L-tectonites defined by stretched fragments (Fig. 2.3 C and D). At higher strain and within the marginal domain of these structures, S-L tectonites dominate. Well-developed foliation and structural features, such as shear bands and boudins are common and provide kinematic indicators suggesting a dextral sense of shear (Fig. 2.3 E and F). The folding and overprinting of earlier generations of foliation is also common (Fig. 2.3 G and H). Closer to the central domain of these shear zones, shear bands and crenulated foliation is replaced by a banded foliation defined by alternating quartz and mica-rich layers (Fig. 2.4 A). Finally, the interpreted central domain of these structures is marked by a relatively narrow zone of phyllitic, mica-rich, S-C and C-C' foliation (Fig. 2.4 B to D).

At the interpreted boundary of mapped shear zones in the Dogpaw and Flint Lake area, measured lineations typically plunge steeply. They largely consist of stretched fragments of pyroclastic rocks. Closer to the interpreted core of these shear zones lineations are typically moderately plunging and defined by the strong preferred alignment of prismatic minerals and ridge-and-grove slickenside striae (Fig. 2.4 E and F). Relatively minor shear zones and faults are also commonly found throughout the northern part of the map area. These structures may be discrete, only several meters in width, and sharply cross-cut primary features (Fig. 2.5 A to D).

A series of feldspar-quartz and felspar-porphyry dykes are found at a number of bedrock exposures in the north end of the Dogpaw-Flint Lake map area. They are found along the boundary of mapped shear zones and are variably deformed within the internal margins of the structures (Fig. 2.5 E and F). They appear identical to the set of dykes found at the Dogpaw deposit that either crosscut gold bearing shear zones or are deformed within the margins of the Dalby Bay shear zone (see Chapter 3).

2.2.2 East-northeast Trending Shear Zones, Cedartree Lake

In the southern half of the map area, around Cedartree Lake, three relatively minor, sinistral, east-northeast trending shear zones were identified. The rocks deformed here consist largely of polymictic tuff-breccia of the Kakagi Lake Group (Fig. 2.6). As with the shear zones found in northern half of the map area, shear zones in the Cedartree Lake area are characterized by a gradation in strain intensity.

At the interpreted boundary of these shear zones there is a dominantly pure strain component, with the transition between massive country rock and the marginal domain of these structures marked by the flattening of tuff-breccia fragments (Fig. 2.6 C and D). Strain appears to be partitioned in melanocratic and fine-grained fragments while relatively quartz and feldspar rich fragments are largely undeformed. In the marginal domain all tuff-breccia fragments show signs of deformation and a foliation develops in the supporting groundmass, becoming progressively better developed closer to the central domain of the shear zones (Fig. 2.6 E to G). This foliation is replaced in the central domain by a relatively narrow, highly foliated zone, identical to the fabric found in the central domain of shear zones found in the northern half of the map area (Fig. 2.6 H).

Although less abundant in the south, S-C foliation close to the central domain of mapped shear zones provide a sinistral sense of shear. Lineations in the southern map area are typically shallow to moderately plunging. Shear zones deform pyroclastic rocks of the Kakagi Lake Group and so lineations are mostly defined by stretched fragments (Fig. 2.4).

2.3 Discussion and Conclusions

Previous to this study the kinematics and trend of the Pipestone-Cameron fault zone in the Dogpaw-Flint Lake map area was largely speculative. Structural data and observations suggest two dominant trends in the map area, an east-southeast trending set of shear zones in the north around Dogpaw and Flink Lake and an east-northeast trending set of shear zones in the south, with dextral and sinistral kinematics, respectively. Conflicting kinematic indicators are rare but do exist suggesting a potential more complex deformation history. However, the common and repeating structural features, gradation in strain intensity and compatible kinematics between the sets in the north and south suggests that activity along these structures may have been largely synchronous. This interpretation does not exclude the possibility that a subsets of shear zones that constitute the Pipestone-Cameron fault zone may have been longer-lived structures relative to others.

The shallow plunging lineations and kinematic indicators in the south part of the map area suggest that east-northeast, sinistral shear zones record dominantly strike-slip and a relatively minor dip-slip component. However, in the north part of the map area, steeply plunging lineations at the boundary of shear zones and shallow plunging lineations at their apparent center suggests a boundary normal component of movement near the boundary of the shear zones and boundary parallel component of movement in the central domain. This change in orientation of lineations and apparent gradation in strain is indicative of transpressional shear zones, a common observation in other shear zones of the Superior Province (Lin et al., 2007).

In the south part of the map area, east-northeast trending shear zones may have been structures that first originated as a result of slip along primary lithological contacts during

refolding of the Emm Bay syncline. Movement along these shear zones and the arcuate form of the Emm Bay syncline near the Pipestone-Cameron fault zone may have been in response to the north-south directed regional stress regime and overall right-lateral movement in the North.

Overall, kinematic and shear sense indicators from the mapped shear zones in the Dogpaw-Flint Lake map area suggest a broad N-S directed compression and coincident, east-southeast, right-lateral sense of movement along several, major shear zones. This interpretation is compatible with the deposit-scale stress regime interpreted for the Dalby Bay shear zone at the Dogpaw deposit. The shared structural features, compatible kinematics, and presence of syn-tectonic dykes spatially associated with other suspected splay of the Pipestone-Cameron fault zone suggests that the Dalby bay shear zone is one such splay and part of the larger network of shear zones that constitute the Pipestone-Cameron fault zone.

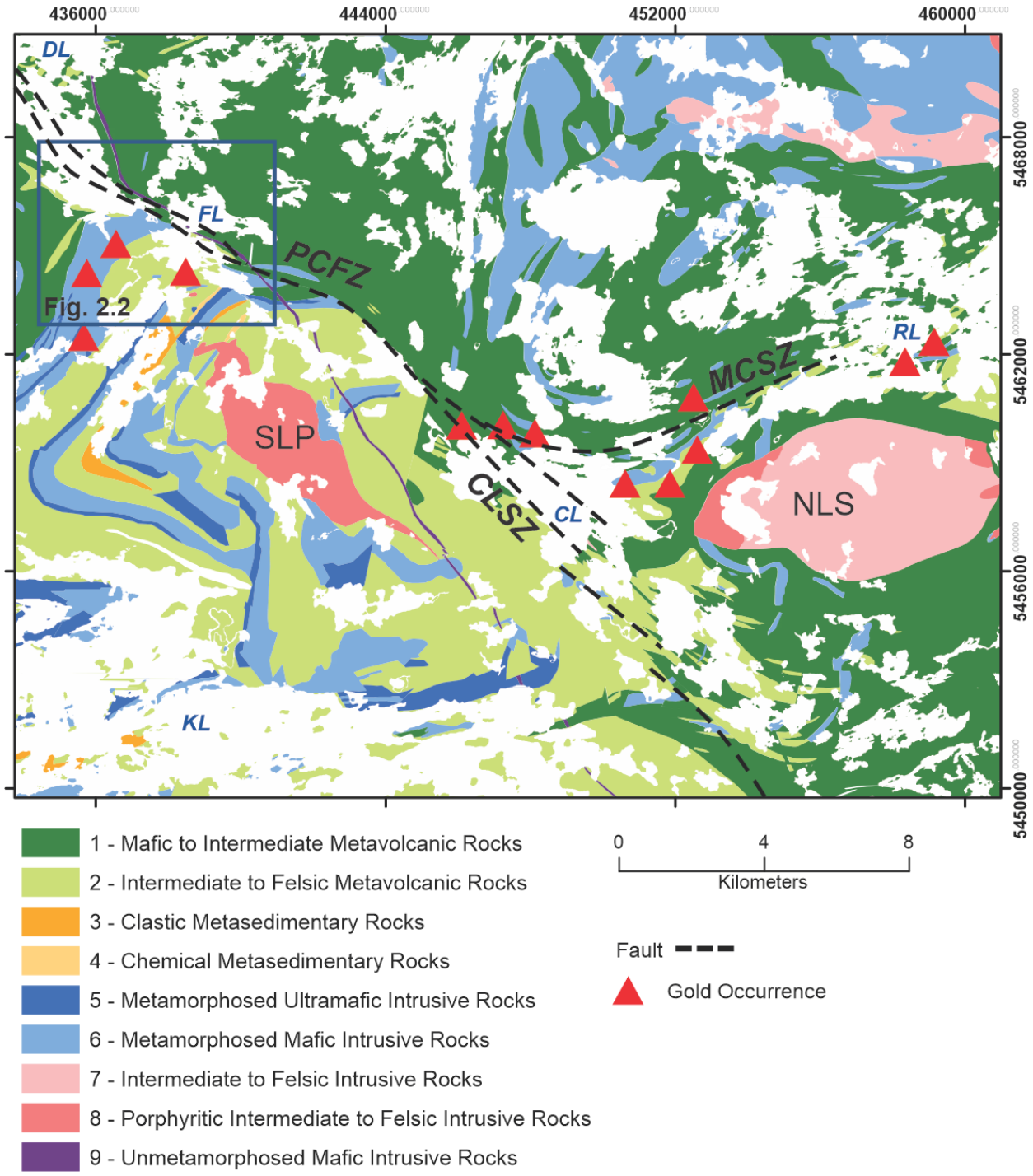

Figure 2.1: Simplified geological map of the Rowan-Kakagi greenstone belt (*modified from* Johns 2007). Figure 2.2 is outlined in blue. The locations of several gold occurrence are indicated. Abbreviations: CLSZ, Cameron-Lake shear zone; MCSZ, Monte-Cristo shear zone; NLS, Nolan Lake stock; PCFZ, Pipestone-Cameron fault zone; SLP, Stephen Lake pluton; Universal Transverse Mercator (UTM) co-ordinates are provided using North American Datum 1983 (NAD83) in Zone 15.

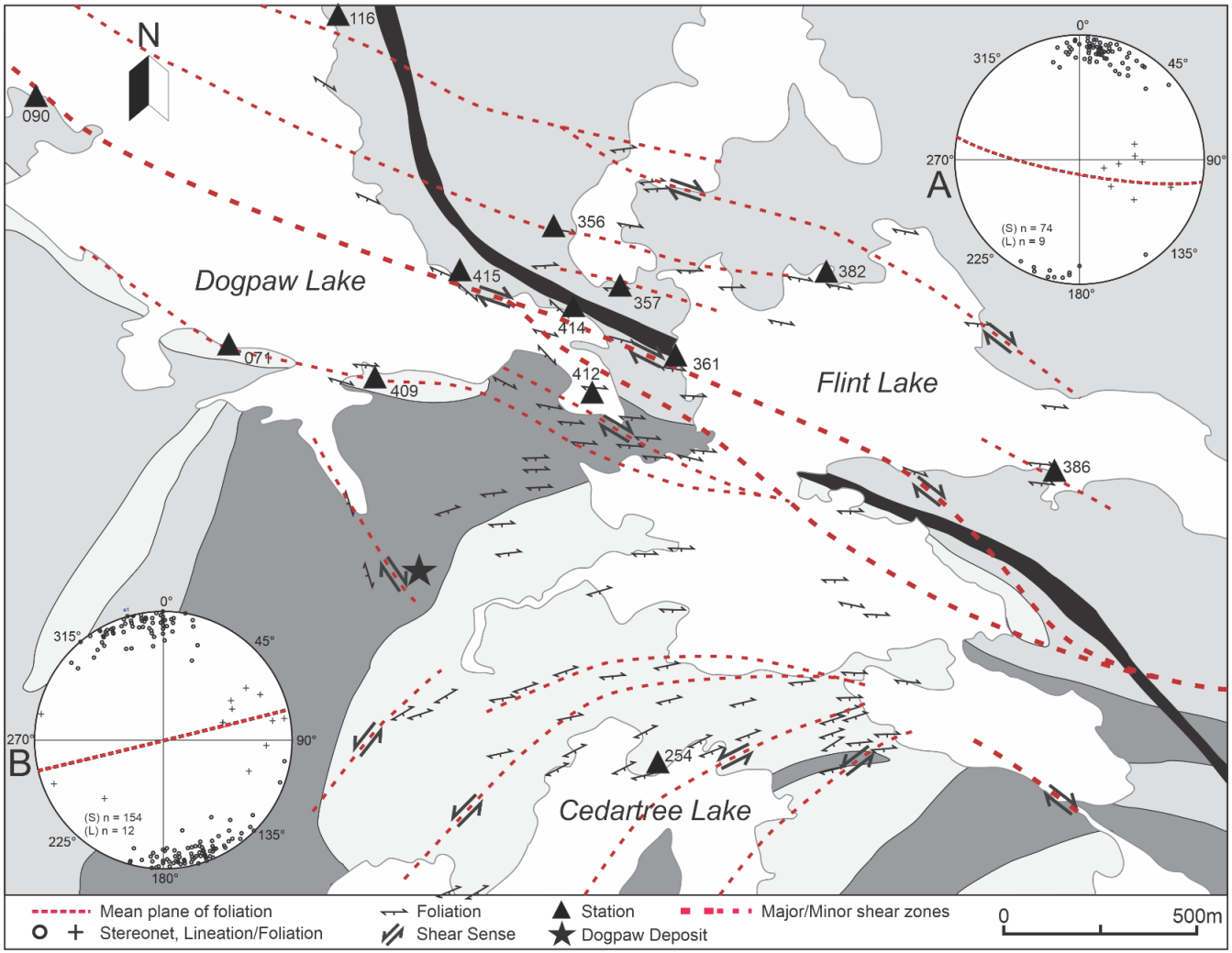

Figure 2.2: A simplified geological map of Dogpaw-Flint Lake map area highlighting the structural geology in the map area (*modified from* Johns 2007). Please refer to Fig. 3.1 and 3.2 for the bedrock geology. The location of the Dogpaw deposit is indicated with a star. Stereonets A and B display structural data collected in the north and south parts of the map area, respectively. Mapped shear zones from this research project that constitute the Pipestone-Cameron fault are displayed in dashed red lines. Stations with outcrop photos in subsequent figures (Fig. 2.3 to Fig. 2.6) are displayed.

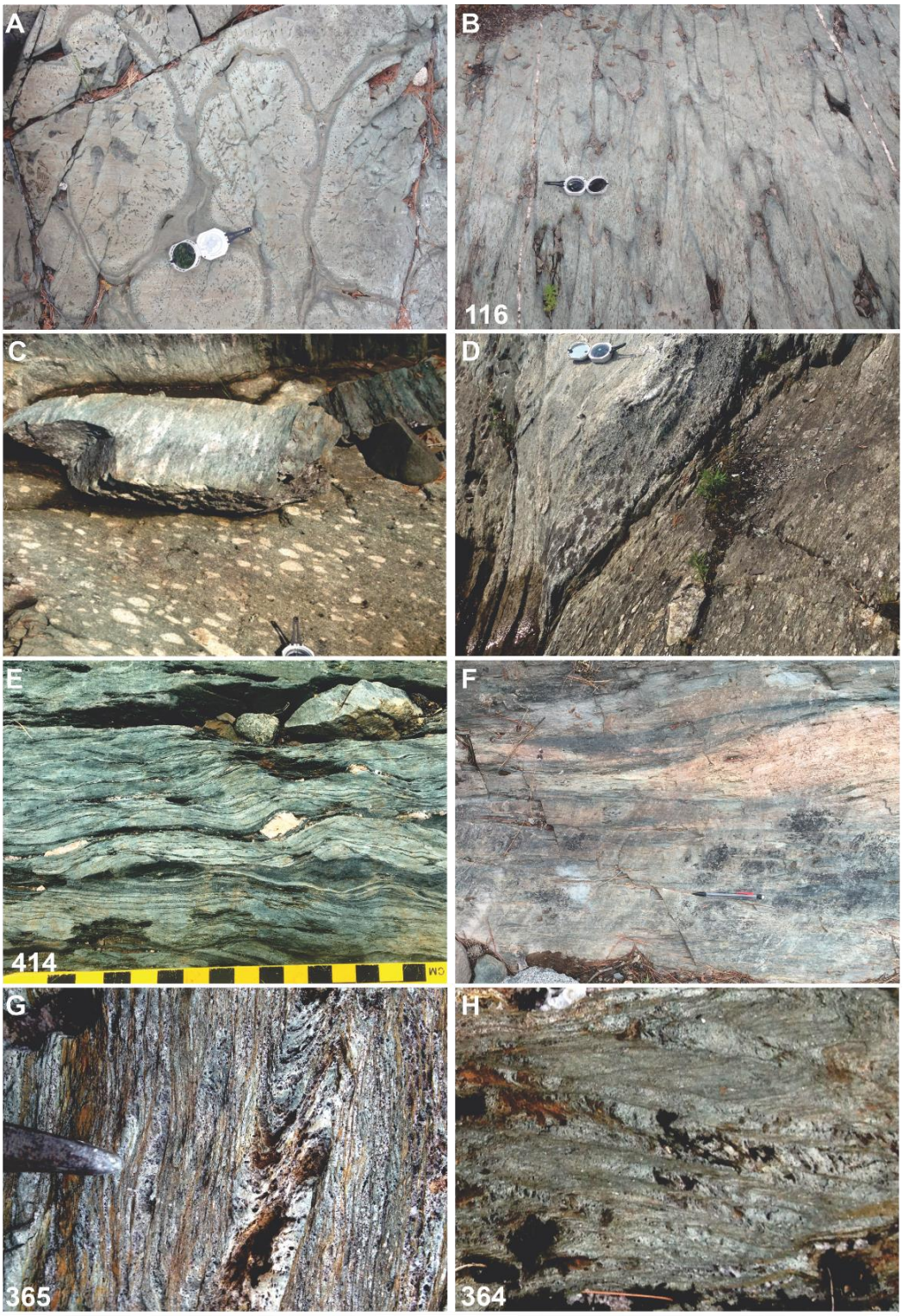

Figure 2.3: Shoreline outcrop photos around Dogpaw and Flint Lake. A) and B) Massive and flattened pillowed basalts. C) and D) Well-developed L-tectonite with steeply plunging stretched fragments and a poorly developed foliation. E) and F) Rotated porphyroclasts in a deformed basalt and shear bands. G) and H) Folding and crenulation of a well-developed foliation closer to the central domain of a shear zone.

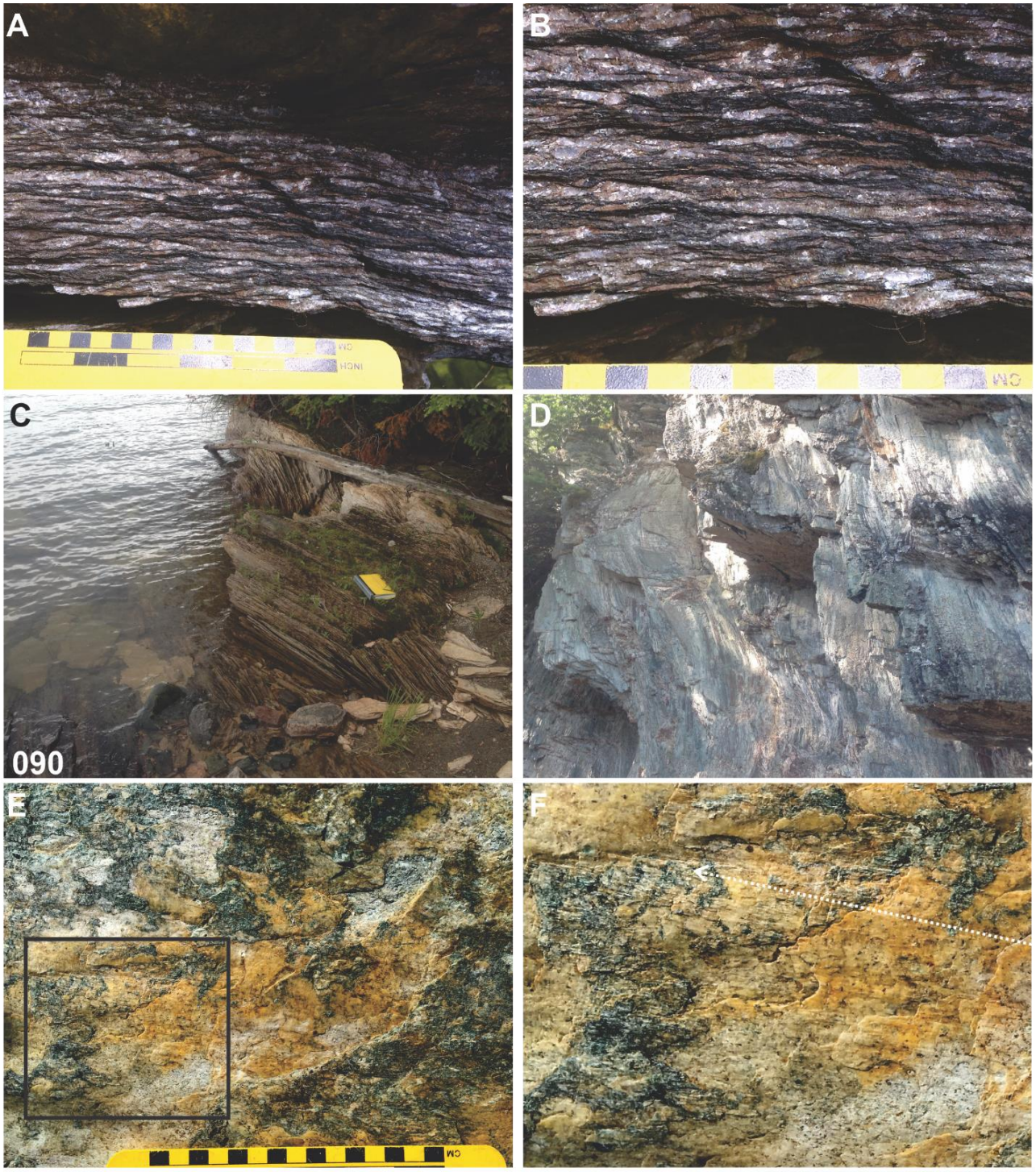

Figure 2.4: Shoreline outcrop photos around Dogaw and Flint Lake. A) and B) Banded foliation found near the central domain of shear zones. C) and D) Phyllitic foliation typical of the central domain of shear zones of the Pipestone-Cameron fault zone. E) and F) Ridge-and-grive slickenside striations. G) and H) Late kink folds and quartz-carbonate veins

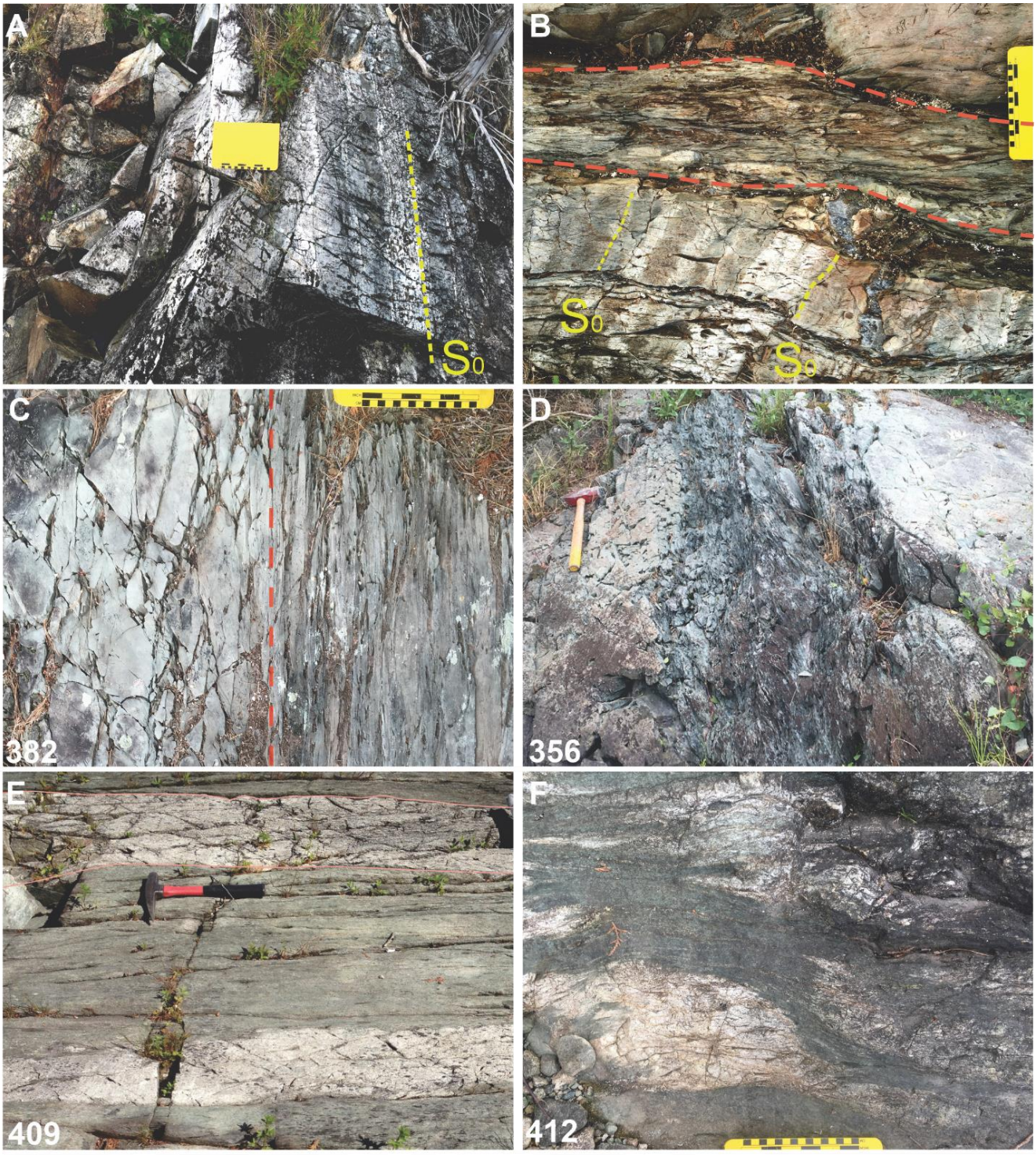

Figure 2.5: Shoreline outcrop photos around Dogpaw and Flint Lake. A) Alternating ash beds of the Kakagi Lake group and B) same beds cut at a high angle by a discrete fault, in red. C) and D) Examples of minor, discrete faults of the Pipestone-Cameron fault zone. E) Relatively undeformed feldspar-quartz porphyry dykes hosted in gabbro. F) Deformed feldspar-quartz porphyry dykes in a shear zone of the Pipestone-Cameron fault zone.

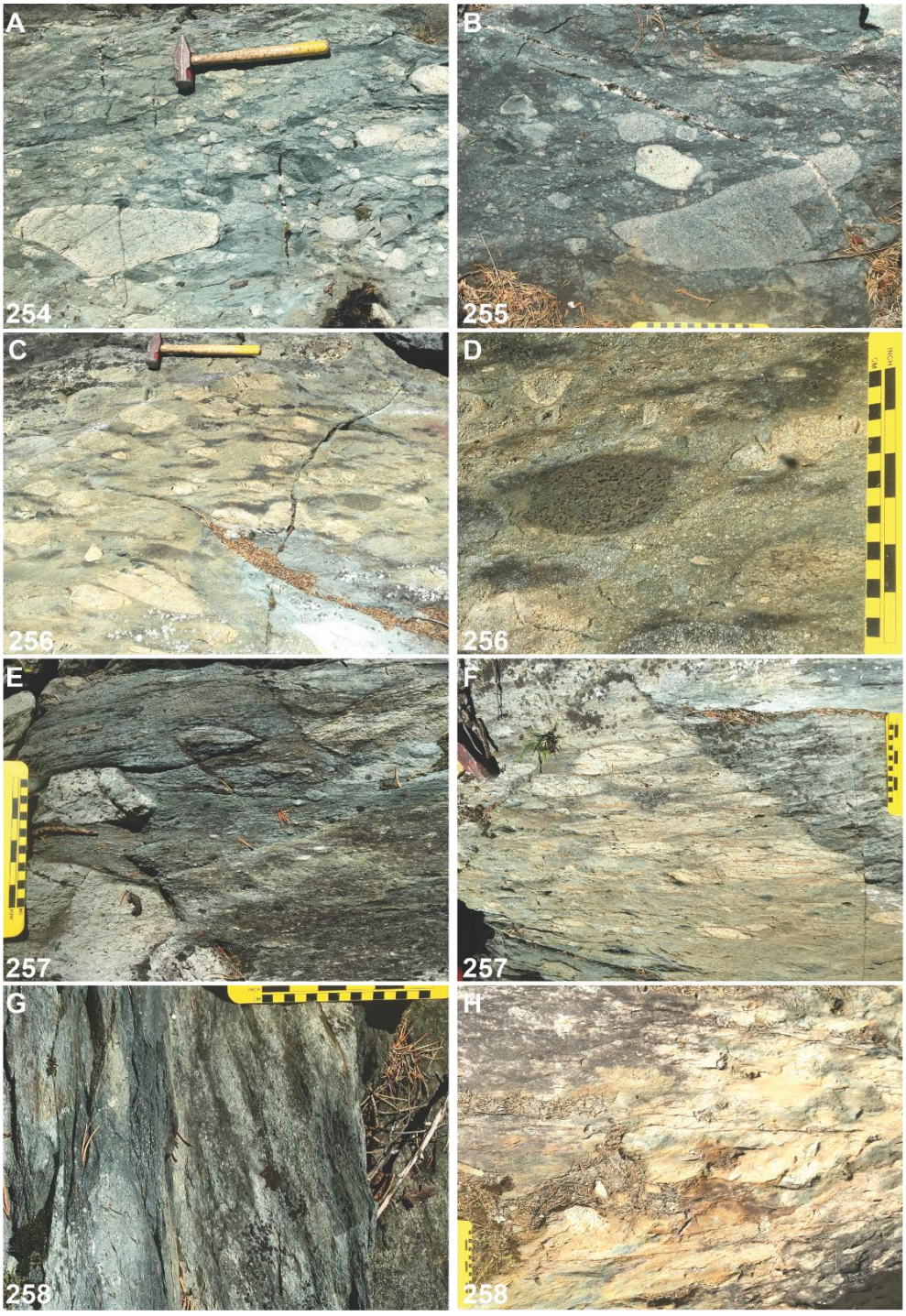

Figure 2.6: Shoreline outcrop photos around Cedartree Lake. Photos are taken along a largely continuous exposure of shoreline. Note the progressive development of a well-developed foliation and loss of primary features with increasing strain. A) and B) Undeformed massive, polymictic fragmental rocks of the Kakagi Lake group C) to G) Development of a foliation and stretching of fragments with increasing strain. H) Loss of primary features at high strain with a phyllitic foliation typical of several shear zones of the Pipestone-Cameron fault zone.

Chapter 3
Structural Geology, Timing and Style of Gold Mineralization at the Dogpaw Gold Deposit, Rowan-Kakagi Greenstone Belt, Western Superior Province, Ontario

3.1 Introduction

The Dogpaw gold deposit is hosted in the Neoarchean rocks of the Rowan-Kakagi greenstone belt of the Western Wabigoon subprovince in northwestern Ontario. It is one of several gold occurrences that occur adjacent to the crustal-scale Pipestone-Cameron fault zone in the greenstone belt.

At the Dogpaw gold deposit, bedrock exposures are of good quality and mineralization is readily identified and accessible at surface, providing an ideal environment to study the structural geology and gold mineralization. Here the bulk of gold mineralization is strictly hosted in a network of conjugate, mylonitic shear zones which have been overprinted by a secondary fault of the Pipestone-Cameron fault zone and are cross-cut by a set of porphyry dykes. Gold is associated with quartz-carbonate breccia veins and sheeted, shear zone parallel quartz-carbonate veins. Field observations suggest that gold was introduced syn-kinematic to the hosting structures with the bulk of mapped mineralization located at the intersection of conjugate shear zone sets. A suite of samples was taken at the Dogpaw deposit for LA-ICP-MS U/Pb analysis. $^{207}Pb/^{206}Pb$ zircon ages from samples collected from the deposit-hosting intrusion and feldspar porphyry dykes that cross-cut gold bearing structures provide the first absolute timing constraints on gold mineralization at the Dogpaw deposit, and a first in the Rowan-Kakagi greenstone belt.

The Pipestone-Cameron fault zone has long been associated with several gold occurrences in the Rowan-Kakagi greenstone belt, including the indicated 0.024 M oz Dogpaw deposit and the measured and indicated, 0.569 M oz Cameron Lake deposit (Drabble et al. 2015, p.155, Table 23.1) (Fig. 3.1). However, a relationship between the structures that host these deposits and the regional fault has remained largely speculative. While gold occurrences in the greenstone belt have received varying levels of attention and locally share similar structural characteristics, camp-scale detailed structural analysis is lacking at many historic gold occurrences in the belt. Additionally, a constraint on the timing of gold mineralization has yet to be attempted. Therefore, details on gold mineralization in the Rowan-Kakagi greenstone belt is lacking relative to other Archean greenstone belts of the Superior Province.

To address these gaps the bedrock geology in proximity to the Dogpaw deposit was mapped at a scale of 1:5 000 (Fig. 3.2) (Krapf-Jones et al., 2016, 2017) in collaboration with regional mapping at a scale of 1:20 000 of bedrock exposures in the Rowan-Kakagi greenstone belt (Meade, 2015, 2016, 2017). Additionally, several mechanically stripped exposures at the deposit were mapped at a scale of 1:200, or in more detail (1:50) when key geological relationships were observed.

This chapter begins with a description of the hosting intrusion, the layered ultramafic to mafic Kakagi sill, and the country rocks it abuts. This is followed by a section detailing the generations of structures and key structural observations local to the Dogpaw deposit. Emphasis is placed on G2 structures, an early network of auriferous, conjugate shear zones unique to the Dogpaw deposit, and G3 structures, specifically the Dalby Bay shear zone, a suspected splay of the Pipestone-Cameron fault zone. This is followed by a section detailing the gold-bearing vein

network at the deposit followed by a section concerning a set of porphyry dykes that cross-cut G2 auriferous structures at the deposit and are themselves variably deformed by the G3, Dalby Bay shear zone. Results from the analysis of a suite of samples for U/Pb geochronology are presented and their implications discussed. Finally, at the end of this chapter, the property and regional-scale implications of this study are discussed.

3.2 Regional Geological Setting

The Rowan-Kakagi greenstone belt consists of two metavolcanic terranes, the Rowan Lake terrane and the Kakagi Lake terrane, separated by the overall northwest-trending Pipestone-Cameron fault zone. The most recent geological map compilation of the greenstone belt is by Johns (2007) at a scale of 1:50 000. The area around the Dogpaw deposits was mapped by Davies and Morin (1976) at a scale of 1:31 360. Field mapping and a high-precision U/Pb geochronological study was carried in the Kakagi Lake area by Davis and Edwards (1982, 1986). Relevant results from these studies are summarized in the following section.

The deposit is hosted by rocks of the Kakagi Lake terrane. The terrane consists of the Katimiagamak Formation and the Snake Bay Formation basalts (U/Pb age of 2731.7 +4.0/−2.9 Ma; Davis and Edwards, 1986), which are overlain by the dominantly pyroclastic rocks of the Kakagi Lake Group (U/Pb age of 2711.1 +1.3/−1.2 Ma; Davis and Edwards, 1986). Metamorphism is dominantly greenschist-grade, however the thoellitic basalts of the Snake Bay formation are reported as locally variably metamorphosed to amphibolite grade along the eastern margin of the Aulneau Batholith (Davies and Morin, 1976).

The metavolcanics of the Kakagi Lake terrane are intruded by a series of coeval, mafic to ultramafic layered sills (U/Pb age of 2724.8 +2.5/−2.3 Ma; Davis and Edwards, 1986), referred

to as the Kakagi sills. These layered intrusions can be up to one and a half kilometers thick and of varying heterogeneity (Davies and Morin, 1976). The sills are well differentiated and are typically comprised of a basal pyroxenite layer overlain by alternating layers of gabbro and pegmatitic gabbro. The Kakagi Lake terrane is also intruded by voluminous felsic plutonic rocks, including the multi-phase Sabaskong batholith (2723.2±1.8 Ma), the Aulneau Batholith (2716.8 +4.9/−2.8 Ma) and the Henry Lake intrusion (2701.0±1.2 Ma; all U/Pb ages from Davis and Edwards, 1986). A suite of syn-tectonic feldspar porphyry and feldspar-quartz porphyry dykes also occur locally along the trend of several major faults of the Pipestone–Cameron fault zone, at several gold occurrences in the Rowan-Kakagi greenstone belt, and cross-cut known gold bearing structures at the Dogpaw deposit.

Major structural features in the Rowan-Kakagi greenstone belt include a network of brittle-ductile faults, referred to as the Pipestone-Cameron fault zone, and a series of macroscopic antiforms and synforms. This includes the Emm Bay syncline in the Kakagi Lake terrane, one of at least three folds superimposed on the larger Kakagi Lake syncline (Fig. 3.1). These folds have an average wavelength of several kilometers and are characterized by steeply dipping, east-west trending, axial planes. The Dogpaw deposit is hosted in the north-west limb of the Emm Bay syncline. The Emm Bay syncline is a prominent belt-scale fold which controls the bedrock pattern in the map area on the south-west side of the Pipestone-Cameron fault zone. Besides the Pipestone-Cameron fault zone, deformation in the Rowan-Kakagi greenstone belt appears to have been largely concentrated along lithological contacts, evident by the lack of bedrock exposure and topographic lows at these locations. Davis and Morin (1976) proposed that the Emm Bay syncline was the result of flexural slip folding, with lithological contacts between

the relatively competent mafic metavolcanics and sills acting as slip surfaces and strain accommodated largely in the less competent intermediate to felsic volcanics of the Kakagi Lake Group.

The Rowan Lake and Kakagi Lake terranes are separated by several brittle-ductile shear zones which constitute a section of the Pipestone-Cameron fault zone within the map area. These shear zones vary in width from tens to hundreds of meters, are well-spaced by blocks of undisturbed country rock, and commonly shouldered by zones of gradational strain. The apparent hinge of several macroscopic folds on either side of the Pipestone-Cameron fault zone are interpreted to arc into the zone of deformation. This suggests the regional fault was active during a later phase of deformation that affected earlier structures of the Rowan-Kakagi greenstone belt. Apart from these structural features the supracrustal rocks of the Rowan-Kakagi greenstone belt are largely undeformed with primary igneous and sedimentary structures well preserved. This aids in the delineation of major deformation zones and distinguishing generations of structures versus the challenges when working in more complex, poly-deformed terranes. Further details on the Pipestone-Cameron fault zone are found in Chapter 2.

The crustal history of the Rowan-Kakagi greenstone belt is interpreted to have occurred in a short time interval of approximately 32 Myr (Davis and Edwards, 1986). This interval is bracketed by the deposition of the Katimiagamak Formation (U/Pb age of 2731.7 +4.0/−2.9 Ma: Davis and Edwards, 1986) and the emplacement two late-tectonic intrusions, the Heronry Lake pluton (U/Pb age of 2701.0 ± 1.2 Ma: Davis and Edwards, 1986) and Stephen Lake pluton (U/Pb age of 2699.2 ± 1.9 Ma: Davis and Edwards, 1986). The emplacement of these intrusions is also interpreted to mark the end of regional deformation. A recent U/Pb age of 2705±5 Ma by Lewis

et al., (2012) was obtained from zircons collected from the Nolan Lake stock in the Rowan Lake terrane. This intrusion is believed to be late-tectonic and provides further constraint on the timing of deformation (Lewis et al., 2012).

3.3 Local Geological Setting

The following description of the local geology is in part the result of field mapping at a scale of 1: 5000 and trench mapping at a scale of 1:100 at the Dogpaw deposit (Krapf-Jones et al., 2016, 2017) within the Dogpaw-Flint lake study area (Fig. 3.1 & 3.2). The Dogpaw deposit is hosted in the mafic to ultramafic rocks of a layered intrusion, a member of the Kakagi sills. A sample collected by Davis and Edwards (1986) from a pegmatitic section of a Kakagi sill in the north-end of Kakagi Lake yielded a U/Pb zircon age of 2724.8 +2.5/−2.3 Ma (Fig. 1.3). The Kakagi sills are interpreted to have been emplaced at the late stages of or following mafic volcanism and during the transition to felsic magmatism in the greenstone belt (Davis and Edwards, 1986). This one-kilometer-wide sill is in contact with a series of mafic metavolcanic rocks of the Snake Bay Formation to the west and in contact with the intermediate to felsic metavolcanics and metasedimentary rocks of the Kakagi Lake Group to the east. The sill is cut by a network of shear zones and faults, some of which host the bulk of known gold mineralization at the Dogpaw deposit. Within the larger study area deformation is typically restricted to discrete zones, dividing the country rock into fault blocks with preserved igneous and sedimentary structures. Faults are also found along lithological contacts between the sill and hosting volcanics, creating localized variability in topographic relief. Additionally, a series of feldspar porphyry and feldspar-quartz porphyry dykes, interpreted as broadly syn-tectonic, cross-

cut known gold bearing shear zones at the Dogpaw deposit and occur in the map area along the trend of several major breaks of the Pipestone–Cameron fault zone.

3.3.1 The Kakagi Sill

The Dogpaw deposit is hosted in the upper gabbroic layer of a kilometer thick, layered, mafic to ultramafic sill of the Kakagi sills (Fig. 3.2 & 3.3). The Kakagi sills consists of five, well differentiated layered intrusions (Davies and Morin, 1976). Davis and Edwards (1982) suggested that the Kakagi sill complex may have originated during a time of contemporaneous felsic and mafic magmatism and that the sills were emplaced successively during the buildup of the Kakagi Lake Group volcanic pile. They are typically comprised of a basal pyroxenite/ultramafic layer followed by a gabbro layer and an upper layer of varying proportions of gabbro and gabbro pegmatite. In the study area the Kakagi sills provide some of the greatest topographic relief. The intrusion is well exposed from the south end of Dogpaw Lake to the north shores of Kakagi Lake. The gabbro layer of the sill, which hosts the Dogpaw deposit, is mostly equigranular and varies in texture from coarse to very coarse grained to pegmatitic (Fig. 3.4). Pegmatitic patches, up to several meters in width, occur locally in the upper layer and can constitute over half of a single exposure (Fig. 3.4, C to F). On average the gabbro contains approximately 35% plagioclase and 35% pyroxene minerals with varying proportions of quartz, magnetite and epidote. Both the gabbro and pegmatitic gabbro patches commonly exhibit radiating pyroxene and plagioclase crystals, and in the case of the pegmatite patches, minerals can be several centimeters in size (Fig. 3.4, Photo F).

To the east, the upper contact of the hosting intrusion is in contact with the lower-most formation of the Kakagi Lake Group. Mapping along the eastern margin of the intrusive contact

has provided new details on the relationship between this sill and the volcanics of the Kakagi Lake Group. These two units are separate by a distinct contact zone, referred to here as the Kakagi intrusive contact zone (KICZ). The KICZ is an approximately three-hundred-meter-wide, largely continuous zone that can be followed along the eastern margin, or upper contact, of the intrusion. The KICZ is internally complex, with discrete deformation zones running subparallel to its trend, and includes a network of sills and dykes followed by a metamorphic aureole that extends into the hosting pyroclastic volcanics of the Kakagi Lake Group. Field observations in the KICZ suggest the Kakagi sill intruded a relatively cooler volcanic package resulting in a gradational contact that extends approximately two to three hundred meters into the Kakagi Lake Group volcanics. Davis and Edwards (1982) describe a similar relationship found at the upper contact of the sills and hosting volcanics while mapping other sills of the Kakagi sill complex in the larger Kakagi Lake terrane. The basal layer of the hosting intrusion is in contact with the basalts of the Snake Bay volcanics to the west. In the study area, the contact between the basal ultramafic layer of the sill and the country rock is poorly exposed. There is a notable drop in topography along the suspected contact and it is likely that significant faulting occurred along the western margin of the sill during regional-scale folding and later phases of deformation related to the Pipestone-Cameron fault zone.

3.3.2 The Snake Bay Volcanics

The Snake Bay volcanics are one of two mafic metavolcanics packages of the Kakagi Lake terrane and are overlain by the Kakagi Lake Group (Fig. 3.1). In the map area exposures of the Snake Bay volcanics are chiefly comprised of massive and pillowed basalts. To the west of the hosting intrusion, flow structures are common, often pristinely preserved with abundant

pillow structures providing way-up indicators (Fig. 3.5; A, B). They are dark green to blue on fresh surfaces and pale bluish-green on weathered surfaces. Rarely, porphyritic variants and basaltic layers with plagioclase glomerocrysts in a melanocratic, fine-grained groundmass can be found (Fig. 3.5; C, E, F). Like all the supracrustal rocks in the study area, the metavolcanics have been folded, however, apart from the rarely observed fracture sets and stretched pillow forms found at some exposures, internally, the Snake Bay formation appear to be largely undisturbed.

3.3.3 The Kakagi Lake Group

The Kakagi Lake Group is an intermediate to felsic, dominantly pyroclastic volcanic package with minor metasedimentary units on the south-west side of the Pipestone-Cameron fault zone. Davies and Edwards (1982) described four formations that constitute the Kakagi Lake Group, based on grain size and texture, two of which are found within the Dogpaw-Flint Lake study area. Davis and Morin (1976) detailed the supracrustal rocks of the Kakagi Lake Group found in proximity to Cedartree Lake.

In the study area the deposit-hosting sill is in contact with the lower formation of the Kakagi Lake Group, an approximately 1.5-kilometer-thick layer of polymictic, tuff-breccia (Fig. 3.6). This tuff-breccia unit consists of angular fragments of varying size and lithology supported in a very fine-grained, tuffaceous groundmass. Fragment size can vary substantially, from bombs and blocks (> 64 mm) to individual mineral grains, with more than 50% of fragments by approximate total volume greater than 64mm in size. Fragment composition can vary from diorite to basaltic and texturally from phaneritic to aphanitic to porphyritic (Fig. 3.6 C & D). The lower formation is heterogenous and it is often challenging to follow any one rock unit along strike. Interbedded tuff beds of ash particle size are also rarely found. This lower formation has

been variably disturbed and recrystallized along the eastern margin of the Kakagi sill that hosts the Dogpaw deposit.

The lower formation of the Kakagi Lake Group is followed by an approximately 1-kilometer thick layer of bedded, lapilli-tuff and tuff within the study area (Fig. 3.7). Tuff and lapilli-tuff beds are largely homogenous in the study area relative to the lower formation. Rarely, folds can be found in some exposures (Fig. 3.7 C & D). For example, at one trenched exposure at the Dubenski deposit tuff layers are folded into a series of mesoscopic folds with wavelengths of several meters (Fig. 3.7 C). Davis and Morin (1976) also noted the presence of minor folds of a few feet in width found in the upper formation of the Kakagi Lake Group around the Cedartree Lake area.

3.3.4 Feldspar Porphyry and Quartz-Feldspar Porphyry Dykes

A series of syn-tectonic, feldspar-quartz porphyry and feldspar porphyry dykes are spatially associated with several gold occurrences in the Rowan-Kakagi greenstone belt (Secord 2011, Ball 2014, Drabble et al., 2014 & 2015). In the Dogpaw-Flint Lake map area they are commonly found along the trend of the Pipestone-Cameron fault zone and several correlative ‘splays’ of the regional-scale fault. At the Dogpaw deposit these porphyry dykes are either relatively massive and locally crosscut auriferous shear zones (Fig. 3.9) or, conversely, are orientated subparallel to shear zones and are themselves variably deformed and altered (Fig. 3.10). There has been no attempt to discriminate generations of dykes analytically and they are divided here based on igneous texture, mineralogy, and cross-cutting relationships (Fig. 2.8).

Two varieties of porphyritic dykes are found at surface at mechanically stripped exposures at the Dogpaw deposit: 1) feldspar porphyry dykes and rarer 2) feldspar-quartz porphyry dykes (Fig. 2.8; A, B). Both varieties typically have sharp planar contacts with the undisturbed country rock. Most of these dykes trend northwest, are a few meters wide and, in some cases, can be traced along strike for over one hundred meters. A thin, cm-scale, baked margin commonly extends into the country rock from both varieties (Fig. 3.8 C). At several outcrops, xenoliths of deformed wallrock can be found within the dykes (Fig. 3.8 D). Based on these observations, dykes at the Dogpaw deposit and those found in the large map area are likely related, however any genetic link should be addressed analytically.

3.4 Structural Geology

Three generations of structures, G1 to G3, were identified and distinguished based on cross-cutting relationships and style of deformation while bedrock mapping at a scale 1: 5 000 and 1: 20 000 in the Dogpaw-Flint Lake map area. However, only two of these generations, G2 and G3, are found locally at the Dogpaw deposit and were identified from detailed mapping at a scale of 1:100 and 1:50 of mechanical stripped exposures (Fig 3.2, Fig. 3.3). Second generation (G2) structures are a series of conjugate, mylonite shear zones apparently unique to the Dogpaw deposit property and exposed at trench #1 (T1), trench #3 (T3) and trench #4 (T4). These structures host the bulk of known exposed mineralization at the deposit, are crosscut by a series of porphyry dykes and are variably overprinted by a third generation (G3) of structures. G3 are a series of secondary brittle-ductile shear zones of the Pipestone-Cameron fault zone which offset and/or deforms all previous structures in the larger Dogpaw-Flint Lake map area (see Chapter 2). Locally at the deposit, G3 includes the Dalby Bay shear zone, a prominent deformation zone

exposed at trench #2 (T2) (Fig. 3.10). The Dalby Bay shear zone does not appear to host any significant gold mineralization and the series of porphyry dykes that crosscut G2 structures are strongly deformed within its boundaries. The Dalby Bay shear zone shares many structural characteristics of other suspected splays of the Pipestone-Cameron fault zone. The shear zone is interpreted to have developed during a distinct phase of deformation that overprinted all previous structures and may have fundamentally affected the original geometry of the Dogpaw gold deposit. Associated foliation and lineation for G2 and G3 are termed S2, L2 and S3, L3, respectively.

3.4.1 Second Generation (G_2) Structures; Conjugate Mylonite Shear Zones

G2 structures comprise a series of discrete, ductile-brittle, conjugate shear zones. They are defined by a well-developed, penetrative, mylonitic foliation (S2) and a stretching lineation (L2) readily identified at outcrop exposures and in hand sample. Observations from bedrock mapping at a scale of 1: 5000 suggests these structures are unique to the upper layer of the hosting Kakagi sill. G2 shear zones are least disturbed and best observed outside the margins of the Dalby Bay shear zone at T1 and T4 (Fig. 3.3). An interpreted G2 shear zone is overprinted by the Dalby Bay shear zone at T3.

G2 shear zones typically comprise two sets of discrete orientation, either indicating a sinistral sense of movement or a dextral sense of movement. Shear zones sets have a strong spatial relationship and intersect at a number of mechanically stripped exposure, for example at T1 (Fig. 3.9, inset A). At T1, the two sets intersect, have steeply plunging lineations and dipping foliation and are defined by identical structural elements, S2 and L2. Where the shear zone sets intersect the zone of deformation and alteration widens abruptly, and the internal structure is

complex. At T1 a southwest striking sinistral shear zone intersects with a relatively minor, west striking dextral shear zone. At the point of intersection, the mylonitic fabric of the sinistral shear zone is continuous along the margins of the zone of intersection, while the mylonitic fabric of the dextral shear zone is locally weakly disturbed and discontinuous (Fig. 3.9, inset A). This discrete overprinting of the dextral shear zone set by the sinistral shear zone suggests the latter was the longer-lived structure. Within the zone of intersection there is a notable increase in quartz-carbonate breccia veins, cm-scale en echelon quartz veins, and a myriad of planar quartz veins of varying orientation and cross-cutting relationships.

The inherent heterogeneity of the country rock is interpreted to have had a strong control on the width and length of G2 shear zones. G2 shear zones pinch and swell, wrapping around the more competent, gabbro pegmatite patches. This characteristic is shared by all mapped G2 shear zones at the Dogpaw deposit and suggests strain was preferentially accommodated in the relatively finer-grained gabbro component of the country rock.

The boundary between undeformed country rock and G2 shear zones is very sharp. It is marked by the abrupt development of a curviplanar, mylonitic foliation S2 along the shear zone margin and a sub-vertical lineation (Fig. 3.13; Photos B, C & D). S2 is termed mylonitic based on the presence of strongly aligned plagioclase porphyroclasts in a fine-grained matrix which constitutes over 50% of the rock. Closer to the ‘core’ of the shear zone the single foliation transitions into a well-developed S-C mylonitic foliation (Fig. 3.13 Photo D). S-planes are discontinuous, and their outlines can be traced as they arc into the orientation of continuous C-planes. The C-planes shares the same orientation as the trend of the shear zone boundary. The angular relationship between S-foliation and C-foliation and the angular relationship between the

shear zone boundaries provides an apparent shear sense for the different G2 conjugate shear zone sets.

G2 structures are also characterised by stretched feldspar porphyroclasts, L2, the long axis of which are strongly aligned parallel to and change orientation with S2 (Fig. 3.13 Photo B). At outcrop exposures L2 is best observed in the relatively coarser grained components of the shear zones, assumed to have originally been pegmatitic patches of the protolith. In hand sample L2 appears to be elongated singular grains of plagioclase but in thin sections, L2 are in fact aggregates of plagioclase minerals that have elongated pod like shapes. A comparison between massive wall rock and mylonite suggests L2 originated as individual plagioclase crystals and were subsequently rotated and recrystallised during deformation. In the massive country rock individual plagioclase grains can be several centimetres in length and were likely subsequently dynamically recrystallised within the shear zones. They are defined as stretching lineations based on their striking, elongated cigar-like form.

The spatial relationship between the two sets of shear zones, compatible kinematics of individual sets and identical structural elements indicate that G2 shear zones likely developed as contemporaneous, conjugate sets. G2 shear zones are discrete and detailed mapping suggests there has been negligible disturbance of their original geometry by subsequent phases of deformation. If these gold-bearing structures are in fact conjugate, the angular relationship between the two sets of shear zones could be used to approximate the apparent stress regime during deformation. In the case of the conjugate sets found at T1 the kinematics of the shear zones suggest that the bulk shortening direction bisects the obtuse angle and the bulk stretching direction bisects the acute angle between conjugate sets (Fig. 3.18 A & B). This would indicate a

bulk, northwest-southeast-directed shortening and east-northeast-west-southwest-directed stretching direction during D2. A similar geometry is shared by the conjugate set found at T4 (Fig. 3.18 C).

G2 shear zones are variably disturbed or reactivated by G3 structures. At T3 and T4 G2 conjugate shear zones of similar trends and structural elements to the set found at T1 are located near the interpreted margin of the Dalby Bay shear zone. Although speculative, the arcuate form of the early G2 sinistral shear zone found at T4 may be the result of the structure being "dragged" as a passive marker during a later phase of deformation. In the case of the shear zones found at T3, the northeast-southwest-trending sinistral G2 shear zone has been reactivated by a relatively narrow, east-west-trending brittle-ductile shear zone (Fig. 3.11). This later structure shares the structural elements of the larger Dalby Bay shear zone and is interpreted as a splay of the larger G3 structure.

3.4.2 Third Generation (G_3) Structures: the Dalby Bay Shear Zone

G3 structures are a set of prominent, brittle-ductile shear zones found in the larger Dogpaw-Flint Lake map area. These structures are characterized by a well-developed and distinct phyllitic to schistose foliation (S3A), rarer mylonitic foliation (S3B) and mineral striations (L3). Based on bedrock mapping at a scale of 1: 20,000 and 1: 5,000 in the Dogpaw-Flint Lake map area, these shear zones are correlated with the network of deformation zones that constitute the regional-scale Pipestone-Cameron fault zone (Fig. 2.2). At the Dogpaw deposit the Dalby Bay shear zone, a G3 structure, offsets the lithological contact between the Kakagi sill and Kakagi volcanics (Fig. 3.3). This structure is exposed at Trench #2 (T2) (Fig. 3.10) and is

interpreted to extend from the south end of Dogpaw Lake into the Kakagi Lake Group (Fig. 2.2 & 3.2).

The Dalby Bay shear zone is a prominent, dextral, brittle-ductile deformation zone. The shear zone strikes approximately north-west and dips 65° to the northeast (Fig. 3.16 D). Unlike G2 structures at the Dogpaw deposit, the Dalby Bay shear zone deforms and offsets all lithologies and pre-existing structures within and along its margins. It also offsets the contact between the hosting Kakagi sill and Kakagi Lake Group by an estimated apparent horizontal displacement of 60 meters. Relative to G2 structures, the Dalby Bay shear zones is a wider, approximately 500-meter-long, largely continuous deformation zone. Blocks of relatively undeformed wallrock are found within the shear zone with foliation wrapping around these relatively competent blocks creating local variations in the kinematic sense (Massive gabbro in Fig. 3.10 & Inset). The boundary between the shear zone and the wallrock is relatively less sharp than that for the G2 shear zones and there is a notable gradation in strain, best observed at the northern boundary of the shear zone at T2. Here a single foliation S transitions into a S-C fabric followed by a S-C-C' fabric, from the margin domain of the shear zone to its central domain (Figure 3.14 & 3.15).

In contrast to G2 shear zones found at the Dogpaw deposit, all lithologies are variably deformed within the Dalby Bay shear zone and there is a notable gradation in strain intensity across its width. This gradation in strain and the interpreted role of the textural heterogeneity of the hosting gabbro is best exemplified at several exposures at T2 (Fig. 3.14 C to F; Fig. 3.15 A, B). Here the relatively finer grained component of the gabbro has a well-developed S-C fabric while the coarser, pegmatitic portions of the gabbro have experienced minimal grain size

reductions and brittle offsets are present (Fig. 3.14 E). In the case of the feldspar porphyry dykes found at T2, there is a notable variation in deformation while following individual dykes from the margin of the Dalby Bay shear zone into the core. From the boundary of the shear zone deformation of the dykes is expressed with the moderate preferred alignment of plagioclase grains and rare foliation in hand sample (Fig. 3.14 A). Following the same dyke and moving into the marginal domain of the shear zone, plagioclase grain alignment becomes relatively strong and two measurable foliations, S- and C-surfaces develop (Fig. 3.14 Photo B). In the central domain of the shear zone, individual S- and C-surfaces are replaced by a composite fabric, referred to here as CS-surfaces (Fig. 3.15 Photos C to F). This composite CS foliation is offset by discontinuous planes that have an obtuse angular relationship to the shear zone boundary, labelled C'-surfaces. The angular relationship between S- and C-surfaces and the deflection of CS surfaces by C' all indicate a dextral sense of shear. Alteration and grain size reduction is intense in the central domain of the shear zone and it can be difficult to discern the original protolith. Rotated, sulfide-rich quartz veins are rarely found within the Dalby Bay shear zone, some of which are auriferous. This gradation in strain intensity, progressive fabric development and the timing relationship of porphyritic dykes to the structure is unique to the Dalby Bay shear zone at the Dogpaw deposit but is a common feature of the shear zone network that constitutes the Pipestone-Cameron fault zone. These observations are distinctly different from those for G2 structures, further helping to distinguish the two different generations of structures.

The offset of the lithological contact between the intrusion and metavolcanics and angular relationship between S/C and CS/C' foliation within the Dalby Bay shear zone all indicate dextral shearing (Fig. 3.18 D). Mineral lineations are moderate to shallowly plunging (~

40°), plunging on average to the east south-east. This coupled with a right lateral strike-slip component indicate an overall southwest-side-up sense of movement. CS-C' fabric typically develops in deformation zone where shear strain is high. While the C-surface has an orientation parallel to the shear zone boundary the angle between S and C surfaces decreases to the point that two discernable foliations are replaced by a composite foliation, CS. Following a high degree of accumulated shear strain a third surface can develop, referred to as C'. C' surfaces are discontinuous and are orientated at an oblique angle to the shear zone boundary. The preservation of these structural elements, a visible gradation in strain and offset of lithological contacts suggests that the Dalby Bay shear zone may be a long-lived structure relative to G2 shear zones and records a distinct phase of deformation.

As previously noted, several porphyry dykes are found within the Dalby Bay shear zone. These dykes share many characteristics to those spatially associated with G2 structures. However, in the case of the Dalby Bay shear zone, field observations suggest an early- to syn-tectonic timing of emplacement for the dykes relative to the structure There is a notable gradation in shear fabric development imparted on the dykes relative to their position in the Dalby Bay shear zone, typically transitioning from relatively massive at the boundary to strongly deformed and altered in the central domain. This syn-tectonic timing of emplacement is best exemplified at trench #2 (Fig. 3.10 inset and Fig. 3.15). Here an apparently massive feldspar porphyry dyke is in contact with deformed gabbro with a well-developed S3 mylonitic fabric (Fig. 3.15 B). However, less than a meter away from this contact there is a strong preferential alignment of plagioclase grains in the porphyry dyke followed by the development of a S-C fabric (Fig 3.15 C). This is a common observation of all the mapped feldspar porphyry dykes

found within the Dalby Bay shear zone. Where G2 structures are observed and not overprinted by G3 structures, feldspar porphyry dykes are massive, have no apparent tectonic fabric and crosscut both G2 shear zones and mineralized zones (Fig. 3.9). This not only suggests that the porphyry dykes are syn-tectonic to G3 structures, an observation shared at other suspected G3 structures in the larger map area, but further supports that the Dalby Bay shear zones is related to a later phase of deformation distinct from the conjugate G2 shear zones.

3.5 Gold Mineralization

This section includes information on the gold mineralization and alteration at the Dogpaw deposit following detailed mapping and sampling of five historic, mechanically stripped exposures (Fig. 3.2 & 3.3). Gold mineralization is exposed at surface at several locations at the Dogpaw deposit and consists of a network of veins and vein breccia material of similar structural control and timing. The bulk of identified gold mineralization is hosted in G2 conjugate shear zones which have been variably deformed by the G3, Dalby Bay shear zone. A total 47 Au assay channel samples were taken to delineate gold bearing veins and validate historic information at the deposit (Table B.1). Distinguishing between zones of alteration, mineralization and relative undisturbed wallrock was aided by the intense yet shallow weathering of mechanically stripped outcrops since their original exposure by the previous claim holders.

Field observations suggest a syn-tectonic timing and strong structural control on the localization of gold mineralization at the Dogpaw deposit. The highest returned gold grades were from Au assay channel samples collected from intervals of quartz-carbonate vein breccia and sheeted quartz-carbonate veins, here termed V1 and V2 respectively, that are strictly hosted in G2 conjugate shear zones. These vein sets are both found and best exposed at T1. V1, V2 and the

proximal, strongly altered and mineralized material close to these veins, form easily identified auriferous zones (suspected mineralization in Figs 3.9 to 3.12). They are consistently shouldered by a relatively narrow zone of intense chloritization and mylonitic fabric, S2 of G2 shear zones. Gold barren, feldspar-quartz and feldspar porphyry dykes either crosscut or are spatially associated with the G2 gold-hosting structures. These intrusions have a syn- to late-tectonic relationship with the G3 Dalby Bay shear zone which bisects the deposit and are used to help constrain the timing of deformation and gold mineralization. The relative lack of gold-bearing veins and characteristic alteration in the G3 Dalby Bay shear zone suggests the structure largely post-dates gold mineralization at the deposit.

3.5.1 Macroscopic Structural Controls and Timing Constraints

The bulk of identified and accessible gold mineralization at surface at the Dogpaw deposit is found at Trench #1 (T1) and Trench #4 (T4). Here appreciable gold values were returned from samples collected from zones of intense alteration and quartz-carbonate veining (Table B.1) (Fig. 3.16 C). These zones are shouldered by a zone of relatively moderate alteration and mylonitic fabric, S2 of G2. A waste pile and several boulders of ore of altered and brecciated rock can be found at the Dogpaw deposit, the product of a 500-ton bulk sample taken in 1996 (Ball, 2014). A channel sample from one of these boulders returned 3.591 ppm Au (Table B.1; 16AKJCS036) near Trench #3 (T3).

3.5.2 Gold Bearing Vein System

At least three distinct vein sets are found at the Dogpaw deposit. Vein sets are discriminated here based on minerology, style and cross-cutting relationships. This section summarizes field observations from detailed mapping and is complimented by targeted Au

channel assay sampling. All samples and field descriptions are from five mechanically stripped exposures at the Dogpaw deposit (Fig. 3.2). It should be noted that this section does not provide an exhaustive description of the vein network found at the Dogpaw deposit. There are other distinct vein sets however many of these veins appear brittle in nature and their field relationships suggest they likely post-date the gold hosting structures and, therefore likely mineralization. Distinct vein sets discussed here are termed V1, V2, and V3.

3.5.2.1 V1, Shear-zone controlled, Au-quartz-carbonate breccia veins

V1 veins are a set of gold bearing, breccia veins that are enveloped by, and strictly hosted in, G2 mylonitic shear zones. Texturally, they are comprised of angular fragments of coarse grained to pegmatitic gabbro supported by a network of quartz-carbonate veins, V1 (Fig. 3.17 A & B). In hand sample, breccia fragments consist of strongly altered but undeformed segments of the surrounding wallrock. The preservations of igneous textures and coarse to pegmatitic grain size of the fragments suggests that these fragments experienced negligible deformation during alteration. These veins are best observed at the intersect of the conjugate shear zones found at T1 and T4 and several boulders at the 'Dogpaw pit' at T3. At T1 they are cut by a series of sheeted veins, V2, which also run parallel to the trend of the hosting shear zones. A bulk sample for U-Pb LA-ICP-MS analysis of zircon, 17AKJMS457, was taken from a V1 vein at T1.

3.5.2.2 V2, Shear-zone controlled, Au-quartz-carbonate sheeted veins

V2 veins are a series of sheeted quartz-carbonate veins that crosscut and divide V1 veins into layers (Fig. 3.17 C and D). They are well spaced, steeply dipping, and trend parallel to boundary of their hosting structure. V2 veins can vary in thickness from the 1cm to 20cms, are light yellow to light red on weathered surface and there is a distinct drop in magnetic strength

across their width. Au assay samples strictly taken from the thickest segments of these veins returned notably higher Au values than the surrounding altered and deformed rock (Fig. 3.17 D). As with V1, V2 veins are enveloped by a zone of intense alteration and mylonitic foliation (S2) and do no extend into the wallrock. V2 veins postdate V1 veins based on their sharp planar contacts. Both V1 and V2 veins are strictly found within G2 shear zones.

3.5.2.3 V3, Shear zone hosted, Au-quartz-carbonate veins

Although minor and rare, a set of gold bearing veins are hosted in the G3 Dalby Bay shear zone at T2. V3 veins are typically buckled, discontinuous and steeply dipping veins, 30-40 cm long and 5-15 cm wide (Fig. 3.17 E). A few of these veins have been rotated, likely contemporaneously with deformation that developed the pervasive S-C-C' fabric as their sense of rotation is compatible. They are interpreted as either V1 or V2 veins that originated in earlier G2 structures which were subsequently either fully entrained or variably transposed into the G3 Dalby Bay shear zone.

3.6 Geochronology:

To better constrain the timing of gold mineralization and deformation at the Dogpaw deposit four bulk samples were collected for U-Pb zircon dating by LA-ICP-MS. At the deposit a series of feldspar porphyry and feldspar-quartz porphyry dykes either sharply crosscut known gold-hosting G2 structures and are relatively massive or are deformed within the later G3 Dalby Bay shear zone. Two samples of these dykes (17AKJMS431A and 433A) were collected from T1 and T4, respectively. A bulk sample at T4 of the hosting country rock (16AKJISA602A) and a bulk sample of the ore from a V1 vein (17AKJMS457) at T1 was collected. The location of these samples is indicated on Figure 3.3 and on the respective figures of each trench.

3.6.1 Analytical Methods:

To reduce the risk of contamination, efforts were taken in the field to collect bulk samples from the least fractured, veined and altered exposures of the interested lithology. Each bulk sample was crushed, and zircons separated at the Hebei Regional Geological Survey laboratory in Langfang, Hebei Province, China. Each bulk sample returned over two hundred zircon grains. To avoid highly fractured grains a representative set of zircons were hand-picked using a reflecting microscope, at least one hundred for each sample, at the University of Waterloo. Zircons were then mounted in epoxy and polished to expose a cross section of the grains and cathodoluminescence (CL) images were taken at the Hebei Regional Geological Survey laboratory (Fig. 3.22).

U-Pb analyses of zircons from five samples were performed using LA-ICP-MS (Laser Ablation Inductively Coupled Plasma Mass Spectrometry) at the Metal Isotope Geochemistry Laboratory, University of Waterloo. An Analyte G2 laser system with a HelEx two-volume sample cell was coupled to an Agilent 8800 quadrupole ICP-MS. Isotopes measured include 206Pb, 207Pb, 238U, 232Th and 88Sr (10ms integration times). Zircons were ablated with a laser spot diameter of ~25 um, a fluence of 4 J/cm^2 (measured at sample surface), and a frequency of 5 Hz. Zircons were ablated for 30s (after a 30s gas background was collected) and the aerosol was carried to the torch using ~1 L/min He with an additional ~1 L/min Ar added as a make-up gas in a mixing bulb. Zircon DD85-17 was used to correct for instrumental mass fractionation (3002 ± 2 Ma; Tomlinson et al., 2003) and was analyzed every 5-7 unknowns. Secondary reference materials were Archean zircon DD91-1 (2682.4 ± 1 Ma; Davis 2002) and Proterozoic zircon reference material 91500 (1065 Ma; Wiedenbeck et al., 1995); these were

monitored to assess accuracy and propagate analytical uncertainty. Data were reduced using the Iolite v 3.6 (Paton et al., 2011) and the U-Pb Geochronology4 data reduction scheme. No down hole fractionation correction was applied. Secondary reference material DD91-1 yielded a $^{207}Pb/^{206}Pb$ age of 2678 ± 3 (MSWD = 1.7, n = 29), which is slightly below accepted value; zircon 91500 yielded a weighted mean $^{207}Pb/^{206}Pb$ age of 1061 ± 8 Ma (MSWD = 2.1, n = 12), which is within uncertainty of the accepted values. Weighted mean $^{207}Pb/^{206}Pb$ ages are reported with 95% confidence limits that include incorporation, in quadrature, of the uncertainty in the secondary reference Archean zircon. Select analysis were rejected if they returned highly discordant ages or ages that were significantly different from the main group used to calculate a weighted mean age. Rejected analysis are included in the respective tables of each sample. Results are presented in Table A.5 and A.6. For data from all three samples, Isoplot v. 4.15 (Ludwig 2008) was used to generate concordia plots and calculate weighted mean $^{207}Pb/^{206}Pb$ ages.

3.6.2 Pb-Pb Results:

The reported results of this analysis use $^{207}Pb/^{206}Pb$ ratios, avoiding the complication of U-Pb fractionation during ablation and low U isotope concentrations in Archean age rocks. Analytical data are given in Tables A.1 to A.4. Representative photos of the zircons analyzed are given in Figure 3.22. Concordia and weight mean plots are presented in Figure 3.23 and Figure 3.24. Weighted mean $^{207}Pb/^{206}Pb$ ages from this study and U-Pb ages from previous workers in the Rowan-Kakagi greenstone belt are summarized in Figure 3.25.

3.6.2.1 Gabbro Pegmatite, sample 16AKISIA602

Sample 16AKJISIA602 [NAD 83 Zone 15; 436589E, 5464869N] was collected from a pegmatitic 'patch' of the gabbro commonly found at the Dogpaw deposit at T3 (Fig. 3.4). These pegmatitic patches, up to several meters in width, occur locally in the upper layer of the Kakagi sill.

129 zircons were mounted from sample 16AKISIA602. Grains are subeuhedral to euhedral and have either oscillatory or planar zoning. No clear core and rim structures were observed. 28 spot analyses were conducted. A cluster of 24 spots yielded a weight mean $^{207}Pb/^{206}Pb$ age of 2716.6 ± 2.6 (n=24/28; MSWD = 1.7) (Fig. 3.24).

3.6.2.2 2) Feldspar Porphyry Dykes (samples 17AKJMS431A, 17AKJMS433A)

Samples 431A [NAD 83 Zone 15; 436417E, 5464812N] and 433A [NAD 83 Zone 15; 436589E, 5464919N] were collected from dykes that crosscuts both the G2 shear zones and the identified mineralization at T1 (Fig. 3.9) and T4 (Fig. 3.12), respectively. The dykes are massive, relatively unaltered and are unmineralized. The morphology of zircons collected from these samples appear identical (Fig. 3.22 A and B) and consists of oscillatory zoning, indicative of igneous origin. No clear core and rim structure were observed however, as a precaution, spots were divided between apparent cores, referred to here as the 'interior' of the grains, and rims.

79 zircons were mounted from sample 431A. 28 spot analysis were conducted: 16 from rims and 12 from the interior of the grains. The analysis returned a weighted mean $^{207}Pb/^{206}Pb$ age of 2694.1 ± 2.4 (n=25/28; MSWD = 1.3)

36 zircons were mounted from sample 433A. Oscillatory zoning was observed in all analyzed grains; however, the apparent thickness of this zoning was less than 10μm, below the

spot size of 25µm of analysis. 30 spot analysis were done: 1 from the rim and 29 from the interior of grains. The analysis returned a weighted mean $^{207}Pb/^{206}Pb$ age of 2695.9 ± 2.8 (n=29/30; MSWD = 1.8) for the sample.

3.6.2.3 3) Bulk Ore Sample (17AKJMS457)

Following targeted assay sampling in 2016, several zones of appreciable gold mineralization were identified (Fig 2.17). Sample 457A [NAD 83 Zone 15; 436403E, 5464793N] is a bulk sample of ore hosted in the G2 conjugate shear zones from the Dogpaw deposit exposed at trench #1 (Fig. 3.9 inset B). The bulk sample consisted of strongly and pervasively silicified, quartz-carbonate vein breccia and approximately 20 percent pyrite.

89 zircons were mounted from sample 457A. Grains either display oscillatory zoning or planar zoning, and crystal form varies from anhedral to euhedral. 30 spot analysis were done: 1 from a rim and 29 from the interior of grains. A cluster of 23 spots yielded a weighted mean $^{207}Pb/^{206}Pb$ age of 2717 ± 6.2 (n=23/25; MSWD = 7.7).

3.6.3 Discussion of Results:

The results from the U-Pb LA-ICP-MS analysis of samples taken at the Dogpaw deposit are summarized in Figure 3.25. The results of this analysis are also plotted against other U/Pb ages reported by previous workers in the Rowan-Kakagi greenstone belt.

Samples 17AKJMS431A and 17AKJMS433A, collected from two separate feldspar-porphyry dykes on either side of the Dalby Bay shear zone and returned similar $^{207}Pb/^{206}Pb$ ages, 2694.1 ± 2.4 (n=25/28; MSWD = 1.3) and 2695.9 ± 2.8 (n=29/30; MSWD = 1.8), respectively. These comparable ages and zircon morphology suggest the two sampled dykes are related to the

same swarm. The $^{207}Pb/^{206}Pb$ ages for these samples are also comparable to the reported U/Pb ages for other late-tectonic intrusions in the Rowan-Kakagi greenstone belt (Fig. 3.25). The dykes cross-cut mineralized structures at the Dogpaw deposit and so the $^{207}Pb/^{206}Pb$ ages for these samples may provide a reasonable younger limit on the timing of mineralization at the Dogpaw deposit. The $^{207}Pb/^{206}Pb$ ages for these samples may also provide an approximate younger limit for the age of the G2, gold-hosting shear zones.

In the Dogpaw-Flint Lake map area feldspar- and felspar-quartz porphyry dykes are commonly found along mapped shear zones of the Pipestone-Cameron fault zone and at several gold occurrences in the Rowan-Kakagi greenstone belt. Porphyry dykes reported at other deposits have similar reported relative timings of emplacement to gold bearing structures as the dykes found at the Dogpaw deposit. Although speculative, these dykes found at other gold occurrences may be related and the $^{207}Pb/^{206}Pb$ ages from the Dogpaw deposit may help provide a constraint on the timing of mineralization at other deposits.

Sample 17AKJMS457 was a bulk sample taken from the ore and sample 16AKJISIA602 was collected from a massive portion of the hosting intrusion at the Dogpaw deposit. While the isotope data from the U/Pb analysis of zircons collected from the sample of the ore provided a $^{207}Pb/^{206}Pb$ age with a greater error than the sample of the hosting intrusion, the $^{207}Pb/^{206}Pb$ age fall within error of that for the hosting intrusion. This supports the interpretation from field observations that the protolith of the ore is the hosting intrusion and that zircons that were analyzed from the ore were likely from the hosting intrusion. The observation that data from the ore show a bigger spread and the age is not as precise is likely due to intensive alteration associated with mineralization.

Sample 16AKJISIA602 was collected from a pegmatitic section of the deposit-hosting Kakagi sill and yielded an emplacement age of 2716.6 + 2.6 Ma. A sample collected by Davis and Edwards (1986) from a pegmatitic section of another intrusion of the Kakagi sills, approximately 10 kilometers south of the Dogpaw deposit, yielded a U/Pb TIMS zircon age of 2724.8 +2.5/−2.3 Ma (Fig. 1.3). The base of the Kakagi sill at the Dogpaw deposit is in contact with the Snake Bay volcanics to the west and the upper most layer of the intrusion is in contact with the lower-most formation of the Kakagi Lake Group to the east, making it one of the lowermost sill of the Kakagi sills. Davis and Edwards (1982) interpreted their sample to have also been taken from one of the lower-most sill of the Kakagi sills. Their sample taken from the top of the Kakagi Lake Group volcanics, which yielded a date of 2711 +1.3/-1.2 Ma, along with the age of their sample from the sill provided an upper limit on the deposition of the lower part of the Kakagi Lake Group volcanics, over an interval of approximately 13.7 Myr. While the $^{207}Pb/^{206}Pb$ age of 2716.6 ± 2.6 Ma from sample 16AKJISIA602 from the Kakagi sill at the Dogpaw deposit is notably younger than the sill sampled by Davis and Edwards, the sample collected at the Dogpaw deposit is still in agreement with their interpretation that the Kakagi sills were emplaced during the build-up of the Kakagi Lake Group. However, the sill sampled by Davis and Edwards (1982) may have been taken from one of the many mafic to ultramafic intrusions that are interpreted to have been emplaced contemporaneously with the deposition of the Katimigamak Lake and Snake Bay volcanics, an earlier stage of volcanic activity in the Rowan-Kakagi greenstone belt. If the Kakagi sill sampled at the Dogpaw deposit is truly one of the lower-most sills then the results from sample 16AKJISIA602, along with the sample from

Davis and Edwards (1982) of the Kakagi Lake Group volcanics, may provide a new, minimum time interval for the deposition of the Kakagi Lake Group volcanics of approximately 6 Myr.

3.7 Discussion

3.7.1 Localization and Origin of Auriferous G_2 Shear Zones at the Dogpaw Deposit

Identified and suspected gold mineralization found at surface at the Dogpaw deposit is strictly hosted in several discrete shear zones. The observations presented in the previous sections suggest both a structural control on the localization of gold and a syn-kinematic introduction of gold bearing fluids. The ore-hosting structures are interpreted to have originated in response to the textural heterogeneity of the hosting intrusion during D2 with strain partitioned in the medium to coarse grained gabbro versus the gabbro pegmatitic patches. These structures may have originated as independent shear zones, intersecting during progressive deformation during D2 or originated as intersecting sets. During this same phase of deformation, both the relatively longer-lived structure of the sets and zone of intersection of the conjugate sets likely acted as a preferential conduit for gold bearing fluids. Brecciation of pegmatitic material entrained within these shear zones and rupture parallel to the apparent shear plane created dilational structures for gold bearing fluid, resulting in V1 quartz-carbonate breccia veins and quartz-carbonate sheeted V2 vein sets. The timing of both D2 and gold mineralization is constrained by the emplacement of a set of feldspar porphyry dykes that crosscut both ore and ore-hosting structures.

Shear zones are multi-scaled, generally tabular zones of varying geometry and mechanisms. They are the result of localized strain in response to local and far field stress

regimes. Where a shear zone will nucleate depends chiefly on the inherent heterogeneity of the volume of material being subjected to said stress regime. Heterogeneity is scale dependent, and is influenced by a number of variables, such as the simple competency contrast between two in-contact lithologies, pre-existing structures, either continuous or discontinuous, and microscopic variations in mineralogy and the response of those individual minerals to variations in pressure, temperature and stress. While it may be impossible to elucidate the true, full deformation history of a structure, from its nucleation to its final configuration, the documentation of critical field observations, such as cross-cutting relationships and structural elements, can narrow the potential steps that occurred.

At the Dogpaw deposit a set of discrete, conjugate mylonitic shear zones are interpreted to host the bulk of mapped gold mineralization. They are interpreted to have developed during a distinct phase of deformation, D2, predating the development of the Dalby Bay shear zone. These structures have common orientations and kinematics, and their original geometry was likely largely controlled by the primary textural heterogeneity of the country rock.

This heterogeneity of the country rock is revealed at the outcrop-scale in the upper layer of the hosting intrusion. Here, patches of gabbro pegmatite can constitute over half of the exposed bedrock (Fig. 3.4 C, D, E, F). The mineralogy between coarse grained gabbro and these pegmatitic patches is nearly identical and they differ, although dramatically, only in grain size. G2 shear zones wrap around the more competent pegmatitic patches and strain is localized in the relatively finer grained gabbro. These structures are commonly flanked by pegmatite pods and will pinch and swell dramatically. For example, at T1 the apparent width of a sinistral shear zone varies from as little as 5 meters to 25 meters along its length. At the point of intersection between

conjugate shear zone sets at T1 the shear zones are flanked by relatively finer grained gabbro and the zone of deformation and alteration widens abruptly. A similar relationship between shear zone geometry and gabbro pegmatite is found at T4. Figure 3.20 is provided to help illustrate the apparent role of this igneous textural heterogeneity on the origin of G2 shear zones and localization of auriferous zones at the Dogpaw deposit.

G2 shear zones are interpreted as conjugate sets. This is based on cross-cutting relationships found at their point of intersection, sympathetic kinematics, a shared sharp contrast between shear zone and country rock, and identical tectonic structural elements (S2, L2). Lamouroux et al. (1991) noted a number of key geometrical characteristics of conjugate ductile shear zones and their progressive development. While their work focused on exploring the angular relationship between sets as kinematic indicators, the authors also concluded that the zone of intersection of conjugate shear zones may both thicken and lengthen perpendicular to the direction of finite shortening as a conjugate set develops. In the case of the auriferous shear zones at the Dogpaw deposit, the zone of intersection of conjugate sets is consistently the widest segment of the G2 structures. During progressive deformation G2 shear zones may have widened and over time incorporated more of the country rock with the relatively more competent, pegmatitic segments of the country rock being entrained into the shear zone. These competent 'pods' would deform in a relatively brittle manner, fracturing and brecciating. This brecciation of the competent pods would provide local permeable points in the stressed country rock and a potential path for gold bearing fluids resulting in patches of V1 quartz-carbonate vein breccia supported in a mylonitized groundmass found at T1 and T4 (Fig. 3.20 F).

Following the observations and interpretation presented in the previous sections there are two potential scenarios to account for the structural geology at the Dogpaw deposit (Fig. 3.21). It should be noted that both scenarios are very similar and differ only based on the timing of nucleation of the Dalby Bay shear zone relative to earlier, gold-bearing structures. In either scenario the Dalby Bay shear zone is assumed to be a relatively long-lived structure.

In the first scenario these conjugate shear zones as a distinct generation of structures, G2, that developed during a separate phase of deformation, D2, from the G3 Dalby Bay shear zones. The distinction between G2 and G3 structures is based on the difference in style of tectonic fabric, cross-cutting relationship with the feldspar porphyry dykes, relative gold endowment and arcuate form of G2 shear zones in proximity to the Dalby Bay shear zone. In this scenario gold mineralization occurred contemporaneously with the development of the G2 conjugate, mylonite shear zone, followed by the emplacement of feldspar porphyry dykes. The G3 Dalby Bay shear zone is interpreted as a distinct, later structure during D3, variably deforming pre-existing structures and lithologies along its strike. In this scenario the emplacement of the feldspar porphyry dykes that crosscut G2 shear zones marks the transition between D2 and D3. Mineralization found within the Dalby Bay shear zone is attributed to previously existing mineralized structures being entrained within the shear zone during its development.

In the second scenario the conjugate shear zone network and southeast striking Dalby Bay shear zone to have developed during one overall progressive deformation event, $D2_A$ and $D2_B$. In this scenario the Dalby Bay shear zone would be the principle shear zones, with the relatively minor and discrete conjugate shear zone originating as synthetic and antithetic shear zone sets to the Dalby Bay shear zone. This is evident by the approximate north-south bulk

shortening shared by both generations of structures and compatible kinematics between the conjugate shear zones and the Dalby Bay shear zone. In this model the early structures would consist of one larger conjugate network during $D2_A$. As D2 progressed the conjugate sets at T1 and T4 along the margin of the Dalby Bay shear zone became passive structures at the end of $D2_A$. Activity along the Dalby Bay shear zone would have continued with the Dalby Bay shear zone variably overprinting other conjugate sets along its margins during $D2_B$. In this scenario the emplacement of the feldspar porphyry dykes would mark this transition between $D2_A$ and $D2_B$. This is supported by the relatively massive nature of feldspar porphyry dykes crosscutting earlier D2A structures that were no longer active during their emplacement, for example the dyke found at T1 (Fig. 3.9), versus those found within the Dalby Bay shear zone which have been variably deformed. Due to the crosscutting relationship of the feldspar porphyry dykes with gold bearing shear zones, gold mineralization is still constrained to an earlier point in the deformation history of the deposit, $D2_A$.

3.7.2 Genesis of the Dogpaw Gold Deposit

The bulk of identified gold mineralization at the Dogpaw deposit is associated with V1 and V2 veins. V1 veins are strictly hosted in G2 structures and are crosscut by relatively massive, gold barren, porphyry dykes. They are interpreted to have originated as relatively more competent fragments of the country rock that deformed in a brittle manner. Shear zone-parallel, sheeted V2 veins are interpreted as either shear veins or extensional veins that originated at a small angle to the shear plane. The G2 conjugate sets are interpreted to be overprinted or variably deformed along the trend of the Dalby Bay shear zone, for example at T3 and T4. The same set of feldspar porphyry dykes that crosscut G2 structures are variably deformed and

altered by the G3 Dalby Bay shear zone. Based on field observations at the deposit these dykes are interpreted to have been emplaced post gold mineralization and either prior or syn-tectonic to the G3 Dalby Bay shear zone. Apart from three minor gold bearing V3 veins, there were no identified auriferous veins at surface within the Dalby Bay shear zone. Therefore, this deposit-transecting shear zone is interpreted to have nucleated largely after gold mineralization at the Dogpaw deposit. Any gold bearing material found within the Dalby Bay shear zone is believed to have been entrained into the shear zone from pre-existing mineralized structures.

The V1 and V2 veins and proximal carbonate-ankerite-silica alteration represents zones of mappable gold enrichment at the Dogpaw deposit. Although individual mineral grains that constitute the breccia fragments are strongly altered, igneous textures are well preserved in the fragments and there is a notable complete lack of tectonic fabric. This lack of tectonic fabric in V1 breccia fragments is in contrast to the hosting G2 structures and well developed S2 fabric that surrounds auriferous zones. As previously noted, V1 veins are divided by sheeted quartz-carbonate V2 veins. These veins trend parallel to sub-parallel to the boundary of their hosting shear zones and are mostly continuous over several meters.

These observations can be explained by at least two genetic models for the origin of V1 and V2 veins and their hosting structures. The first is that the brecciation event that resulted in V1 veins occurred contemporaneously but late during the phase of deformation responsible for the hosting G2 structure and S2 fabric. V1 breccia veins may represent entrained, pegmatitic and/or competent fragments of the country rock that deformed in a relatively brittle manner, while the surrounding relatively less competent material deformed in a more ductile manner. Following brecciation, repeated failure along the shear zone may have generated the V2 sheeted

veins (Fig. 3.20). The second is that G2 shear zone may have been reactivated during a later phase of deformation, potentially during the development of the Dalby Bay shear zone during D3. Due to the lack of tectonic fabric, V1 breccia veins would still have originate during D2 but the sheeted, shear zone-parallel V2 veins may be a result of cyclic failure/reactivation of the then passive G2 shear zones in proximity to the active G3 Dalby Bay shear zone.

The model for the genesis of the Dogpaw gold deposit places emphasis on an early generation of structures, G2, based on observations made during mapping of trenched exposures at the deposit. In particular this model highlights the significance of competency contrasts inherent in the hosting intrusion suggesting this as the main control on both the localization of strain and development of dilational structures. The important role of competency contrast in both the partitioning of strain and its effect on local stress regimes has been recognized in many orogenic gold occurrences in Ontario. For example, major contacts between rocks of differing properties, such as those found at the Cameron Lake (*see* Melling 1989) and the Angle Hill gold deposit, have long been recognized as a major control for the foci of gold-bearing structures. The Dogpaw deposit differs from other occurrences in the Rowan-Kakagi in that it is the internal, primary structures of the hosting intrusion that is interpreted to have provided the contrast. Furthermore, the model for the deposit suggests that a single gold mineralization event occurred and is the result of the development of an early set of structures, G2. These structures are interpreted as early in the tectonic history of the Dogpaw-Flint Lake map area, in particular in contrast to the Pipestone-Cameron fault zone and its subsidiary faults (Fig. 2.2). G2 structures at the deposit are variably deformed by the Dalby Bay shear zone, interpreted in this model to be a subsidiary shear zone of the Pipestone-Cameron fault zone. The model highlights the role of this

later structure in modifying the geometry of G2 structures at the Dogpaw gold deposit. This timing relationship has been discussed at other gold occurrences in the Rowan-Kakagi greenstone belt. From the primary structures of the hosting intrusion to later modification of gold-bearing structures by a network of regional shear zones and faults, the model for the genesis of the Dogpaw gold deposit calls attention to the importance of studying and accounting for all structures, either pre, syn or post gold mineralization.

3.8 Conclusion

Several gold occurrences in the Rowan-Kakagi greenstone belt consist of auriferous quartz veins reported as either hosted in or spatially related to faults and shear zones. These deposits-hosting structures have received varying levels of study. They have been speculatively correlated to the regional-scale Pipestone-Cameron fault zone and therefore the previous model for their genesis assumes a genetic link to the regional fault. This is reflected in the number of documented and developed gold occurrences of the Rowan-Kakagi found along the trend of the Pipestone-Cameron fault zone where exploration efforts have clearly been focused. However, this research project has demonstrated that, at least at the Dogpaw deposit, earlier structures are the main host of gold mineralization. This concept is well rooted in previous work on Archean gold deposits in Ontario (see Colvine et al. 1984, 1988). In the Rowan-Kakagi greenstone belt, work by Melling (1989) on several gold occurrences suggested that the geometry of many ore bodies had been fundamentally disturbed or entirely overprinted by structures correlative to the Pipestone-Cameron fault zone. The result of this later overprinting is that these later structures host the bulk of mineralization although they may post-date the gold mineralizing event at the occurrences. Subsequently, these later structures, such as the Dalby Bay shear zone, Cameron

Lake shear zone or Flint Lake shear zone, have been the focus of study and exploration, while early structures outside of the shear zones may have been relatively overlooked.

This appears to be the case at the Dogpaw deposit. Here, gold is intricately associated with and hosted in a set of discrete, conjugate mylonite shear zones. Field observations suggest that the primary igneous textural anisotropy of the hosting gabbro resulted in the partitioning of strain into the relatively finer grained component of the country rock resulting in the localization of strain and thus the origin of the auriferous shear zones at the deposit. G2 shear zones differ markedly from the later G3 Dalby Bay shear zone which transects the deposit and variably alters the geometry of G2 gold-bearing shear zones. Field relationships documented at exposures at the deposit suggest these G2 gold-hosting structures pre-date the brittle-ductile G3 Dalby Bay shear zone, a structure correlative to the Pipestone-Cameron fault zone. The increase in apparent width of the mineralized zone at the intersection of G2 conjugate sets suggest gold mineralization is syn-kinematic with G2 shear zone. U/Pb zircon dating results from samples at the Dogpaw deposit has provide a constraint on the timing of gold. The timing of gold mineralization at the Dogpaw deposit is bracketed by the emplacement of the hosting Kakagi sill at 2716.6 ± 2.6 Ma, and the intrusion of the cross-cutting feldspar porphyry dykes at 2692 ± 2.4 Ma and 2695.9 ± 2.8 Ma. This also provides a potential timing constraint on a gold mineralization event in the Rowan-Kakagi greenstone belt, between 2717 to ~2696 Ma.

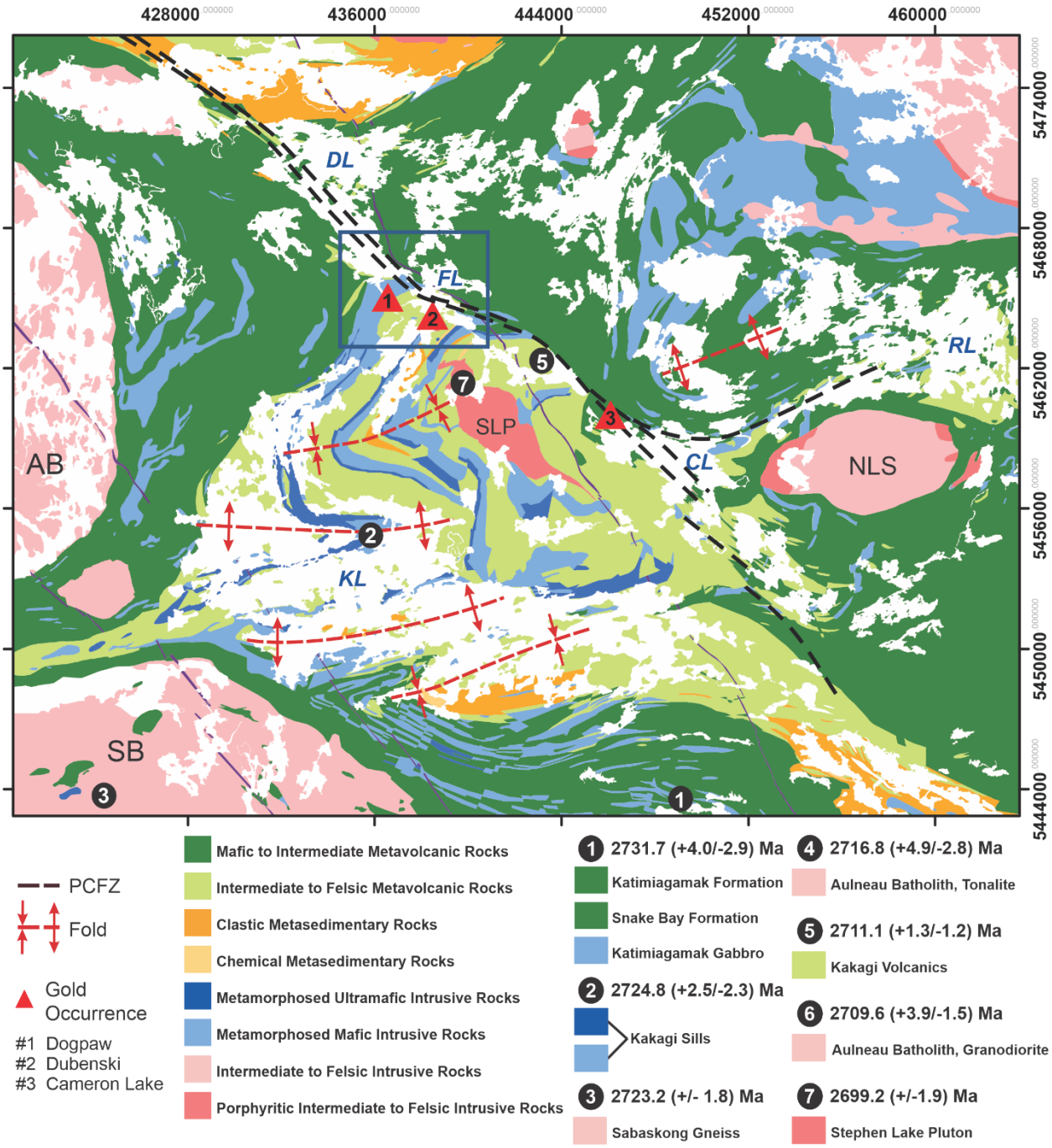

Figure 3.1: A simplified geological map of the Rowan-Kakagi greenstone belt (*modified from* Johns 2007). Sample locations from Davis and Edwards (1986) are numbered from 1-7 with sample locations 4 and 6 from the interior of the Aulneau batholith. Abbreviations: AB, Aulneau Batholith; AtB, Atikwa Batholith; CL, Cameron Lake; DL, Dogpaw Lake, FL, Flint Lake; NLS, Nolan Lake stock; KL, Kakagi Lake; RL, Rowan Lake; SB, Sabaskong Batholith; SLP, Stephen Lake pluton; Universal Transverse Mercator (UTM) coordinates are provided using North American Datum 1983 (NAD83) in Zone 15.

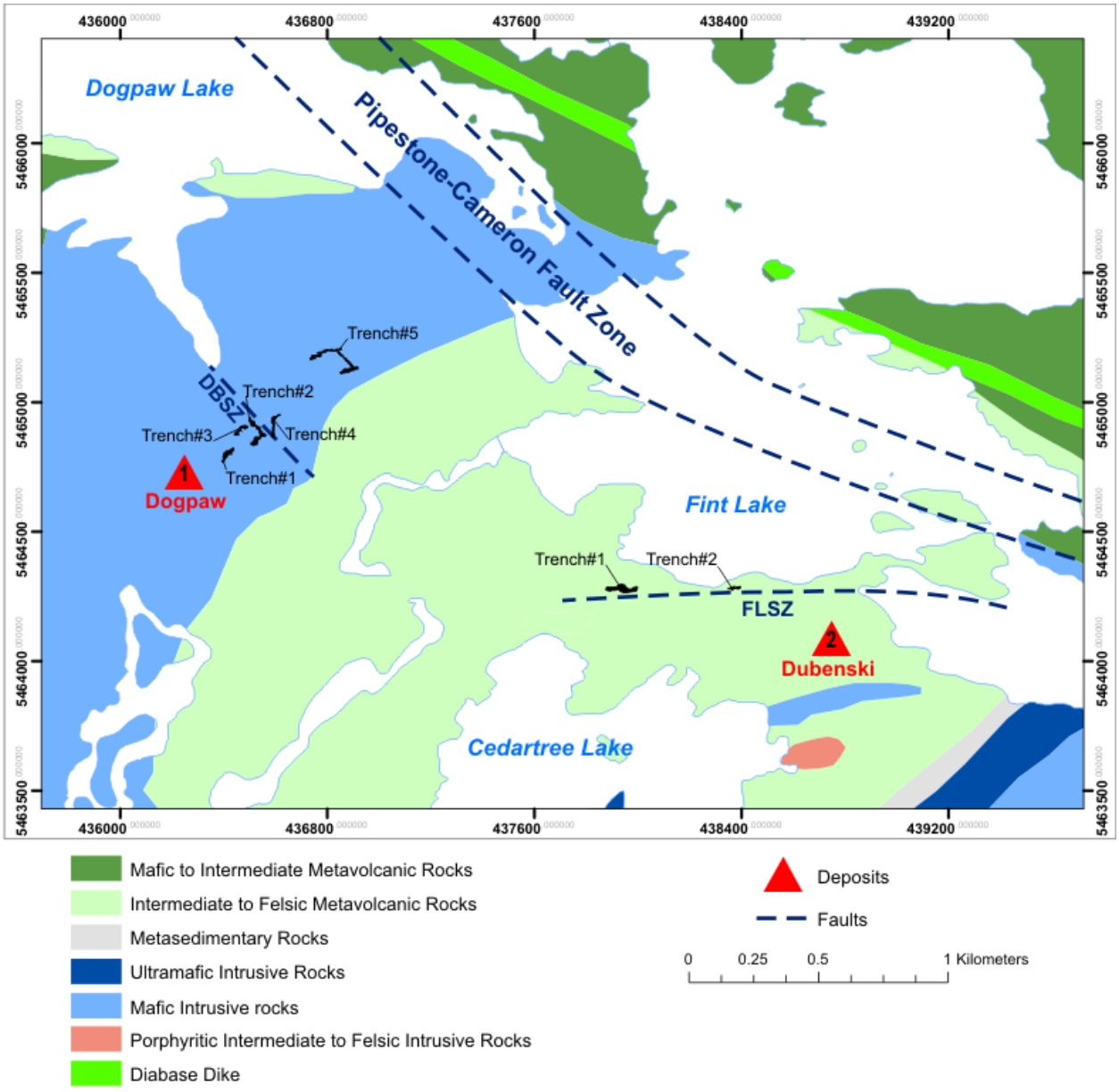

Figure 3.2: Geological map showing the location of the 1) Dogpaw deposit (red triangle number 1) and 2) Dubenski deposit (red triangle number 2) and mapped trenched exposures (*modified from* Johns 2007). The location of 5 trenches at the Dogpaw deposit and 2 trenches at the Dubenski deposit were mapped during the 2016 and 2017 field seasons and are shown. Abbreviations: DBSZ, Dalby Bay shear zone; FLSZ, Flint Lake shear zone. Universal Transverse Mercator (UTM) coordinates are provided using North American Datum 1983 (NAD83) in Zone 15.

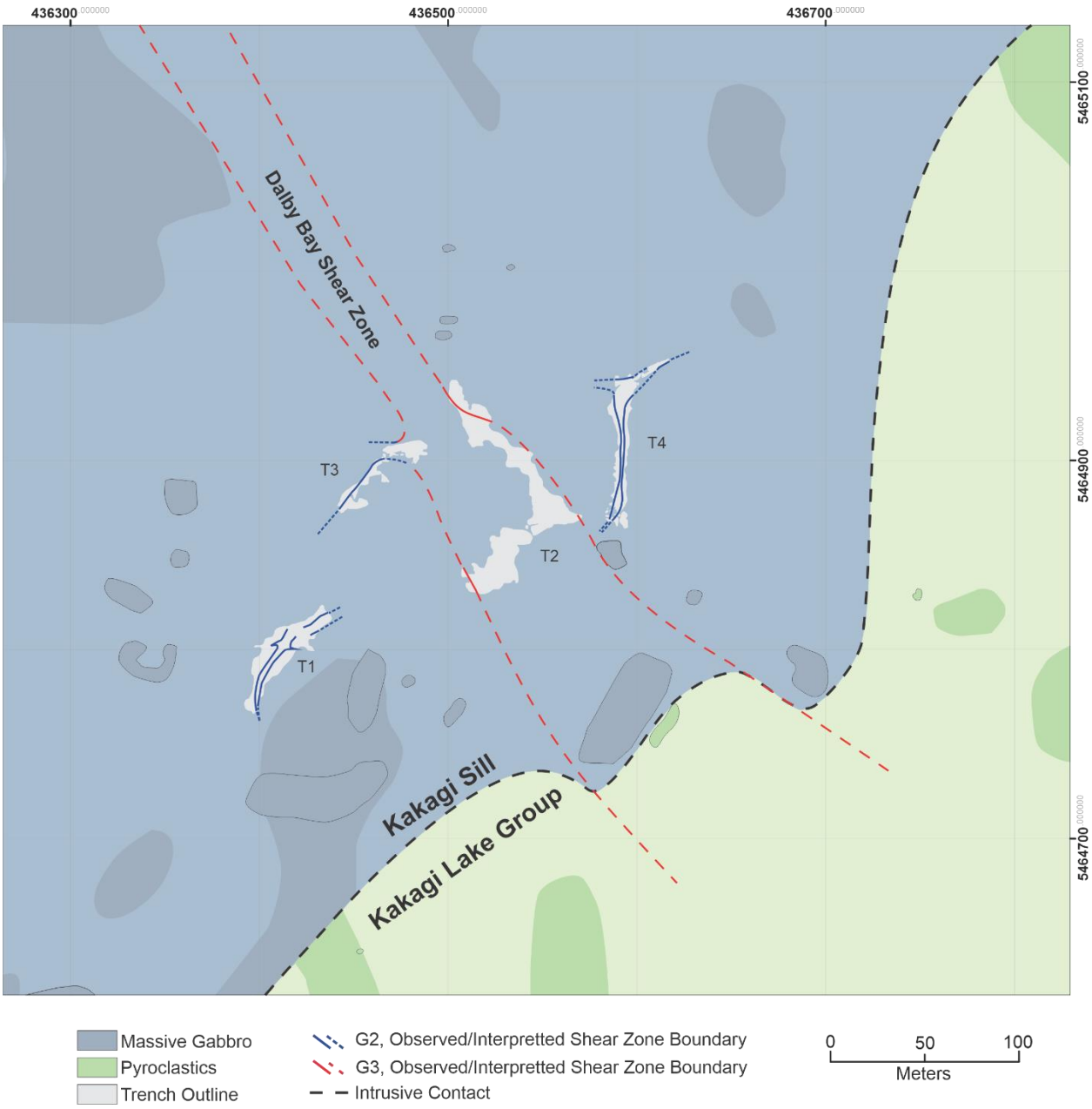

Figure 3.3: Geological map of the Dogpaw deposit. Exposures and contacts without outlines are compiled from Davies and Morin (1976) while those with outlines are exposures mapped during the 2016 and 2017 field season and shaded geology is inferred. The outlines of trenches 1 to 4 are shown in white and labelled. Observed shear zone boundaries of G2 and G3 structures are shown. An expression of the Dalby Bay shear zone was not found to the south-east of the map area and so it is illustrated to end at the lithological contact between the Kakagi sill and Kakagi Lake Group volcanics. Universal Transverse Mercator (UTM) coordinates are provided using North American Datum 1983 (NAD83) in Zone 15.

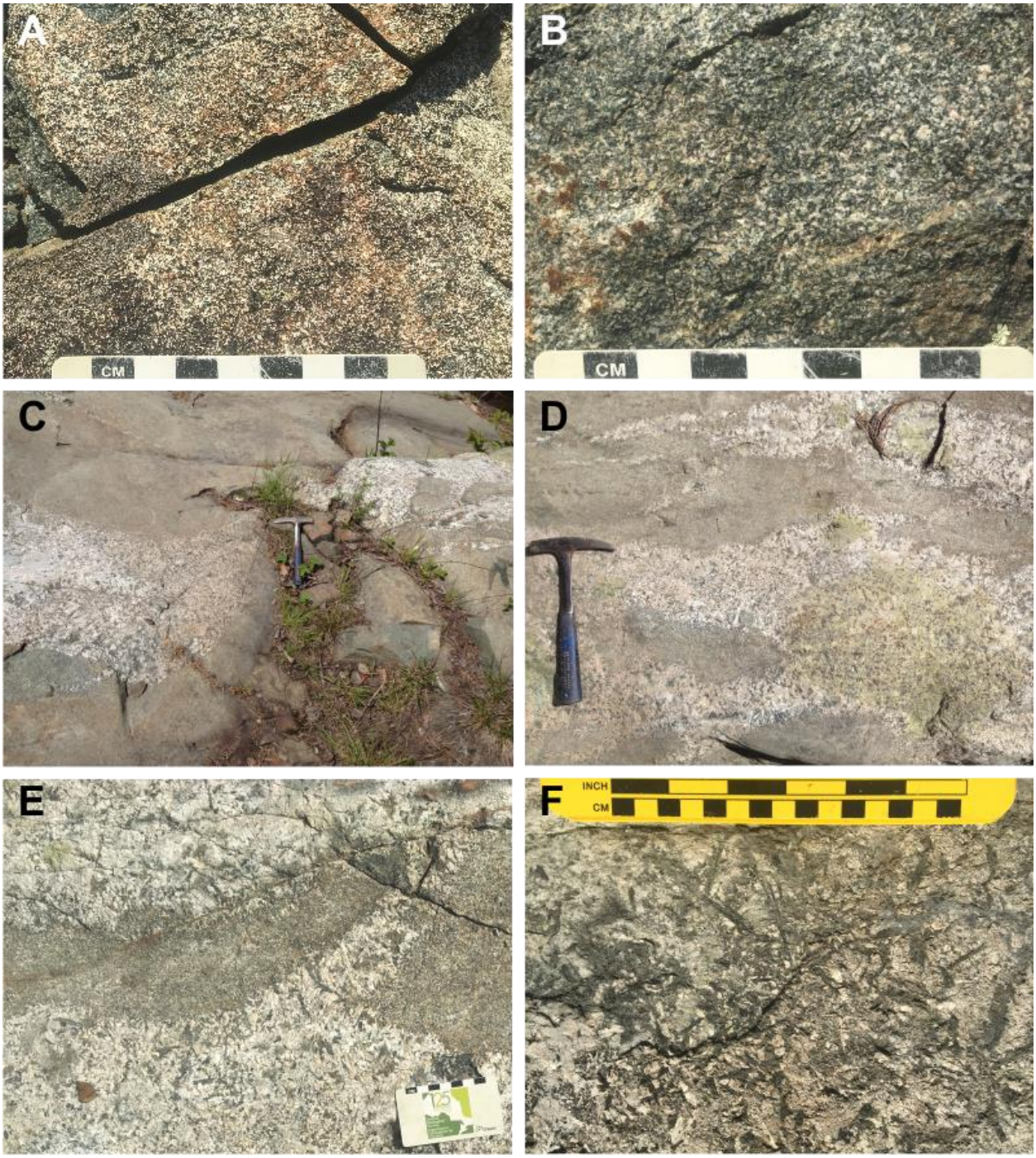

Figure 3.4: Outcrop photos from the Dogpaw deposit of the hosting country rock, the Kakagi sill (when available photo locations provided as UTM coordinates using NAD83 in Zone 15). A), B) Massive, coarse grained gabbro, weathered and fresh surface, respectively [436534] [5465002]. C), D), E), F) coarse grained gabbro with gabbro pegmatite patches [436593] [5464800]. Note that the proportion of plagioclase and pyroxene minerals of pegmatitic patches can vary depending on the exposure.

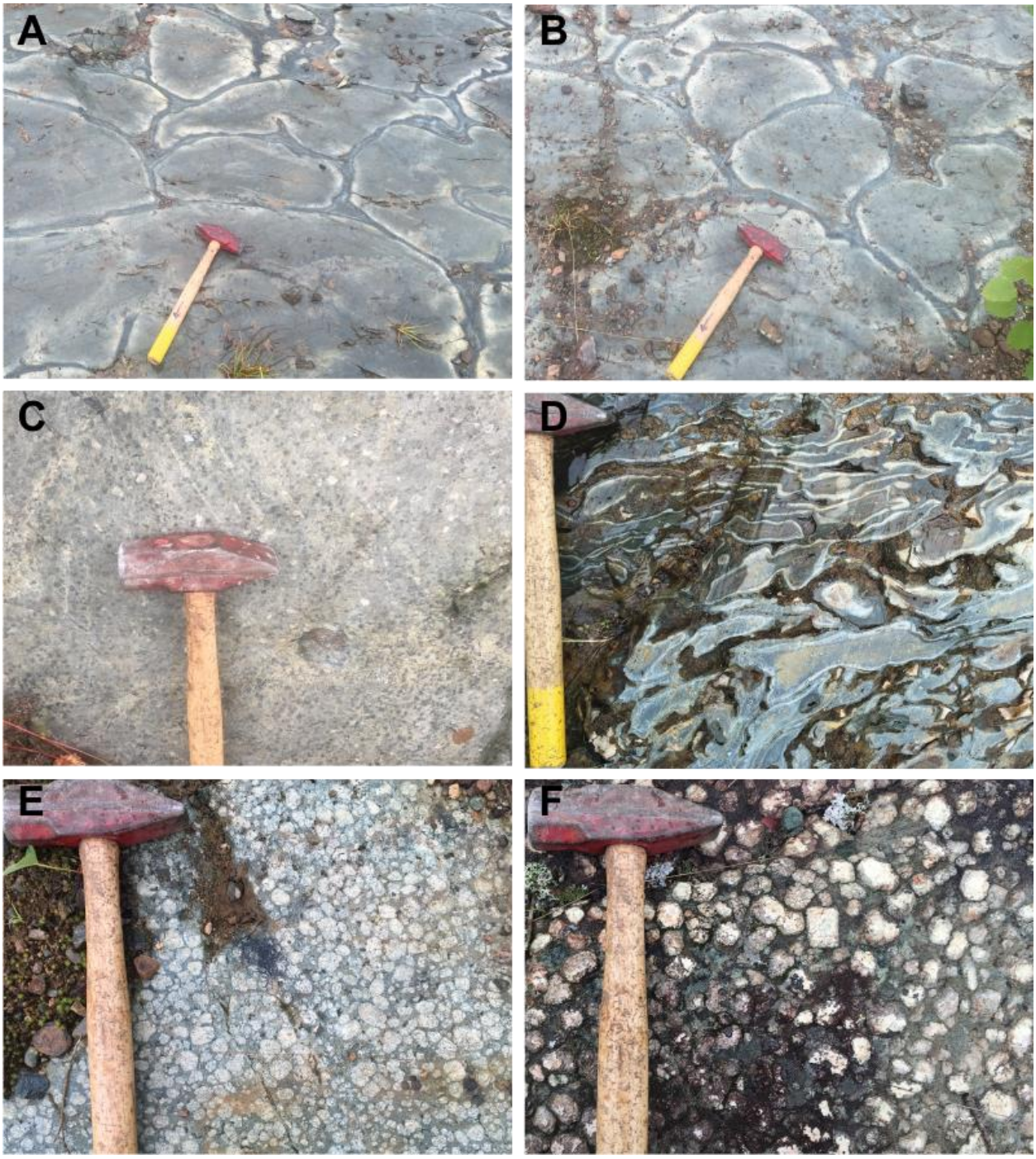

Figure 3.5: Outcrop photos from the Snake Bay formation, west of the Kakagi sill (when available photo locations provided as UTM coordinates using NAD83 in Zone 15). A), B) D) Basalt with flow structures, arrow on hammer is pointing north when displayed [431512] [5463610]. C), porphyritic basalt with phenocrysts of pyroxene in a fine-grained mafic groundmass. E), F) Basalt with glomerocrysts of plagioclase, relatively fresh and weathered surfaces respectively [431676] [5463263].

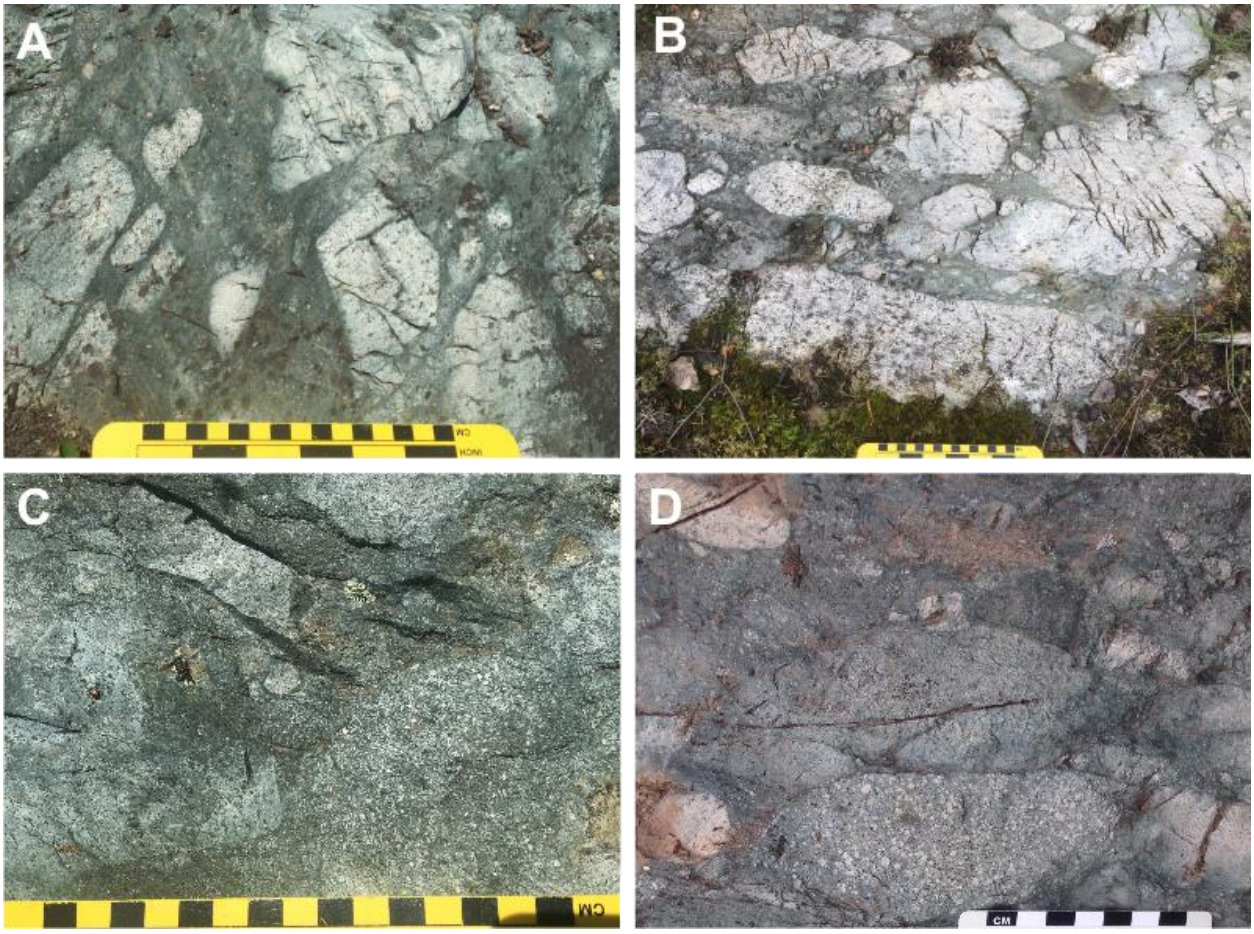

Figure 3.6: Outcrop photos of tuff-breccia from the lower formation of the Kakagi Lake Group east of the Kakagi sill (when available photo locations provided as UTM coordinates using NAD83 in Zone 15). A), B) Tuff-breccia with angular to sub-angular fragments supported by a fine-grained groundmass at fragments of varying size [436823] [5464581]. C), D) Fragments of varying lithology and texture, [436989] [5464869] and [436511] [5464250] respectively.

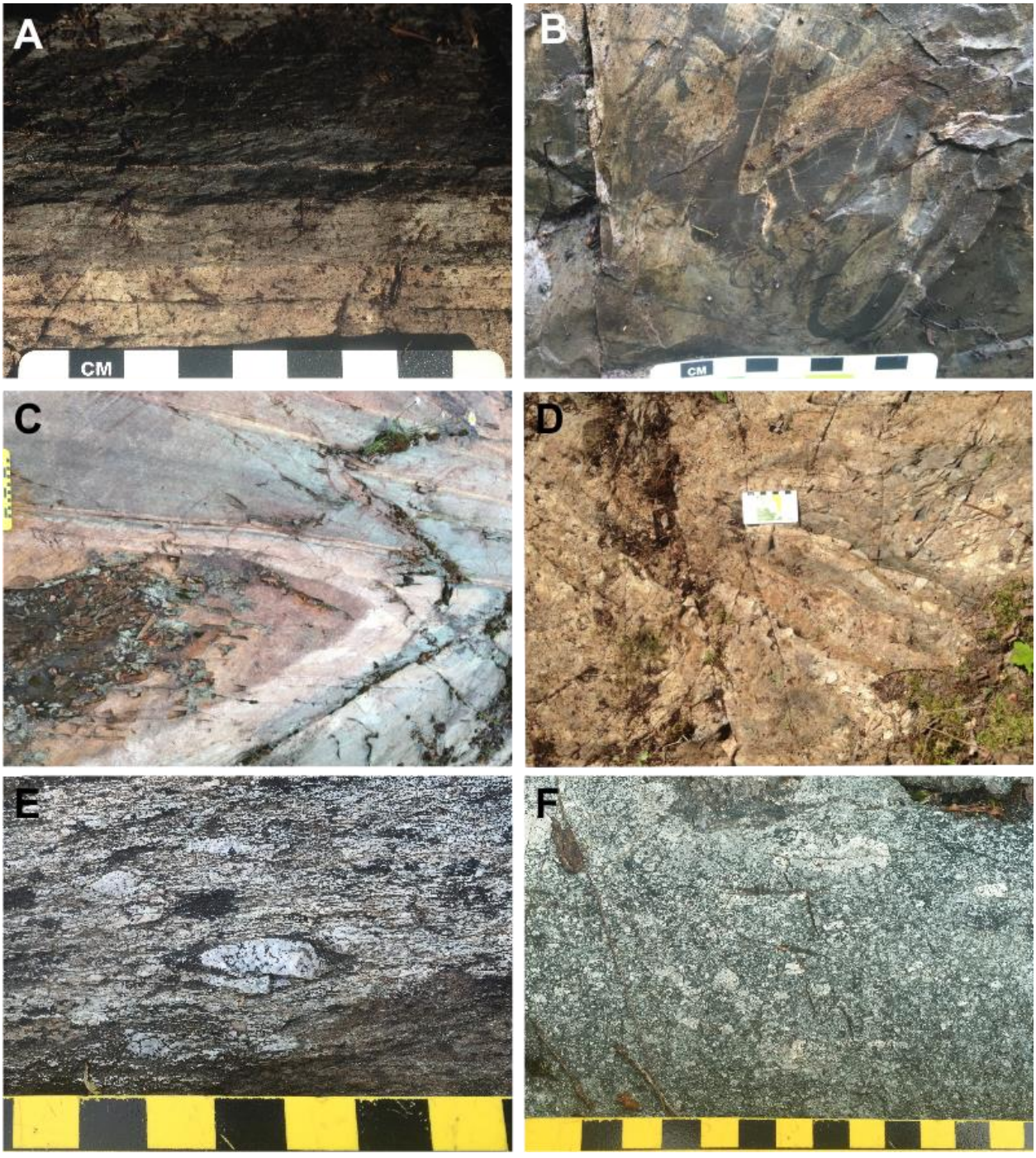

Figure 3.7: Outcrop photos of tuff and lapilli-tuff from the upper formation of the Kakagi Lake Group east of the Kakagi sill (when available photo locations provided as UTM coordinates using NAD83 in Zone 15). A) Tuff layers of apparent varying composition [438885] [5464016] B), Tuff layers with syn-depositional structures C), Macroscopic folds at the Dubenski gold deposit [437914] [5464280] D) Folded layers of tuff and tuff-breccia E), F) bedded lapilli-tuff [438413] [5463965] and [438881] [5464109] respectively. Scale is provided in centimeters unless labelled otherwise.

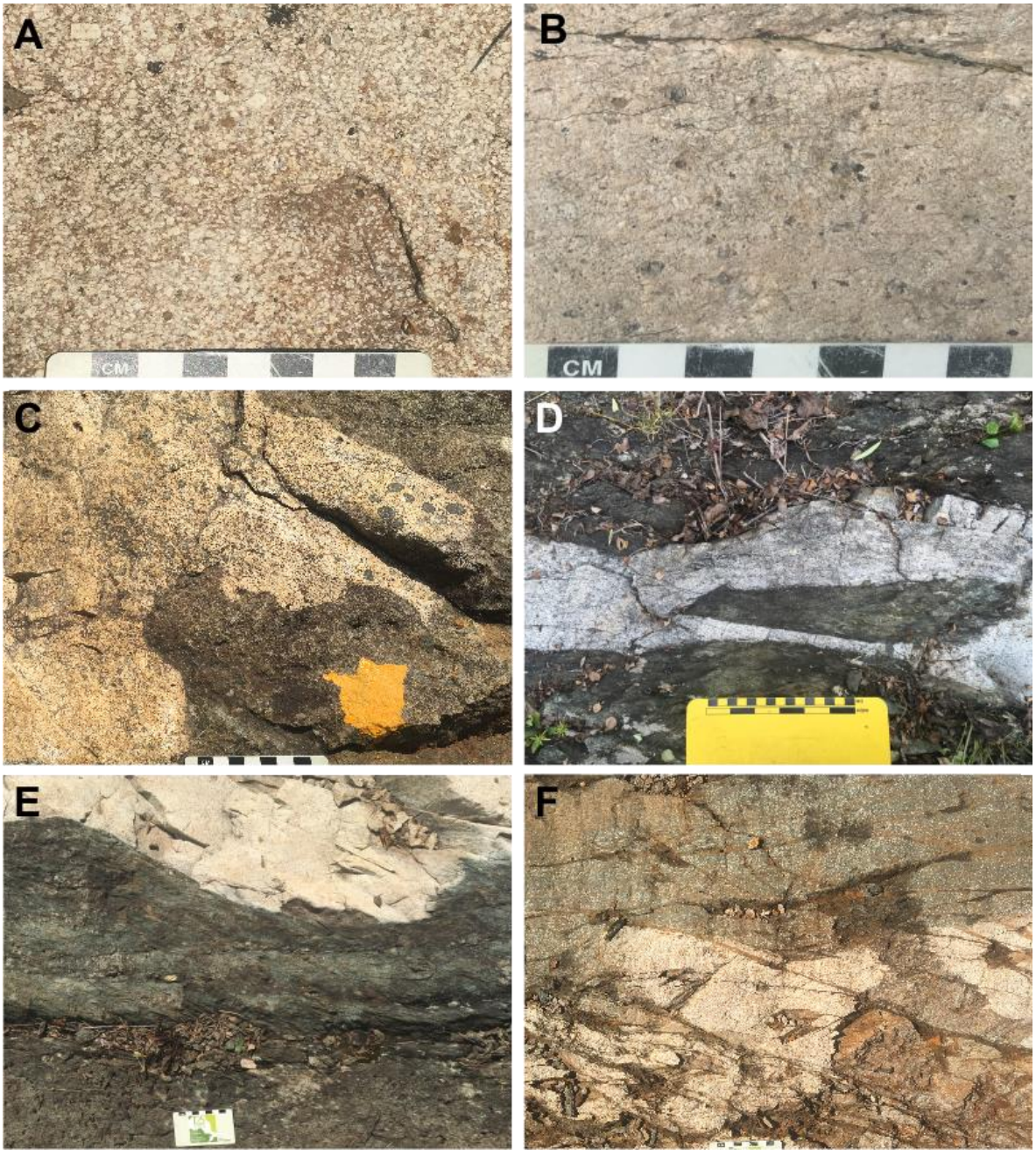

Figure 3.8: Outcrop photos from the Dogpaw deposit of porphyry dykes and intrusive contact relationships with the hosting country rock, the Kakagi sill (when available photo locations provided as UTM coordinates using NAD83 in Zone 15). A) Massive feldspar porphyry dyke [436512] [5464925] B) Massive feldspar-quartz porphyry dyke [436817] [5465201] C) Feldspar porphyry dyke in contact with coarse grained gabbro, a baked margin extends from the dyke into the gabbro [436424] [5464810]. D) Feldspar porphyry dyke with a xenolith of deformed gabbro [436603] [5464945]. E) Massive feldspar porphyry dyke in contact with deformed and altered gabbro [436543] [5464872]. F) Deformed and altered feldspar porphyry dyke and coarse-grained gabbro, note the offset of the contact between both units and alignment of plagioclase minerals in the gabbro [436508] [5464912]. Scale is provided in centimeters unless labelled otherwise.

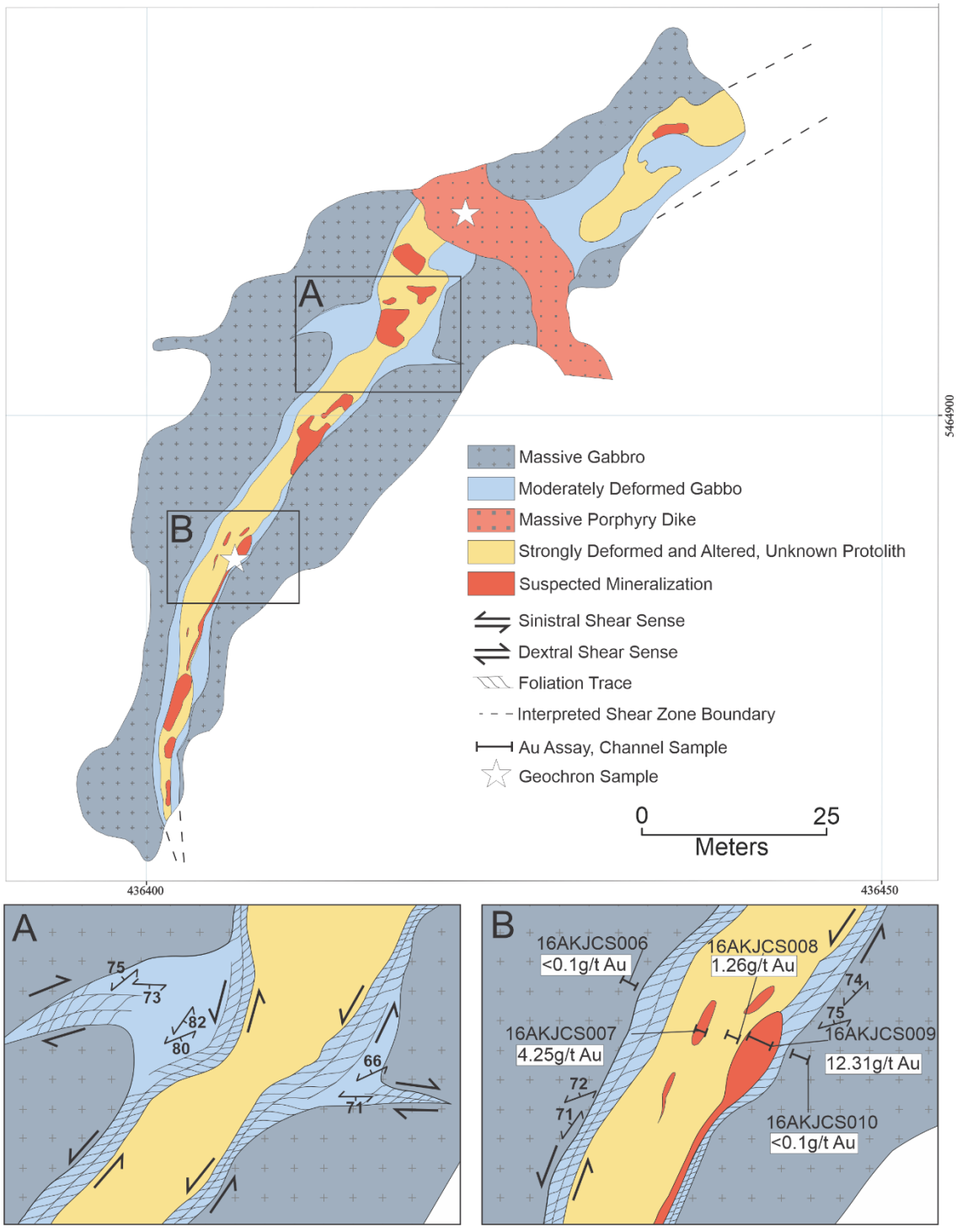

Figure 3.9: Detailed trench map of trench #1 (T1) at the Dogpaw deposit. Insert A and B are provided and outlined to better illustrate the mapped conjugate set and sample assay sample location at the trenched exposure. In inset B some of the au assay samples taken in 2016 are shown, please refer to Table 3.1. Universal Transverse Mercator (UTM) coordinates are provided using North American Datum 1983 (NAD83) in Zone 15.

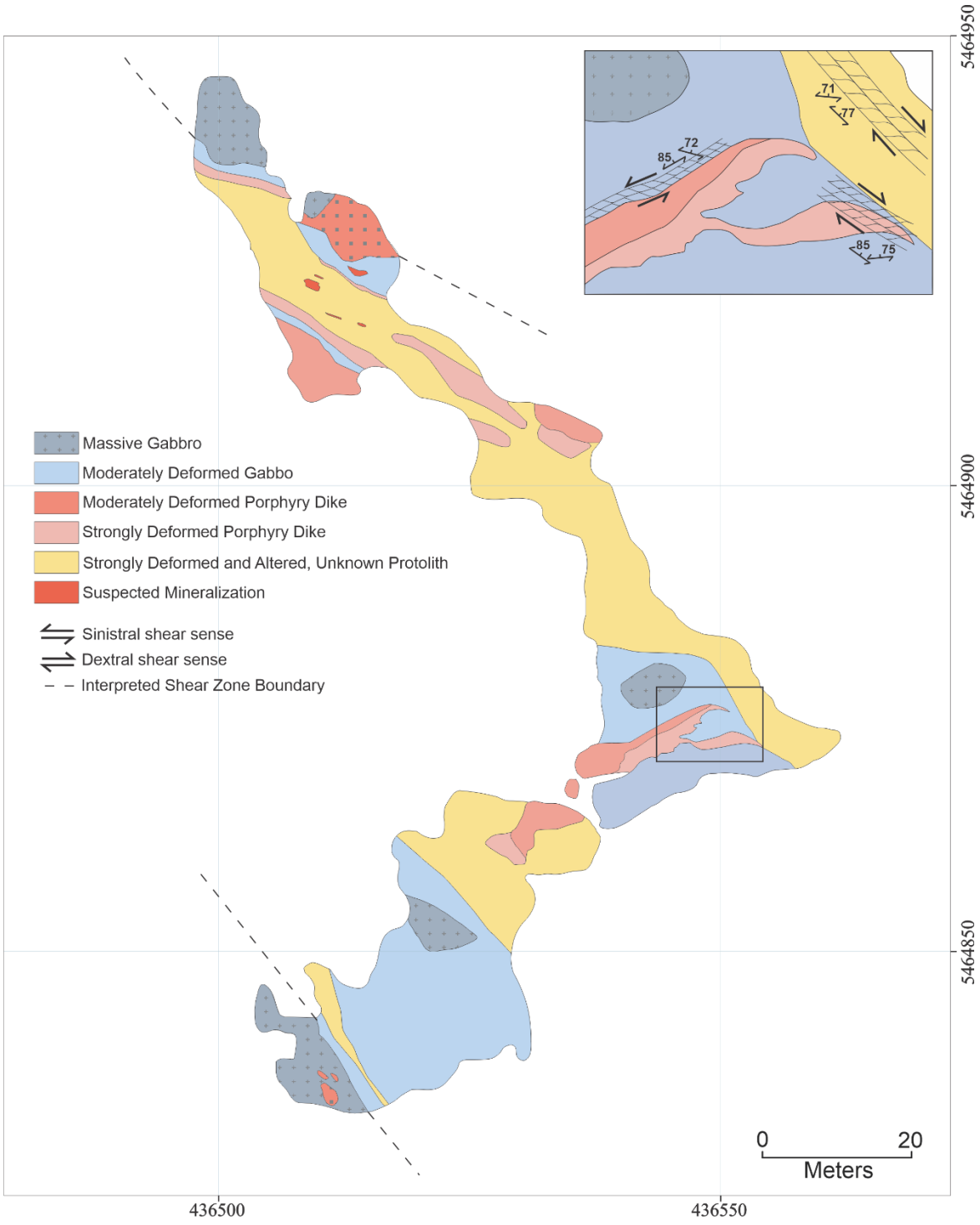

Figure 3.10: Detailed trench map of trench #2 (T2) at the Dogpaw deposit. The insert is outlined and provided to better illustrate the syn-tectonic relationship between one of the mapped feldspar porphyry dykes and the hosting Dalby Bay shear zone (*see* Fig. 3.19). Universal Transverse Mercator (UTM) coordinates are provided using North American Datum 1983 (NAD83) in Zone 15.

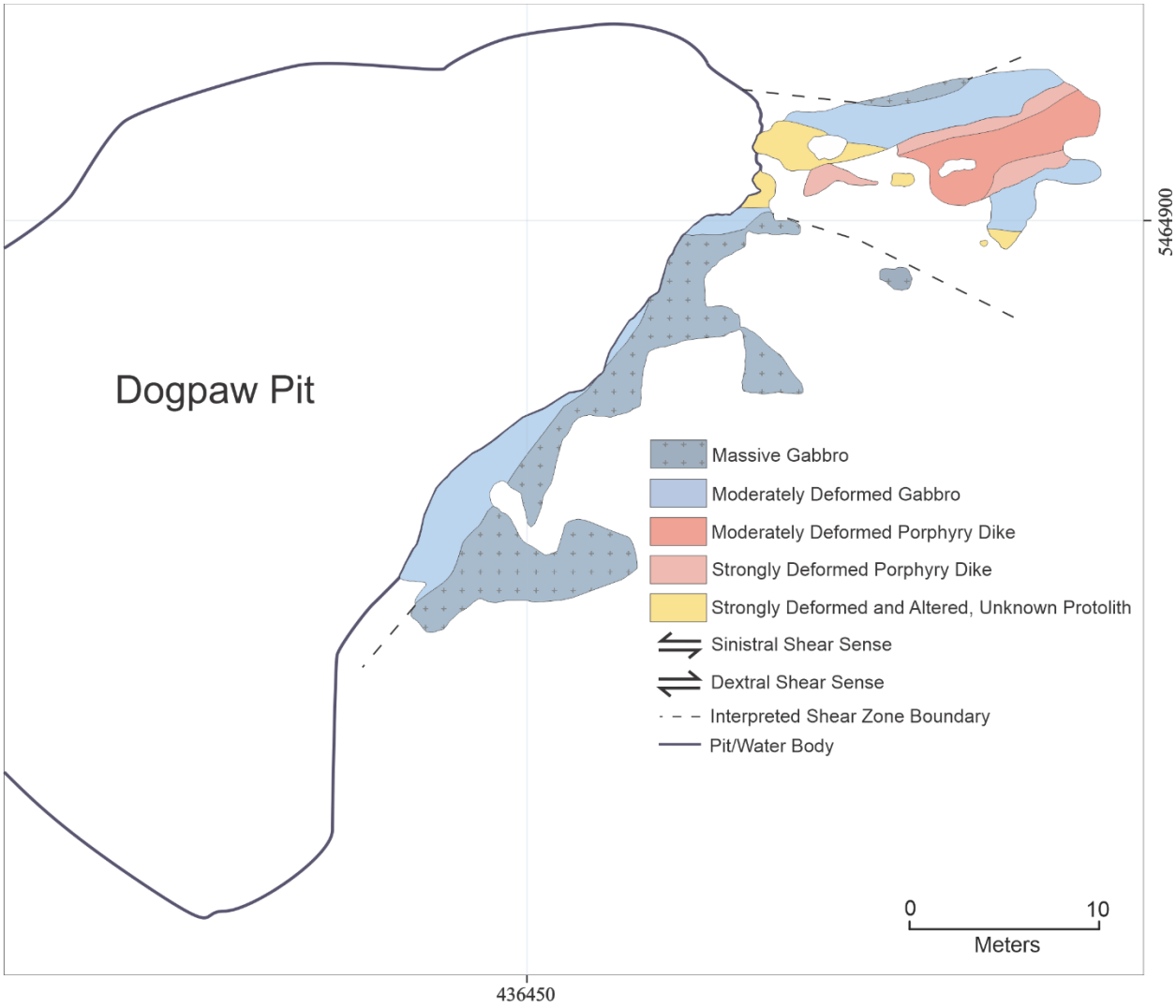

Figure 3.11: Detailed trench map of trench #3 (T3) at the Dogpaw deposit. The Dogpaw pit is outlined. Open pit excavation in 1996 produced a 500-imperial ton, bulk sample at this site, averaging 6.53g/t of gold after dilution (Ball, 2014)/ Boulders of ore are found around the pit. Universal Transverse Mercator (UTM) coordinates are provided using North American Datum 1983 (NAD83) in Zone 15.

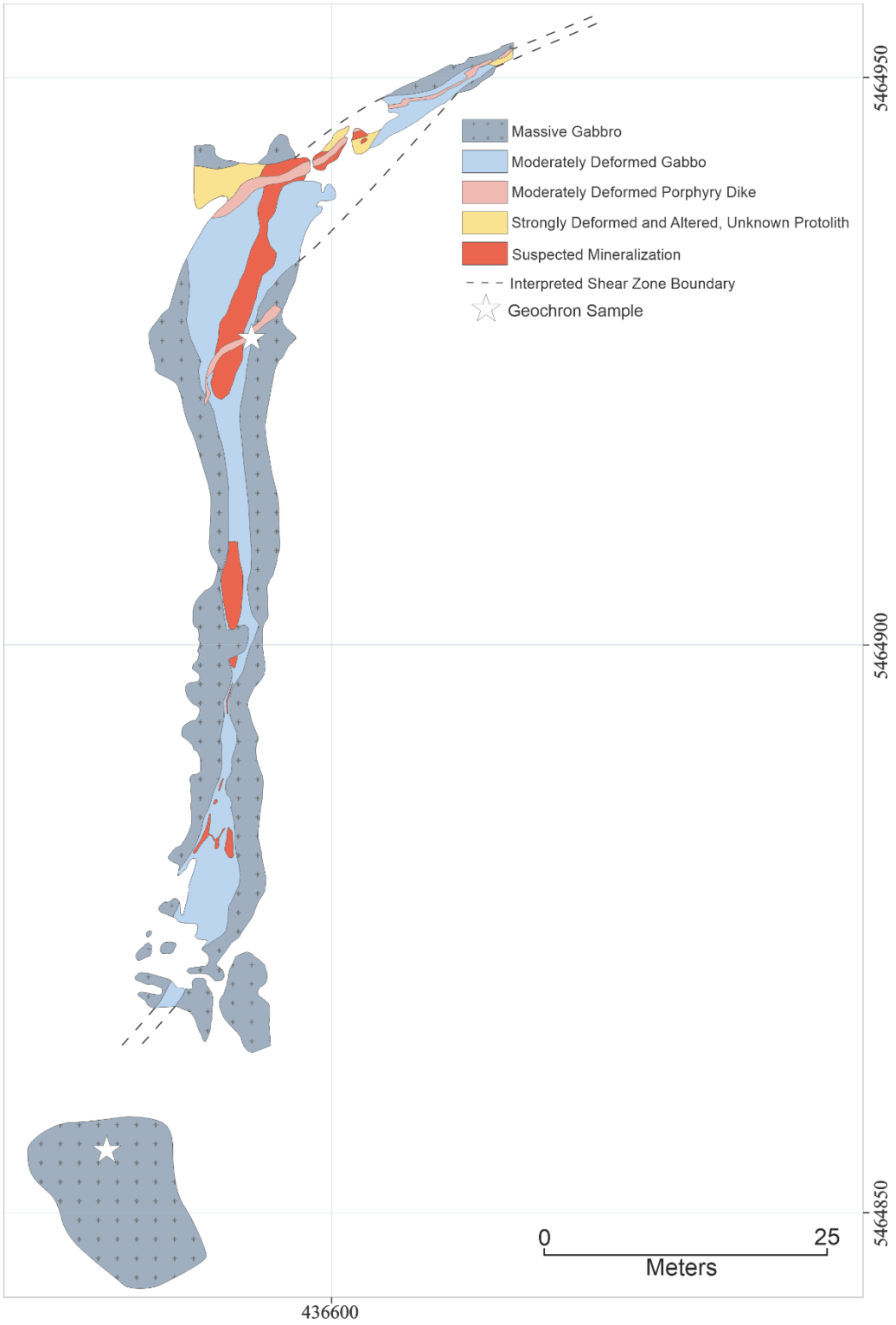

Figure 3.12: Detailed trench map of trench #4 (T4) at the Dogpaw deposit. Universal Transverse Mercator (UTM) coordinates are provided using North American Datum 1983 (NAD83) in Zone 15.

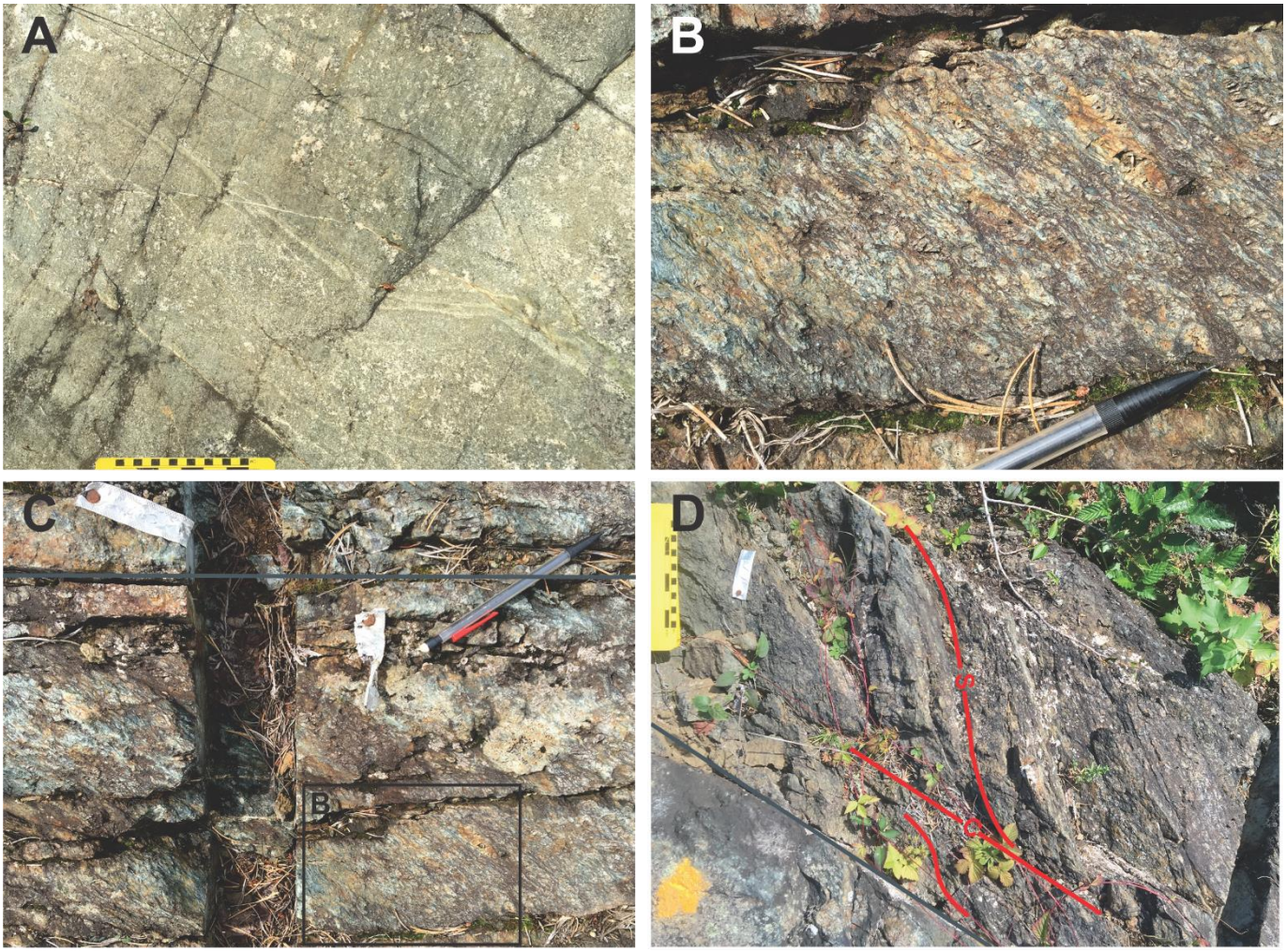

Figure 3.13: Outcrop photos taken at T1 at the Dogpaw deposit. A) Massive, coarse grained to pegmatitic gabbro found only a few feet from the boundary of the conjugate shear zones found at T1. B) Well developed gabbro Mylonite (S2). C) The boundary between shear zone and massive country rock is sharp and easily identified at T1, outlined in dark green. D) A sharp boundary between massive wall rock and shear zone followed by the development of an S-C fabric

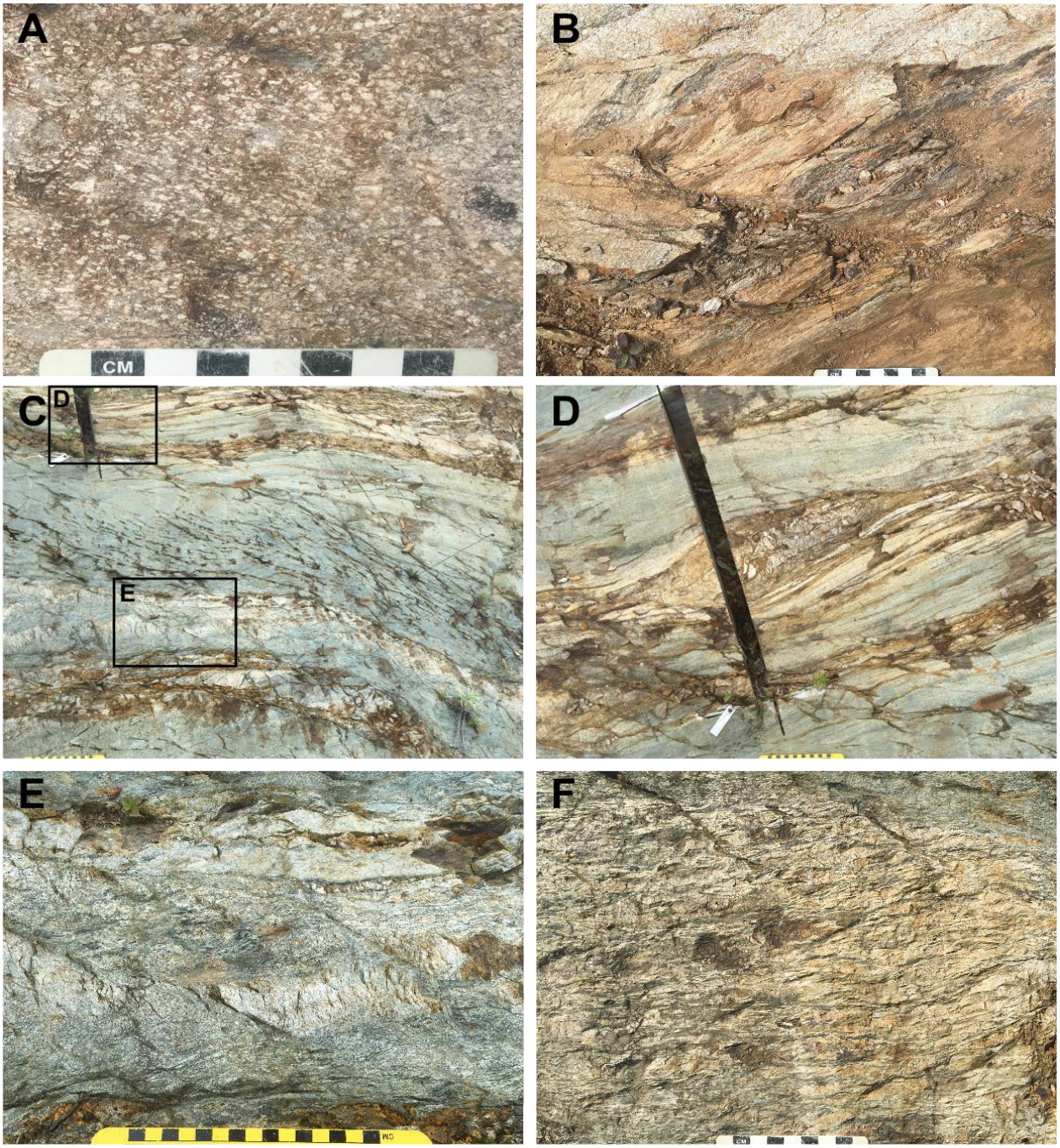

Figure 3.14: Outcrop photos at the Dogpaw deposit at T2 within the margins of the Dalby Bay shear zone. Note the textural variability of the foliations developed in the two lithologies, porphyry dykes (A to B) and gabbro (C to F). For the hosting gabbro layer, the resulting texture is largely controlled by the inherent textural heterogeneity of the gabbro with varying proportions of pegmatite. S-C foliation is well developed in both lithologies near the margins of the Dalby Bay shear zone and transitions into a well-developed CS-C' foliation towards the apparent center of the structure (see Figure 3.15).

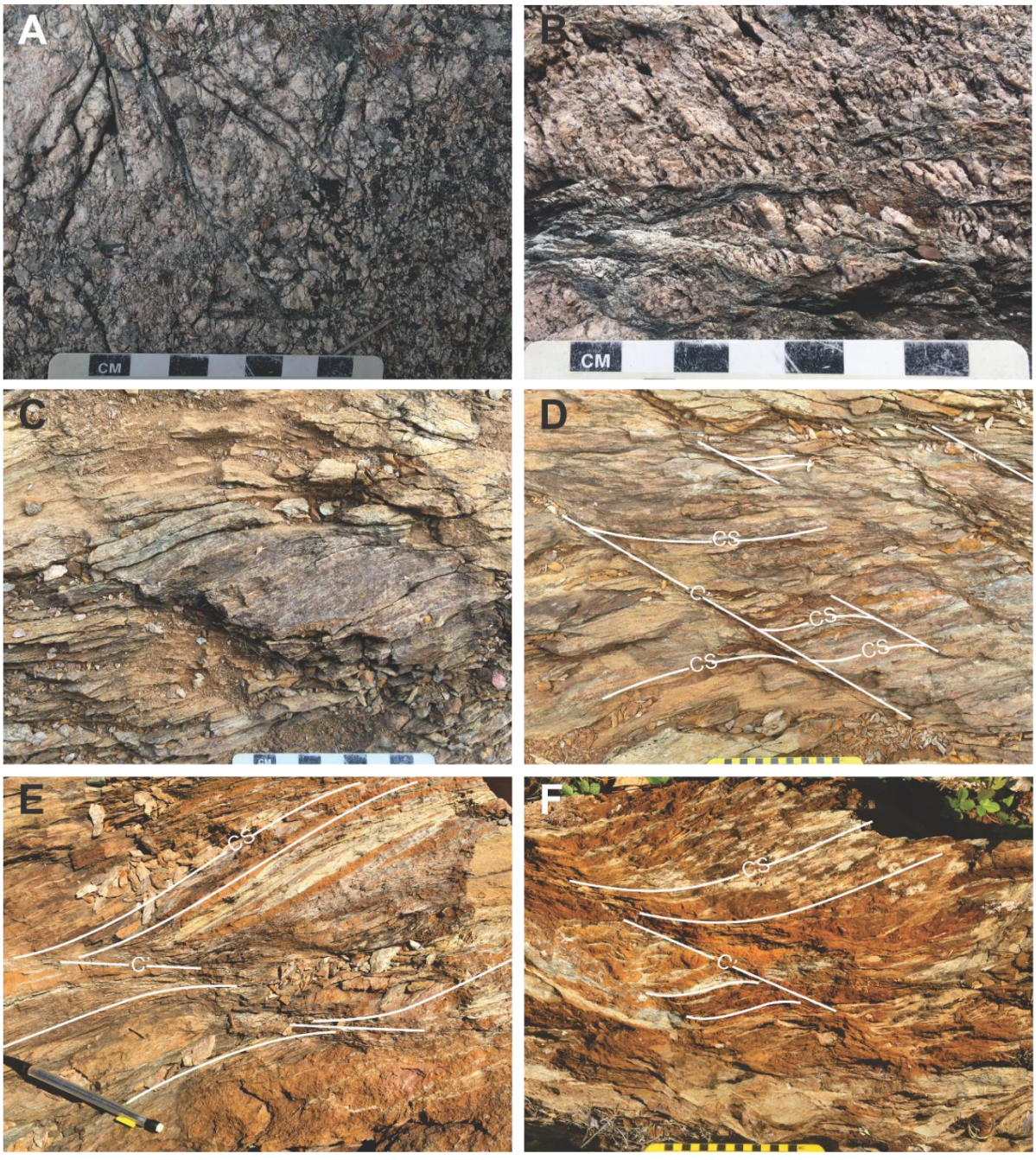

Figure 3.15: Outcrop photos of deformed country rock at T2 within the margins of the Dalby Bay shear zone at the Dogpaw deposit (when available photo locations provided as UTM coordinates using NAD83 in Zone 15). A) Massive, plagioclase rich portion of gabbro pegmatite outside the margins of the Dalby Bay shear zone. B) The same rock within the margins of the Dalby Bay shear zone, note the development of a protomylonite fabric, the presence of a fine-grained groundmass that wraps around strongly aligned and fractured plagioclase grains [436516] [5464845]. C) and D) deformed feldspar porphyry dyke. E) and F) are examples of S-C and CS-C' foliation within the margins of the Dalby Bay shear zone [436509] [5464921].

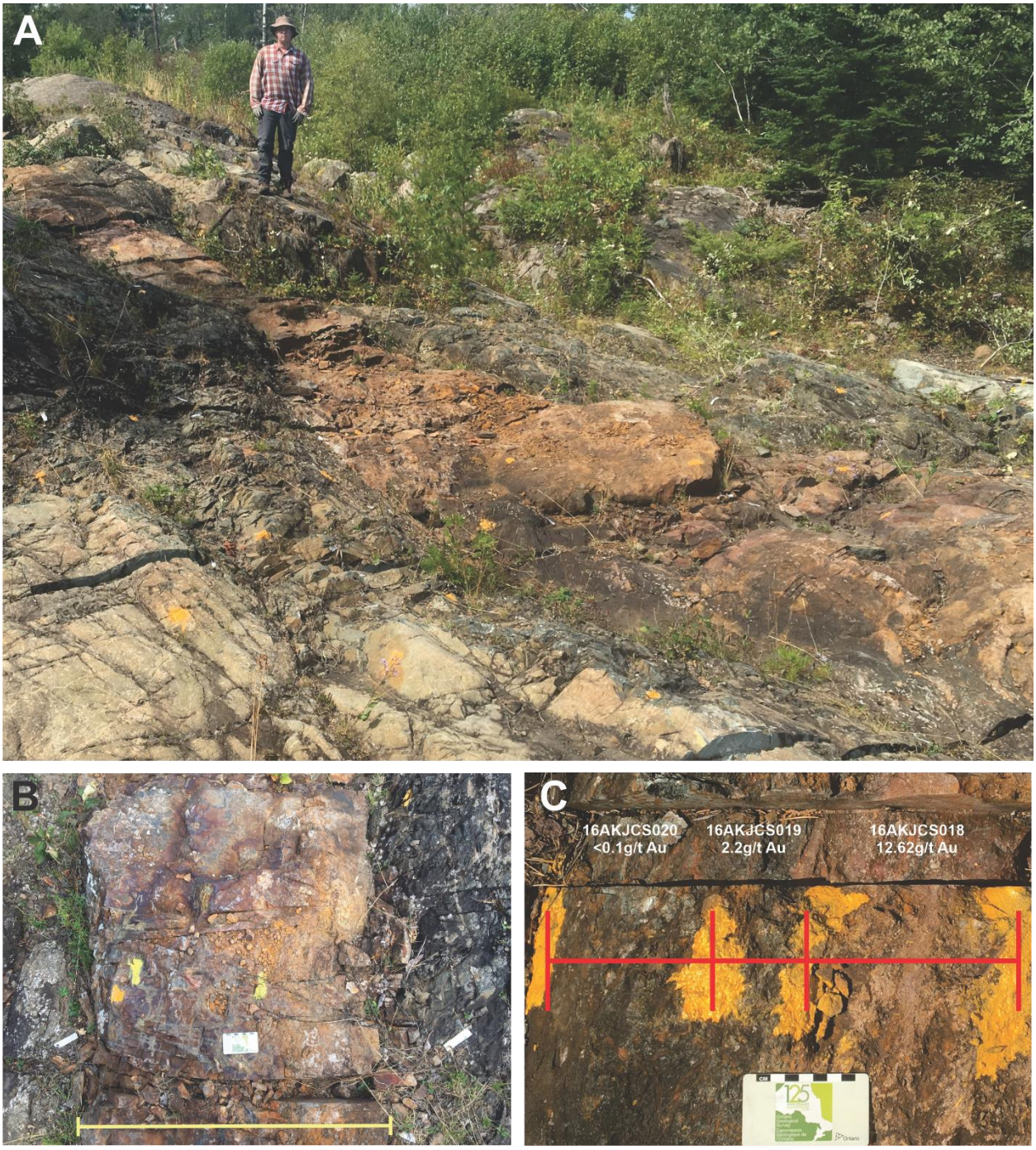

Figure 3.16: Outcrop photos at the Dogpaw deposit at T1. Photos A to C show the typical weather profile of gold mineralization exposed at surface. B) and C) note the stark contrast in weather between mineralized zones (yellow line on B) and the enveloping mylonite zone. C) This stark contrast in weather is also reflected in the relative au endowment aiding in the mapping of prospective zones.

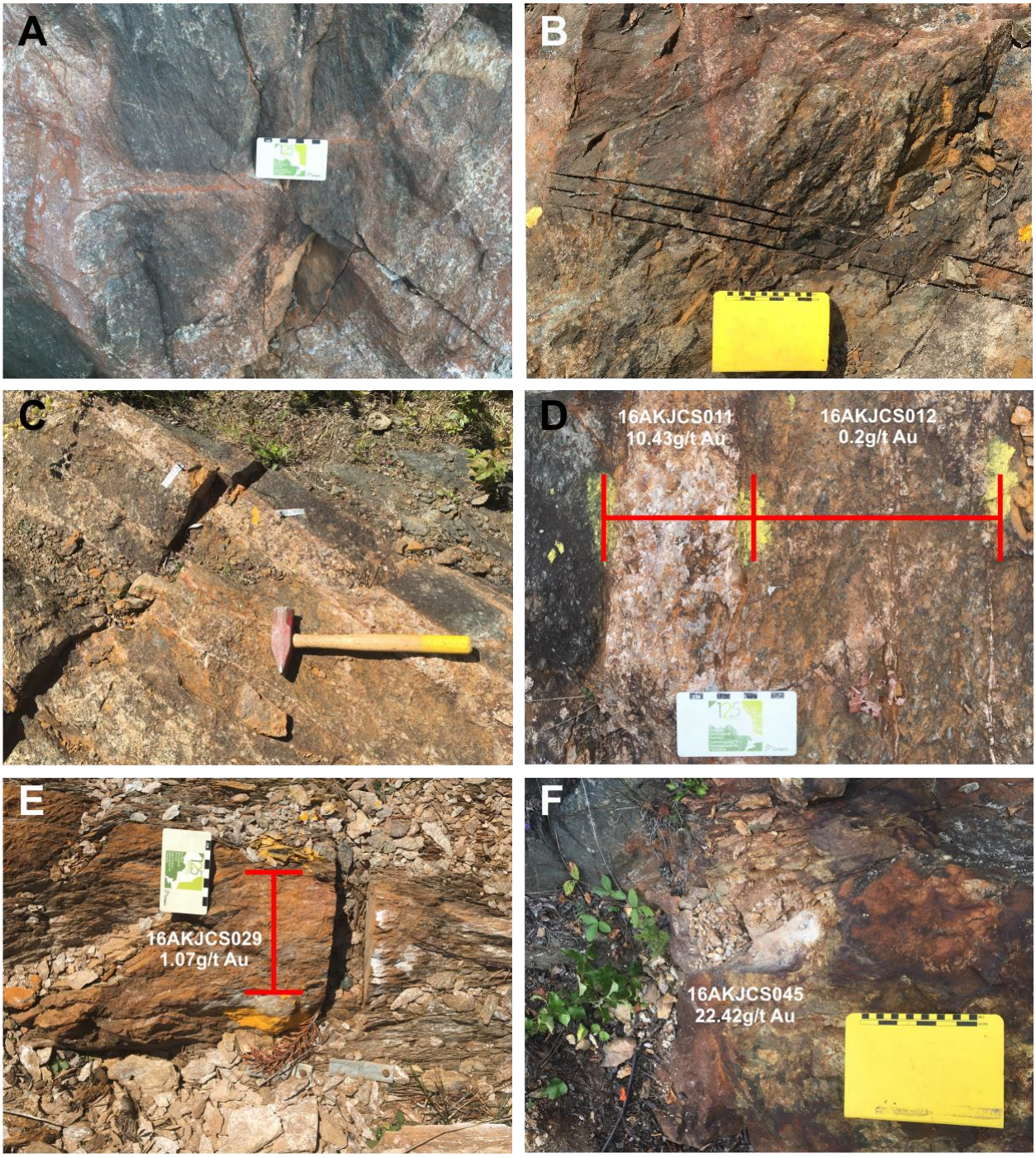

Figure 3.17: Outcrop photos at the Dogpaw deposit of au bearing veins. A) and B) V1 quartz-carbonate breccia veins. C) and D) V2 sheeted quartz-carbonate veins. E) V3 G3 hosted quartz-carbonate veins. F) Quartz-carbonate vein of unknown origin hosted in a shear zone at trench #5 at the Dogpaw deposit.

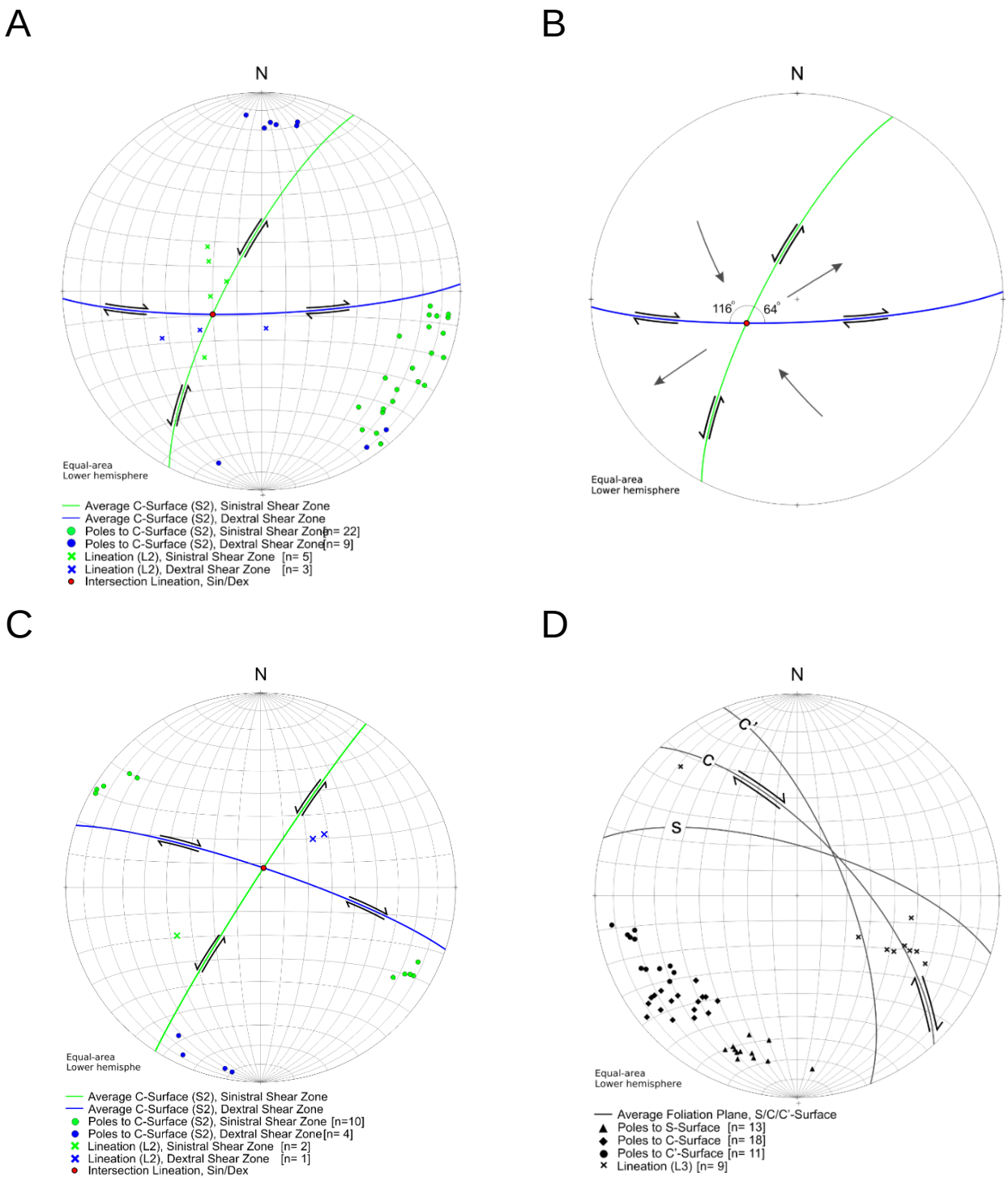

Figure 3.18: Equal-area lower hemisphere projects of structural data collected at the Dogpaw deposit. Projection A) foliation and lineation data from the G2 conjugate shear zone set found at T1 and projection B) the apparent local stress regime elucidated from the structural data. Projection C) the structural data collected from the G2 conjugate shear zone set found at T4. Projection D) structural data collected from the G3 Dalby Bay shear zone.

Figure 3.19: Outcrop photos at the Dogpaw deposit at T2 of a feldspar porphyry dyke. A) An early, syn-tectonic feldspar porphyry dyke B) apparently massive and in contact with foliated gabbro and C) deformed in another location. Photographs are taken at the same location as the inset provided in Figure. 3.10.

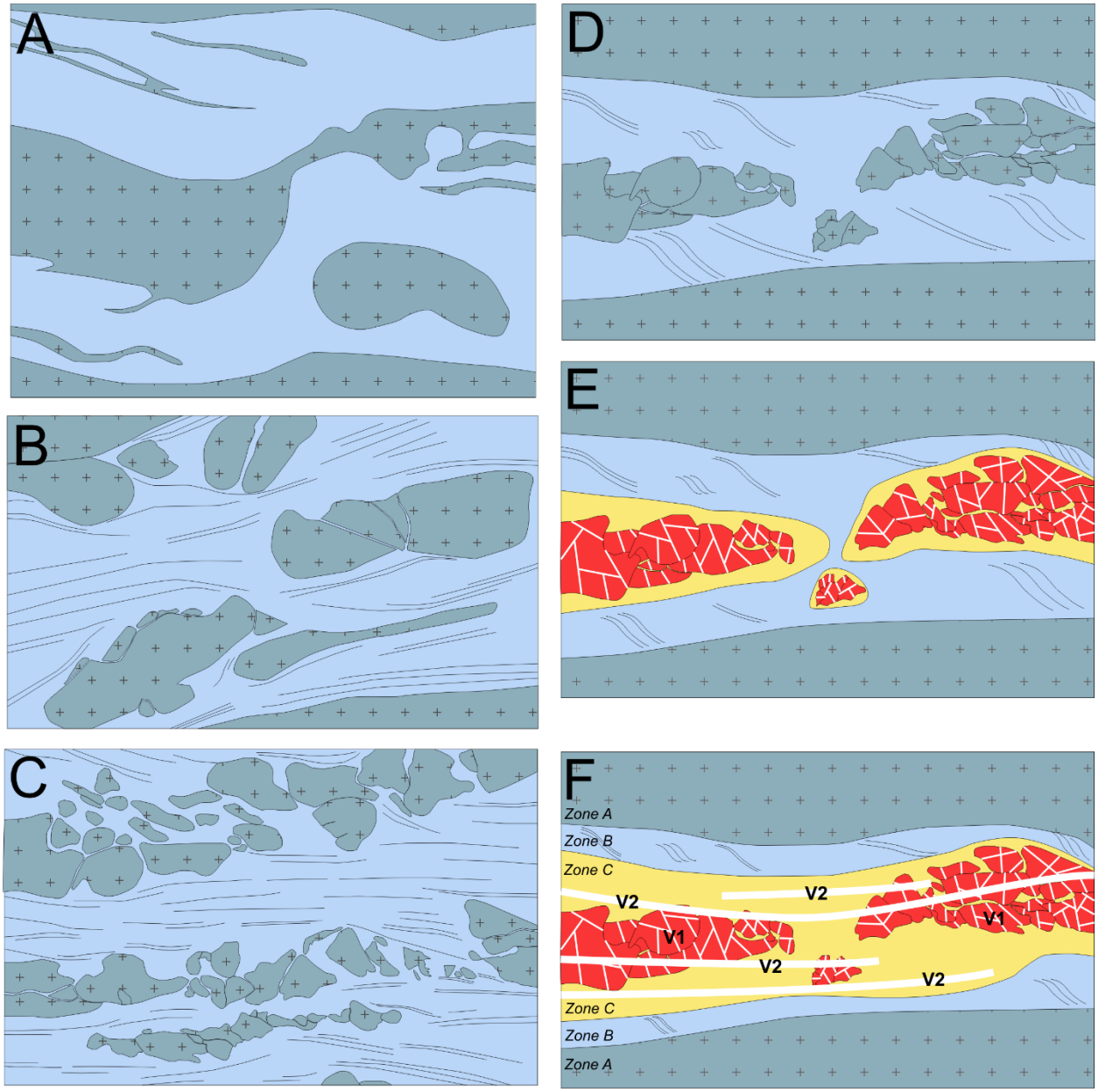

Figure 3.20: Conceptual figure illustrating the generation of V1 and V2 veins. A) Original country rock before deformation. On average host rock is composed of 50% gabbro pegmatite 'patches' which provided an inherent, primary textural heterogeneity. B) and C) During deformation the relatively finer grained, coarse-grained gabbro beings to develop a foliation while the pegmatitic gabbro patches brittlely deform. D) Panning out, a shear zone has developed bounded by massive pegmatite wall rock. Shear zone consists of lenses of gabbro pegmatite surrounded by a matrix of gabbro mylonite. E) The first generation of veins, V1, are generated by the brecciation of these lenses of gabbro pegmatite. Auriferous fluids infill these fractures between fragments and an alteration halo develops. F) Finally, sheeted V2 veins are emplaced and divide up V1 veins and alteration. All these elements are enveloped by a well develop mylonitic foliation and so deformation is interpreted to be ongoing during these illustrated steps.

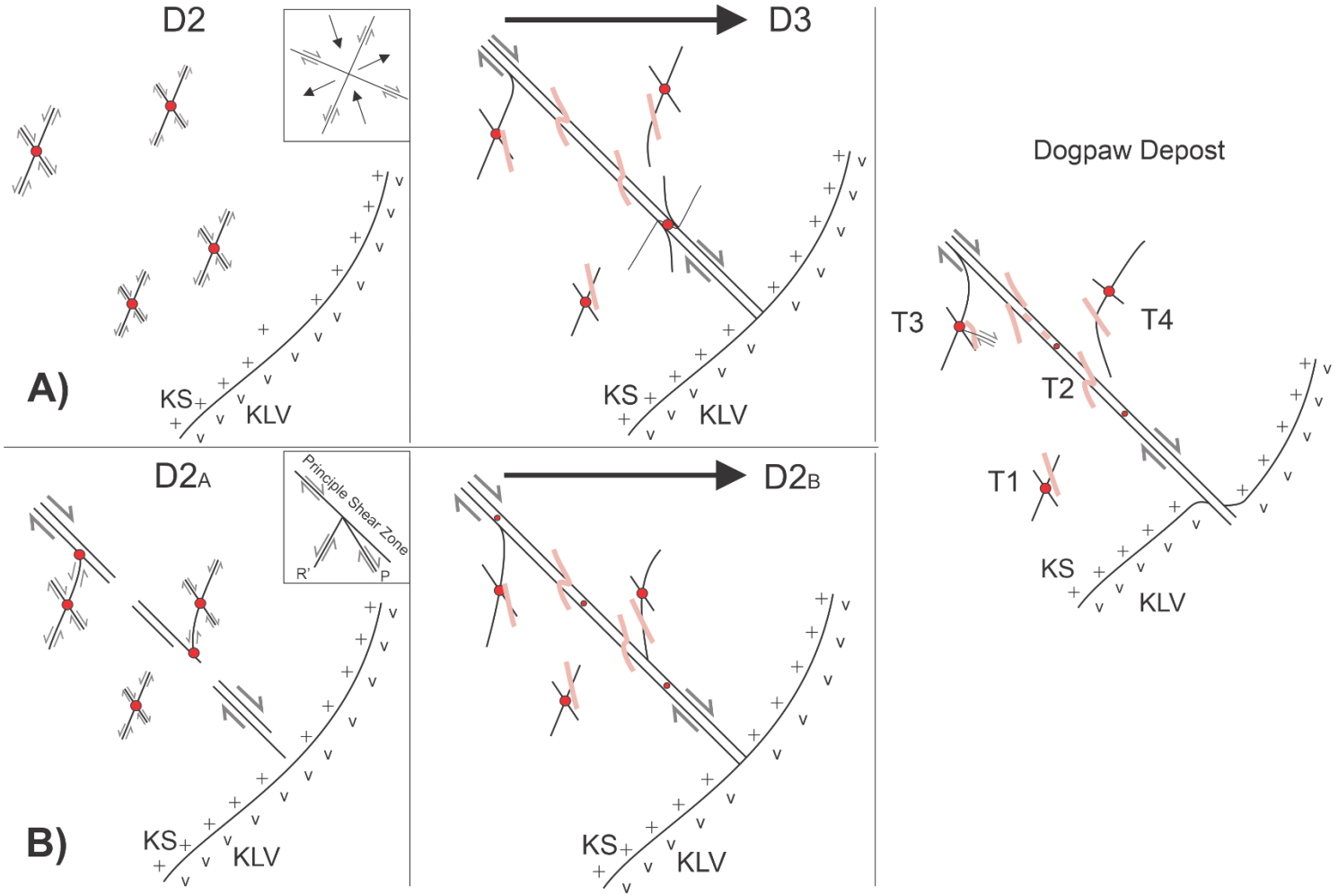

Figure 3.21: Conceptual figure illustrating the two scenarios for the development of the structural geology at the Dogpaw deposit. The final configuration of structures, trenches, and the contact between the Kakagi sill (KS) and Kakagi Lake volcanics (KLV) are shown, not to scale. Red circles show the interpreted loci of gold mineralization at the intersection of structures and feldspar-quartz porphyry dykes are shown in pink. A) Gold-bearing conjugate shear zones develop in D2 in response to broadly N-S directed compression followed by the emplacement of dykes and development of the Dalby Bays shear zone during D3 which variably deforms all structures and lithologies. B) Development of a principal shear zone, the Dalby Bay shear zone, and a network of gold-bearing, relatively minor structures consisting of antithetic and synthetic shear zones during $D2_A$. During $D2_B$ activity continues along the Dalby Bay shear zone and earlier gold-bearing structures and dykes are variably deformed depending on their proximity to the Dalby Bay shear zone.

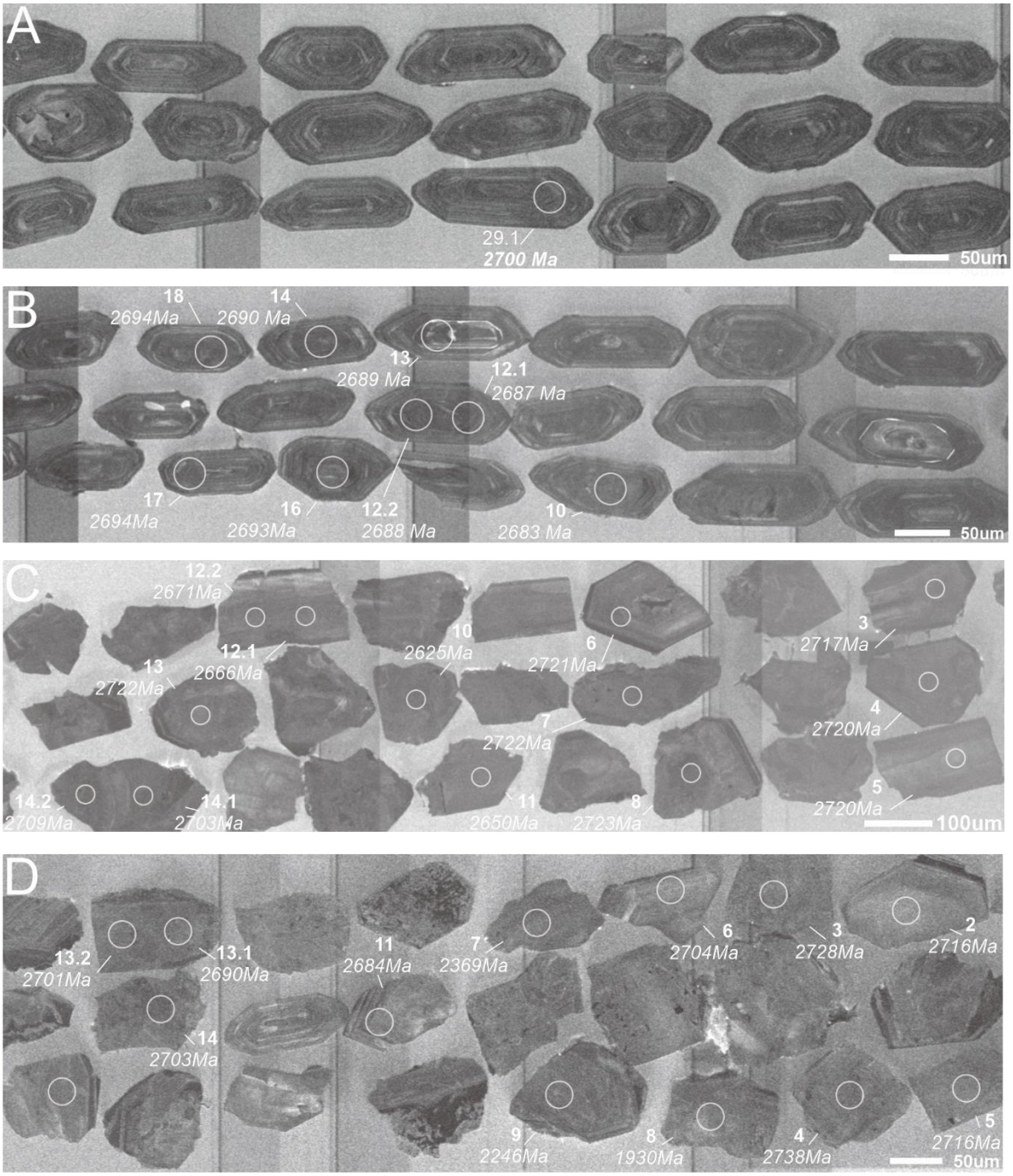

Figure 3.22: Representative photos of zircons recovered from each sample. A) 17AKJMS431A, B) 17AKJMS433A, C) 16AKJISIA602, and D) 17AKJMS457. A set of spots, spot number in bold and $^{207}Pb/^{206}Pb$ ages, are provided for each sample. Note the comparable morphology of grains and $^{207}Pb/^{206}Pb$ ages between A) and B) separated from samples of felspar porphyry dykes and C) and D) collected from the hosting intrusion and ore, respectively, at the Dogpaw deposit.

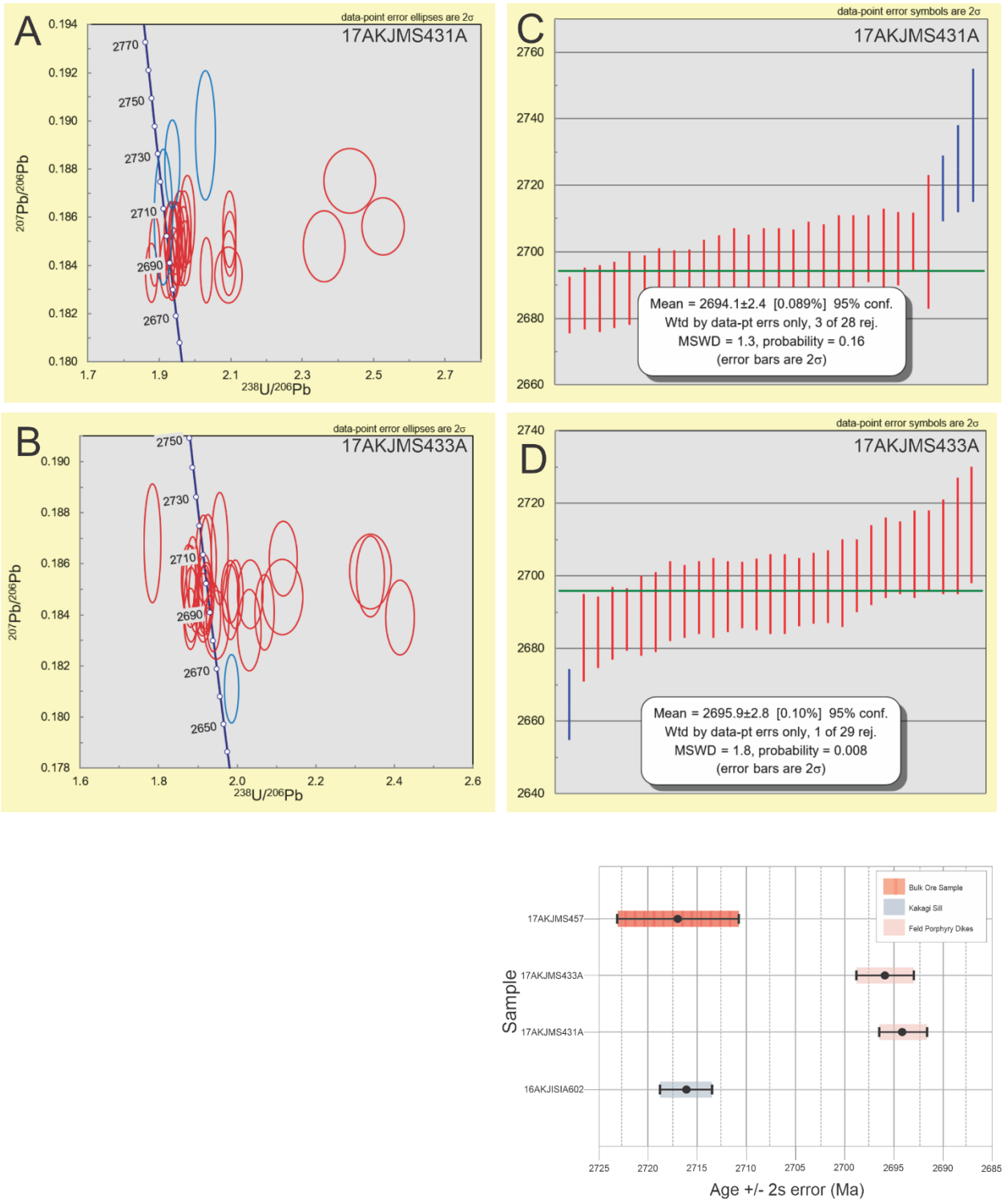

Figure 3.23: Concordia and $^{207}Pb/^{206}Pb$ weight average plots of data from LA-ICP-MS analysis of samples 17AKJMS431A and 433A. Final graph displays the weighted mean $^{207}Pb/^{206}Pb$ ages of each sample. Blue ellipses/bars indicate spots that were not included in the final weighted mean age.

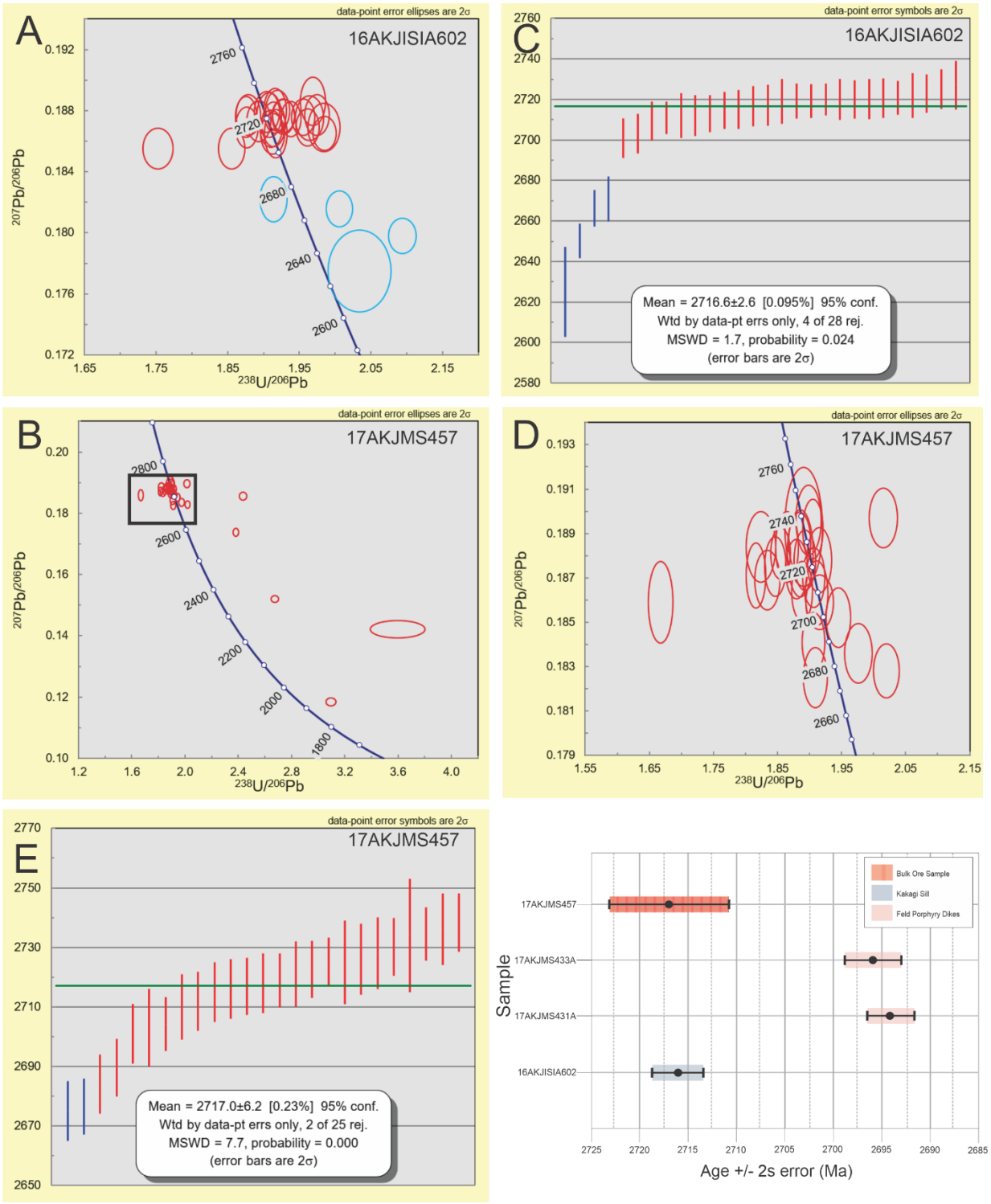

Figure 3.24: Concordia and $^{207}Pb/^{206}Pb$ weight average plots of data from LA-ICP-MS analysis of samples 17AKJMS457 and 16AKJISIA602. Final graph displays the weighted mean $^{207}Pb/^{206}Pb$ ages of each sample. Blue ellipses/bars indicate spots that were not included in the final weighted mean age.

Figure 3.25: Graph displaying the results from this study and U-Pb ages yielded from other studies in the Rowan-Kakagi greenstone belt (Davis and Edwards 1982, 1986). Samples from this study are bolded and italicized.

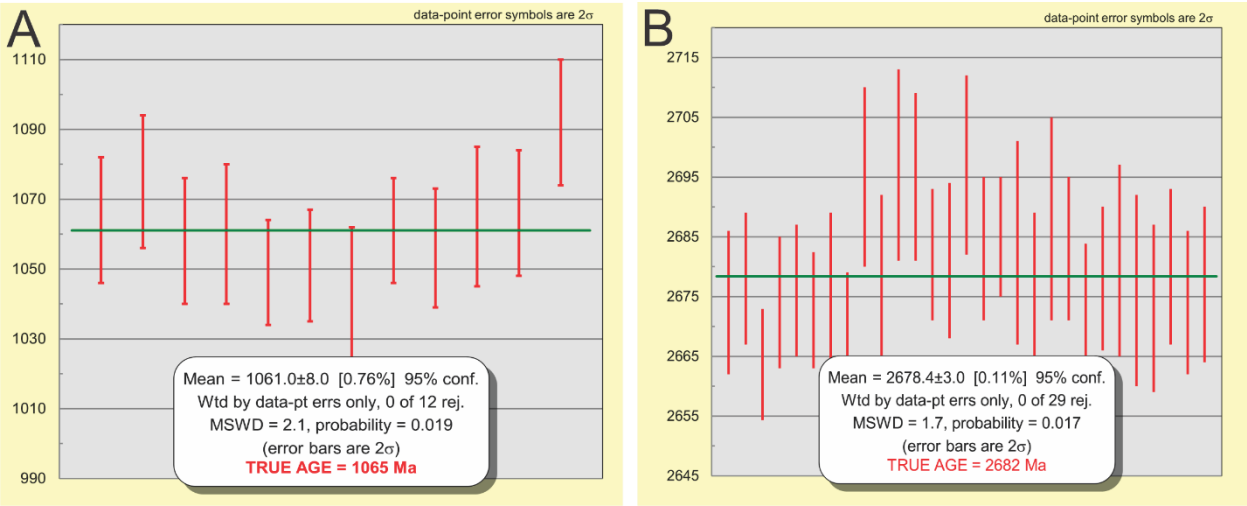

Figure 3.26: Weighted mean $^{207}Pb/^{206}Pb$ plots of data from LA-ICP-MS analysis of standard samples 91500 and DD85, A and B, respectively.

Chapter 4
Summary of Conclusions

4.1 Summary of Thesis

This thesis has provided new information on both structural and timing constraints on gold mineralization at the Dogpaw deposit, in the Rowan-Kakagi greenstone belt. Mineralization at the deposit is limited to upper layer of the hosting intrusion. It is interpreted that gold hosting structures at the deposit were localized in this upper layer due to the inherent textural heterogeneity of the hosting rock. Mineralized zones widen at the point of intersection of these hosting structures, suggesting the point of intersection was a preferential path of Au bearing fluids. These structures are interpreted to have been overprinted by a later fault, which is correlated with the major regional fault zone in the greenstone belt. Furthermore, a series of dykes at the deposit bracket both gold mineralization and activity along this later structure. An interpreted timing of emplacement for these dykes agrees with previously reported ages of major, syn to late-tectonic intrusions in the greenstone belt.

This research project also provides observations from a detailed study on the Pipestone-Cameron fault zone. The kinematics and style of deformation of several splays of the fault zone where delineated. Structural data and field observation in the map area suggest the Pipestone-Cameron fault zone is the result of a broad north-south directed compression resulting in a network of east-southeast trending dextral, and minor, east-northeast trending sinistral shear zones. Based on these observations the Dalby Bay shear zone is interpreted as an arcuate splay of the Pipestone-Cameron fault zone.

4.2 Main Conclusions

4.2.1 Structure and Gold Mineralization at the Dogpaw Deposit

- Gold bearing structures at the deposit are restricted to the upper, gabbroic layer of the hosting ultramafic to mafic Kakagi sill.
- Au-quartz veins are strictly hosted in G2, conjugate shear zones, overprinted by the G3 Dalby Bay shear zone, correlated with the regional Pipestone-Cameron fault zone.
- Geometry of the ore body is controlled by the geometry of the hosting G2 conjugate shear zones, with the ore body plunging subparralel to the intersection of the conjugate set and stretching lineation.
- Geometry of the ore body has been affected by activity along the G3, Dalby Bay shear zone

4.2.2 Geochronological Constraints at the Dogpaw Deposit

- U/Pb LA-ICP-MS analysis of zircon grains and $^{207}Pb/^{206}Pb$ ages differ but broadly agree with previously reported TIMS U/Pb ages for the deposit hosting intrusion and place an upper constraint on the timing of gold mineralization at 2715 ± 3Ma.
- U/Pb LA-ICP-MS analysis and $^{207}Pb/^{206}Pb$ ages of zircon grains recovered from 2 dykes that crosscut G2, gold bearing structures, yielded Pb/Pb ratio suggesting an age of emplacement of 2694.1 ± 2.4 Ma and 2695.9 ± 2.8 Ma. These interpreted ages place a minimum age constraint on gold mineralization and agree with previously reported TIMS U/Pb ages for interpreted syn- to late- tectonic intrusion in the Rowan-Kakagi greenstone belt.

4.3 Recommendations for Future Work

The results of this research project suggest a strong structural control on the localization of gold occurrences at the Dogpaw deposit. Exploration efforts have been focused along the trend of the Pipestone-Cameron fault zone in the greenstone belt and, at least at the Dogpaw deposit, these later structures may postdate gold mineralization and have relatively longer tectonic histories. The exploration for gold occurrences along the trend of these later structures has proved fruitful and so further mapping of the Pipestone-Cameron fault zone and other belt-scale structures will likely provide a greater understanding on gold-bearing structures at known gold occurrences in the belt. The observations included in this project on the structural geology, alteration and style of mineralization at the Dogpaw deposit are common observations reported at other gold occurrences in the Rowan-Kakagi greenstone belt. There is a wealth of information available on the geology of the belt thanks to the contributions by previous workers. It is recommended that further study on the gold mineralization in the Rowan-Kakagi involve a deeper compilation of published work, including 43-101 compliant industry reports and isotopic data from previous studies, and a more comprehensive study at other gold occurrences.

At the Dogpaw deposit results from this research project suggests that gold mineralization is both linked to the development of the hosting conjugate shear zones and largely limited to these structures. Several mineralized structures were identified at the Dogpaw deposit. These structures are discrete and laterally discontinuous with the zones of mineralization widest at the intersection of G2, conjugate shear zone sets. The discontinuous nature of the mineralization at the Dogpaw deposit may have hampered development if exploration efforts in the past were concentrated along trend of these gold-bearing structures. While laterally

discontinuous, mineralization may be relative continuous down plunge, approximately parallel to the intersection of conjugate sets. It is recommended that future exploration efforts focus on delineating additional conjugate sets and testing the down-plunge extent of the mineralization. There is also a notable drop in the magnetic properties of the rock, from massive country rock to mineralized zones, which may aid in identifying mineralized structures not exposed at surface. The Dalby Bay shear zone variably deforms these gold bearing structures. The overprinting effect of the Dalby Bay shear zone should be considered when delineating mineralization close to this structure.

A set of feldspar porphyry and quartz-feldspar porphyry dykes crosscut gold bearing structures at the Dogpaw deposit. The dykes have a clear, late timing of emplacement with gold-bearing structures at the Dogpaw deposit and absolute ages from samples collected from these intrusions has placed a timing constraint on gold mineralization at the deposit. Of all the samples collected for U-Pb zircon dating by LA-ICP-MS, samples collected from these dykes at the Dogpaw deposit provided results of the highest confidence. Other such dykes are commonly reported at other gold occurrences in the Rowan-Kakagi greenstone belt and share the same apparent timing of emplacement. It is recommended that a suite of samples be collected from these dykes reported at other gold occurrences to better constrain the timing of gold mineralization, deformation, and magmatic activity in the Rowan-Kakagi greenstone belt.

References

Ball, P., 2014. Technical report, Cameron gold camp project, mineral resource summary, western Ontario, Canada, prepared by DATAGEO Geological Consultants for Chalice Gold Mines Limited; Chalice Gold Mines Limited, NI 43-101 Technical Report, filed July 28, 2014 with SEDAR®, *see* SEDAR Home Page, 267p. [accessed November 9, 2016]

Beakhouse, G.P., 2007. Structurally controlled, magmatic hydrothermal model for Archean lode gold deposits: a working hypothesis; Ontario Geological Survey, Open File Report 6193, 133p.

Beakhouse, G.P., Stott, G.M., Blackburn, C.E., Breaks, F.W., Ayer, J., Stone, D., Farrow, C., and Corfu, F., 1996. Western Superior province; Fieldtrip guidebook, Ontario Geological Survey, Open File Report 5924

Beard. R.C., and Garratt, G.L., 1976. Gold deposits of the Kenora-Fort Frances area, districts of Kenora and Rainy River; Ontario Division of Mines, MDC 16, 46p. Accompanied by Chart A, scale 1:253 440 or 1 inch to 4 miles.

Bedard, J.H., 2006. A catalytic delamination-driven model for coupled genesis of Archean crust and sub-continental lithospheric mantle; Geochimica et Cosmochimica Acta, 70, (2006), 1188-1214

Blackburn, C.E., 1980. Towards a mobilist tectonic model for part of the Archean of Northwestern Ontario; Geoscience Canada, v.7, number 2

Blackburn, C.E., Johns, G.W., Ayer, J., and Davis, D.W., 1991. Wabigoon Subprovince; *in* Geology of Ontario, Ontario Geological Survey, Special Volume 4, Part 1

Card, K.D., Ciesielski, A., 1986. Subdivisions of the Superior Province of the Canadian Shield. Geosci Canada 13:5-13

Colvine, A.C. et al., 1984. An integrated model for the origin of Archean lode gold deposits; Ontario Geological Survey, Open File Report 5524, 98p.

Colvine, A.C., Fyon, J.A., Heather, K.B., Soussan Marmont, P.M., and Troop, D.G., 1988. Archean Lode Gold Deposits in Ontario; Ontario Geological Survey, Miscellaneous Paper 139, 136p

Cutting, D.R., and Anthony, E.G., 2005. Exploration summary and mineral resource estimate for the Angel Hill gold zone, West Cedartree gold project, Houston Lake Mining Inc. Kenora Mining District. Ontario

Davies, J.C. and Morin, J.A., 1976. Cedartree Lake area, District of Kenora; Ontario Division of Mines, Map 2319, scale 1:31 360.

Davis, D.W. and Edwards, G.R., 1982. Zircon U–Pb ages from the Kakagi Lake area, Wabigoon Subprovince, northwest Ontario; Canadian Journal of Earth Sciences, v.19, p.1235-1245.

——— 1986. Crustal evolution of Archean rocks in the Kakagi Lake area, Wabigoon Subprovince, Ontario, as interpreted from high-precision U–Pb geochronology; Canadian Journal of Earth Sciences, v.23, p.182-192.

de Wit, M.J., 1998. On Archean granites, greenstones, cratons and tectonics: Does the evidence demand a verdict?; Precambrian Research, v. 91, p. 181-226

Davies, D.W., 2002, U-Pb geochronology of Archean metasedimentary rocks in the Pontiac and Abitibi subprovinces, Quebec, constraints on timing, provenance and regional tectonics: Precambrian Research, v. 115, p.97-117.

Davies, J.C., and Pryslak, A.P., 1967, Kenora-Fort Frances Sheet: Ontario Geological Survey; Map 2115, scale 1 inch to 4 miles.

Drabble, M., Froud, J., Cervoj, K. and Morgan, R., 2015. Technical report on the Cameron gold deposit, Ontario, Canada December 2015 mineral resource estimate, prepared by Optiro Pty Limited for Chalice Gold Mines Limited; NI 43-101 Technical Report, filed December 21, 2015 with SEDAR®, *see* SEDAR Home Page, 278p. [accessed September 19, 2016].

Dube, B., and Gosselin, P., 2007. Greenstone-hosted quartz-carbonate vein deposits, *in* Goodfellow, W.D., ed., Mineral Deposits of Canada; A Synthesis of Major Deposit-Types, District Metallogeny, the Evolution of Geological Provinces, and Exploration Methods; Geological Association of Canada, Mineral Deposits Division, Special Publication No. 5. p. 49-73

Dunbar, P., and Morton, S., 2008. Assessment report on the 2008 Dubenski shaft zone gold deposit diamond drilling program, West Cedartree gold project, Kenora, Ontario for Houston Lake Mining Inc.

Groves, D.I., Santosh, M., Goldfarb, R.J., and Zhang, L., 2018. Structural geometry of orogenic gold deposits: Implications for exploration of world-class and giant deposits. Geoscience Frontiers 2018; https://doi.org/10.1016/j.gsf.2018.01.006

Johns, G.W., 2007. Precambrian geology, Kakagi–Rowan lakes area; Ontario Geological Survey, Preliminary Map P.3594, scale 1:50 000.

Kinney, P.D. and Maas, R., 2003. Lu-Hf and Sm-Nd isotope systems in zircon; *in* Reviews of Mineralogy and Geochemistry, 53(1): 327-341, doi: 10.2113/050327

Krapf-Jones, A.D., Meade, S.R. and Lin, S., 2016. A structural study of the Dogpaw and Dubenski deposits, Rowan–Kakagi greenstone belt, Western Wabigoon Subprovince; *in* Summary of Field Work and Other Activities, 2016, Ontario Geological Survey, Open File Report 6323, p.15-1 to 15-7.

Krapf-Jones, A.D., Meade, S.R. and Lin, S., 2017. Preliminary results from a structural study of the Dogpaw and Dubenski deposits, Rowan-Kakagi greenstone belt, Western Wabigoon Subprovince; *in* Summary of Field Work and Other Activities, 2017, Ontario Geological Survey, Open File Report 6333, p.10-1 to 10-9.

Lawson, A.C., 1888. Report on the geology of the Rainy Lake region. Geological and Natural History Survey of Canada. Dawson Brothers, Montreal 1888

Lewis, D. and Woolgar, S. 2011. Structural controls and alteration patterns of gold mineralization at Rowan Lake, northwest Ontario; *in* Summary of Field Work and Other Activities 2011, Ontario Geological Survey, Open File Report 6270, p.10-1 to 10-9

Lewis, D., Kamo, S.L. and Lodge, R.W.D. 2012. New geochemical and geochronological results from the Rowan Lake area, northwestern Ontaro; *in* Summary of Field Work and Other Activities, 2012, Ontario Geological Survey, Open File Report 6280, p.9-1 to 9-10.

Lin, S. and Beakhouse, G.P., 2013. Synchronous vertical and horizontal tectonism at late stages of Archean cratonization and genesis of Hemlo gold deposit, Superior craton, Ontario, Canada; Geology, v/41; no. 3; p.359-362; doi: 10.1130/G33887.1

Lin, S., Jiang, D., and Williams, P., 2007. Importance of differentiating ductile slickenslide striations from stretching lineations and variation of shear direction across a high-strain zone; Journal of Structural Geology, vol.29, p.850-862

Ludwig, K., 2008. Isoplot version 4.15: A geochronological toolkit for Microsoft Excel. Berkeley Geochronology Center, Special Publication, 4.

Mackasey, W.O., Blackburn, C.E., and Trowell, N.F., 1974. A regional approach to the Wabigoon-Quetico belts and its bearing on exploration in northwestern Ontario; Ontario Div. Mines, MP58, 30p.

Meade, S.R., 2015. A new mapping project in the Rowan Lake-Kakagi Lake Area, Western Wabigoon Subprovince; *in* Summary of Field Work and Other Activities, 2015, Ontario Geological Survey, Open File Report 6313, p12-1 to 12-6.

Meade, S.R., 2016. Precambrian geology of the Flint Lake area, Rowan–Kakagi greenstone belt, Wabigoon Subprovince; *in* Summary of Field Work and Other Activities, 2016, Ontario Geological Survey, Open File Report 6323, p10-1 to 10-6.

Meade, S.R., 2017. Precambrian geology of the Rowan–Kakagi Greenstone Belt, Western Wabigoon Subprovince: Flint Lake and Otterskin Lake Areas; *in* Summary of Field Work and Other Activities, 2017, Ontario Geological Survey, Open File Report 6333, p9-1 to 9-6.

Melling, D.R., and Watkinson, D.H., 1985. The Cameron Lake deposit *in* Field Trip Guidebook, Institute of Lake Superior Geology Thirty-First Annual Meeting, Kenora, Ontario 1985

Melling, D.R., and Watkinson, D.H., 1986. The geological setting and genesis of the Cameron Lake gold deposit *In* Geoscience Research Grant Program, Summary of Research, 1985-1986, edited by V.G. Mine, Ontario Geological Survey, Miscellaneous Paper 130, 235p.

Melling, D.R., 1986. Geological setting, structure, and alteration associated with gold-pyrite mineralization in mafic volcanic rocks at Cameron Lake, Wabigoon Subprovince, Northwestern Ontario. M.Sc. thesis, Carleton University, Ottawa, Ontario

Melling, D.R., 1988. Geological setting, structure and alteration associated with gold mineralization in mafic volcanic rocks at Cameron Lake, Wabigoon Subprovince, northwestern Ontario; Ontario Geological Survey, Open File Report 5689, 112p.

Melling, D.R., 1989. The geological setting and distribution of gold in the Cameron-Rowan Lakes area, District of Kenora, with emphasis on the Monte Cristo and Victor Island prospects; Ontario Geological Survey, Open File Report 5713, p108

Melnyk, M., Davis, D.W., Cruden, A.R., and Stern, R.A., 2005. U-Pb ages constraining structural development of an Archean terrane boundary in the Lake of the Woods area, western Superior Province, Canada; Canadian Journal of Earth Science. 43: 967-993 (2006)

Ontario Geological Survey 1992. Tectonic assemblages of Ontario, west-central sheet; Ontario Geological Survey, Map 2576, 1:1 000 000.

Paton, C., Hellstrom, J., Paul, B., Woodhead, J. & Hergt, J. 2011. Iolite: freeware for the visualisation and processing of mass spectrometric data. Journal of Analytical Atomic Spectrometry 26, 2508-2518.

Percival, J.A., Skulski, T., Sanborn-Barrie, M., Stott, G.M., Leclair, A.D., Corkery, M.T., and Boily, M. 2012. Geology and tectonic evolution of the Superior Province, Canada. Chapter 6 *In Tectonic Styles in Canada:* The LITHOPROBE Perspective. *Edited by J.A. Percival, F.A. Cook, and R.M. Clowes. Geological Association* of Canada, Special Paper 49, pp. 321–378.

Percival, J.A., Sanborn-Barrie, M., Skulski, T., Stott, G.M., Helmstaedt, H., and White, D.J., 2006. Tectonic evolution of the western Superior Province from NATMAP and Lithoprobe studies. *Edited by R. Clowes.* Can. J. Earth Sci. 43: 1085-1117. doi:10.1139/E06-062

Sanborn-Barrie, M., and Skulski, T., 2006. Sedimentary and structural evidence for 2.7 Ga continental arc-oceanic-arc collision in the Savant-Sturgeon greenstone belt, wester Superior Province, Canada. Canadian Journal of Earth Science. Vol. 43, 2006

Secord, S.R., 2011. Geochemistry and au mineralization within the Kakagi-Rowan Lakes greenstone belt: a study of the Angel Hill gold zone. M. Sc. Thesis, Lakehead University, Thunder Bay, Ontario

Tetclock, C., Dumas, K., and Lengyel, P., 2016. Assessment report trenching program Cameron Lake gold property Chalice Gold Mines limited .

Tomlinson, K.Y., Davis, D.W., Stone, D., and Hart, T.R., 2003. U-Pb age and Nd isotopic evidence for Archean terrane development and crustal recycling in the south-central Wabigoon subprovince, Canada. Contrib Mineral Petrol (2003) 144: 687-702. DOI 10.1007/s00410-002-0423-0

Tomkins, A.G., 2013. On the source of orogenic gold. Geology, 2013; v. 41; no. 12; p. 1255-1256; doi: 10.1130/focus122013.1

Wiedenbeck, M., Allé, P., Corfu, F., Griffin, W.L., Meier, M., Oberli, F., von Quadt, A., Roddick, J.C., Spiegel, W., 1995. Three natural zircon standards for U-Th-Pb, Lu-Hf, trace element and REE analyses. Geostand. Newslett. 19, 1-23.

Appendix A: Geochronological Data

Table A.1: LA-ICP-MS U-Pb data from analysis of zircons from sample 16AKJISIA602, Kakagi sill, Dogpaw deposit

Analysis Name	*207Pb/ 235U*	*2S*	*206Pb/ 238U*	*2S*	*ρ*	*238U/ 206Pb*	*2S*	*207Pb/ 206Pb*	*2S*	*207Pb/ 235U Age*	*2S*	*206Pb/ 238U Age*	*2S*	*207Pb/ 206Pb Age*	*2S*	*Appx. Th/U*	*Rejected*
16AKJISIA602																	
16AKJISIA602_8	8.11	0.08	0.3781	0.0027	0.38	2.645	0.019	0.1548	0.0010	2242	9	2067	13	2398	11	10.0	x
16AKJISIA602_14.2	12.25	0.34	0.4916	0.0087	0.92	2.034	0.036	0.1775	0.0022	2622	27	2574	38	2625	22	0.6	x
16AKJISIA602_1	11.77	0.10	0.4775	0.0036	0.80	2.094	0.016	0.1798	0.0009	2588	9	2516	16	2650	9	2.8	x
16AKJISIA602_14.1	12.69	0.10	0.4985	0.0038	0.79	2.006	0.015	0.1816	0.0010	2657	8	2608	16	2666	9	1.2	x
16AKJISIA602_10	13.23	0.14	0.5224	0.0042	0.88	1.914	0.015	0.1822	0.0012	2694	10	2710	18	2671	11	2.9	x
16AKJISIA602_2	14.52	0.14	0.5707	0.0056	0.83	1.752	0.017	0.1855	0.0011	2785	9	2912	23	2701	10	2.2	
16AKJISIA602_18	13.89	0.09	0.5389	0.0044	0.68	1.856	0.015	0.1855	0.0011	2742	6	2778	18	2703	10	0.7	
16AKJISIA602_32.2	13.64	0.09	0.5228	0.0037	0.69	1.913	0.014	0.1865	0.0011	2724	6	2710	16	2709	10	1.3	
16AKJISIA602_6	12.87	0.09	0.5037	0.0034	0.78	1.985	0.013	0.1865	0.0009	2671	7	2629	14	2711	8	1.6	
16AKJISIA602_3	12.88	0.12	0.5039	0.0046	0.72	1.985	0.018	0.1869	0.0013	2670	8	2633	20	2712	11	1.0	
16AKJISIA602_12.2	13.58	0.10	0.5216	0.0035	0.25	1.917	0.013	0.1865	0.0013	2720	7	2705	15	2712	10	1.6	
16AKJISIA602_32.1	13.71	0.09	0.5234	0.0034	0.68	1.911	0.012	0.1868	0.0010	2730	6	2714	14	2713	9	1.3	
16AKJISIA602_9.1	13.16	0.09	0.5098	0.0035	0.67	1.962	0.013	0.1869	0.0010	2693	6	2655	15	2715	9	2.5	
16AKJISIA602_50.2	14.01	0.09	0.5329	0.0036	0.65	1.877	0.013	0.1869	0.0011	2750	6	2753	15	2715		1.2	
16AKJISIA602_36	13.80	0.10	0.5282	0.0038	0.61	1.893	0.014	0.1873	0.0011	2735	7	2733	16	2717	10	1.4	
16AKJISIA602_26	13.69	0.11	0.5224	0.0036	0.67	1.914	0.013	0.1871	0.0012	2728	7	2709	15	2717	10	1.1	
16AKJISIA602_4	13.10	0.11	0.5091	0.0042	0.71	1.964	0.016	0.1875	0.0012	2686	8	2652	18	2719	11	3.6	
16AKJISIA602_9.2	13.28	0.08	0.5114	0.0034	0.66	1.955	0.013	0.1876	0.0010	2699	6	2662	14	2719	9	2.5	
16AKJISIA602_11	13.54	0.08	0.5159	0.0030	0.58	1.938	0.011	0.1875	0.0010	2717	5	2681	13	2719	8	1.1	
16AKJISIA602_20	13.55	0.09	0.5187	0.0034	0.74	1.928	0.013	0.1876	0.0009	2718	6	2693	14	2720	8	1.1	
16AKJISIA602_12.1	13.68	0.11	0.5242	0.0038	0.17	1.908	0.014	0.1877	0.0012	2727	7	2718	16	2720	10	1.6	
16AKJISIA602_54	14.03	0.09	0.5332	0.0035	0.62	1.875	0.012	0.1876	0.0011	2752	6	2756	15	2720	10	4.7	

16AKJISIA602_50.1	13.98	0.10	0.5323	0.0040	0.63	1.879	0.014	0.1877	0.0011	2747	7	2750	17	2720	10	1.2	
16AKJISIA602_7	13.09	0.08	0.5065	0.0036	0.49	1.974	0.014	0.1877	0.0011	2686	6	2641	16	2721	10	2.1	
16AKJISIA602_19	13.55	0.08	0.5187	0.0035	0.68	1.928	0.013	0.1876	0.0010	2719	5	2694	15	2721	8	1.2	
16AKJISIA602_31	13.77	0.09	0.5218	0.0035	0.20	1.916	0.013	0.1880	0.0012	2734	6	2708	15	2722	11	1.4	
16AKJISIA602_21	13.70	0.10	0.5250	0.0040	0.73	1.905	0.015	0.1879	0.0011	2731	7	2721	17	2723	10	1.7	
16AKJISIA602_13	13.70	0.10	0.5209	0.0038	0.66	1.920	0.014	0.1880	0.0011	2729	7	2702	16	2725	10	1.7	
16AKJISIA602_5	13.20	0.11	0.5079	0.0037	0.07	1.969	0.014	0.1886	0.0013	2693	8	2647	16	2727	12	1.9	

Table A.2: LA-ICP-MS U-Pb data from analysis of zircons from sample 17AKJMS431A, feldspar porphyry dyke, Dogpaw deposit.

Analysis Name	*207Pb/ 235U*	*2S*	*206Pb/ 238U*	*2S*	*ρ*	*238U/ 206Pb*	*2S*	*207Pb/ 206Pb*	*2S*	*207Pb/ 235U Age*	*2S*	*206Pb/ 238U Age*	*2S*	*207Pb/ 206Pb Age*	*2S*	*Appx. Th/U*	*Rejected*
17AKJMS431A																	
17AKJMS431A_1	11.06	0.15	0.4464	0.0060	0.88	2.240	0.030	0.1770	0.0010	2529	13	2382	26	2624	10	1.0	x
17AKJMS431A_9	12.19	0.18	0.4776	0.0072	0.95	2.094	0.032	0.1836	0.0010	2618	14	2514	32	2684	9	0.7	
17AKJMS431A_8	13.58	0.09	0.5323	0.0038	0.74	1.879	0.013	0.1837	0.0010	2721	7	2752	16	2686	9	0.4	
17AKJMS431A_13	12.56	0.08	0.4921	0.0033	0.62	2.032	0.014	0.1838	0.0011	2647	6	2581	14	2686	10	0.5	
17AKJMS431A_14	13.18	0.11	0.5203	0.0045	0.71	1.922	0.017	0.1840	0.0011	2693	8	2700	19	2687	10	0.2	
17AKJMS431A_16.2	13.11	0.10	0.5150	0.0036	0.60	1.942	0.014	0.1841	0.0012	2687	7	2677	15	2689	11	0.4	
17AKJMS431A_18.1	12.07	0.10	0.4775	0.0038	0.77	2.094	0.017	0.1841	0.0011	2610	8	2516	17	2689	10	0.4	
17AKJMS431A_7	13.24	0.10	0.5167	0.0037	0.65	1.935	0.014	0.1839	0.0011	2697	7	2686	16	2690	11	0.3	
17AKJMS431A_10	13.05	0.08	0.5099	0.0030	0.60	1.961	0.012	0.1844	0.0010	2683	6	2656	13	2691	9	0.6	
17AKJMS431A_16.1	12.99	0.09	0.5129	0.0036	0.72	1.950	0.014	0.1843	0.0010	2680	7	2670	16	2692	9	0.3	
17AKJMS431A_12	12.98	0.10	0.5073	0.0038	0.69	1.971	0.015	0.1845	0.0011	2677	8	2645	16	2694	10	0.3	
17AKJMS431A_21	13.39	0.09	0.5300	0.0034	0.55	1.887	0.012	0.1846	0.0012	2708	7	2741	15	2694	11	0.4	
17AKJMS431A_20	13.04	0.10	0.5125	0.0045	0.12	1.951	0.017	0.1849	0.0014	2682	7	2666	19	2695	12	0.4	
17AKJMS431A_15	12.18	0.09	0.4769	0.0032	0.70	2.097	0.014	0.1849	0.0011	2619	7	2513	14	2695	10	0.4	
17AKJMS431A_3	10.95	0.23	0.4235	0.0086	0.95	2.361	0.048	0.1848	0.0012	2514	20	2276	39	2696	11	0.5	x
17AKJMS431A_19.1	13.09	0.10	0.5142	0.0041	0.64	1.945	0.016	0.1851	0.0012	2686	7	2675	18	2697	10	0.4	

17AKJMS431A_22.1	12.94	0.09	0.5082	0.0034	0.69	1.968	0.013	0.1851	0.0011	2675	6	2650	15	2697	10	0.5	
17AKJMS431A_5.1	13.30	0.09	0.5175	0.0039	0.56	1.932	0.015	0.1851	0.0012	2703	7	2688	17	2698	11	0.4	
17AKJMS431A_19.2	13.10	0.10	0.5145	0.0037	0.67	1.944	0.014	0.1853	0.0011	2687	7	2675	16	2699	10	0.4	
17AKJMS431A_5.2	13.17	0.11	0.5075	0.0040	0.63	1.970	0.016	0.1855	0.0013	2692	8	2645	17	2700	11	0.2	
17AKJMS431A_22.2	12.19	0.09	0.4771	0.0035	0.62	2.096	0.015	0.1855	0.0013	2619	7	2514	15	2700	11	0.6	
17AKJMS431A_17	13.24	0.12	0.5173	0.0042	0.74	1.933	0.016	0.1853	0.0011	2695	9	2690	18	2701	10	0.2	
17AKJMS431A_18.2	12.91	0.13	0.5054	0.0045	0.67	1.979	0.018	0.1859	0.0015	2672	9	2636	19	2701	12	0.2	
17AKJMS431A_29.1	12.99	0.10	0.5110	0.0045	0.36	1.957	0.017	0.1855	0.0013	2680	7	2660	19	2701	11	0.3	
17AKJMS431A_4	10.23	0.19	0.3959	0.0076	0.95	2.526	0.048	0.1856	0.0010	2456	17	2154	35	2703	9	0.5	x
17AKJMS431A_6.1	13.55	0.18	0.5234	0.0057	0.47	1.911	0.021	0.1860	0.0023	2719	12	2714	24	2703	20	0.4	
17AKJMS431A_2	10.77	0.26	0.4110	0.0100	0.96	2.433	0.059	0.1875	0.0011	2494	24	2215	47	2719	10	0.8	x
17AKJMS431A_11	13.42	0.15	0.5164	0.0045	0.60	1.936	0.017	0.1882	0.0015	2709	10	2685	19	2725	13	0.5	
17AKJMS431A_6.2	13.04	0.17	0.4927	0.0055	0.51	2.030	0.023	0.1894	0.0022	2682	12	2585	23	2735	20	0.4	

Table A.3: LA-ICP-MS U-Pb data from analysis of zircons from sample 17AKJMS433A, feldspar porphyry dyke, Dogpaw deposit.

Analysis Name	***207Pb/ 235U***	***2S***	***206Pb/ 238U***	***2S***	***ρ***	***238U/ 206Pb***	***2S***	***207Pb/ 206Pb***	***2S***	***207Pb/ 235U Age***	***2S***	***206Pb/ 238U Age***	***2S***	***207Pb/ 206Pb Age***	***2S***	***Appx. Th/U***	***Rejected***
17AKJMS433A																	
17AKJMS433A_3.2	12.59	0.11	0.5036	0.0039	0.77	1.986	0.015	0.1811	0.0011	2650	8	2629	17	2665	10	0.5	x
17AKJMS433A_23	12.49	0.16	0.4924	0.0061	0.80	2.031	0.025	0.1834	0.0013	2642	12	2582	27	2683	12	0.4	
17AKJMS433A_21	13.02	0.17	0.5137	0.0067	0.89	1.947	0.025	0.1836	0.0011	2679	13	2676	28	2685	10	0.3	
17AKJMS433A_7.2	13.04	0.10	0.5157	0.0040	0.69	1.939	0.015	0.1839	0.0011	2682	7	2680	17	2687	10	0.4	
17AKJMS433A_17	13.43	0.10	0.5317	0.0039	0.74	1.881	0.014	0.1839	0.0010	2709	7	2750	16	2688	9	0.3	
17AKJMS433A_1.1	10.46	0.12	0.4141	0.0052	0.85	2.415	0.030	0.1839	0.0012	2476	11	2235	24	2689	11	0.3	
17AKJMS433A_10	12.26	0.12	0.4833	0.0047	0.77	2.069	0.020	0.1841	0.0012	2625	9	2542	21	2690	11	0.3	
17AKJMS433A_12.1	13.50	0.10	0.5313	0.0043	0.65	1.882	0.015	0.1844	0.0012	2716	7	2748	18	2693	11	0.4	
17AKJMS433A_14	12.84	0.11	0.5042	0.0044	0.75	1.983	0.017	0.1845	0.0012	2667	8	2633	19	2693	10	0.3	
17AKJMS433A_15	13.30	0.10	0.5216	0.0041	0.70	1.917	0.015	0.1846	0.0011	2702	7	2705	17	2694	10	0.2	

17AKJMS433A_18	13.35	0.11	0.5226	0.0049	0.78	1.914	0.018	0.1844	0.0012	2704	8	2709	21	2694	11	0.3	
17AKJMS433A_9	12.75	0.10	0.5012	0.0040	0.70	1.995	0.016	0.1848	0.0011	2660	8	2620	17	2694	10	0.4	
17AKJMS433A_6	13.29	0.12	0.5231	0.0050	0.82	1.912	0.018	0.1844	0.0010	2699	9	2711	21	2695	9	0.4	
17AKJMS433A_7.1	12.49	0.15	0.4919	0.0065	0.91	2.033	0.027	0.1848	0.0011	2641	12	2577	28	2695	10	0.6	
17AKJMS433A_16	12.03	0.24	0.4728	0.0095	0.93	2.115	0.042	0.1847	0.0012	2602	19	2491	42	2695	11	0.2	
17AKJMS433A_19.1	13.38	0.10	0.5280	0.0040	0.65	1.894	0.014	0.1848	0.0012	2706	7	2732	17	2695	11	0.3	
17AKJMS433A_4	12.86	0.12	0.5045	0.0047	0.81	1.982	0.018	0.1849	0.0010	2669	9	2632	20	2696	9	0.4	
17AKJMS433A_20	13.17	0.11	0.5204	0.0042	0.74	1.922	0.016	0.1847	0.0011	2692	8	2702	18	2697	10	0.3	
17AKJMS433A_2.3	13.32	0.10	0.5219	0.0042	0.74	1.916	0.015	0.1849	0.0012	2702	7	2706	18	2697	10	0.3	
17AKJMS433A_12.2	13.57	0.10	0.5314	0.0047	0.26	1.882	0.017	0.1851	0.0013	2719	7	2746	20	2698	12	0.4	
17AKJMS433A_11	13.60	0.11	0.5331	0.0043	0.71	1.876	0.015	0.1854	0.0011	2721	7	2754	18	2700	10	0.6	
17AKJMS433A_3.1	10.94	0.14	0.4274	0.0053	0.90	2.340	0.029	0.1855	0.0013	2516	12	2295	24	2703	11	0.5	
17AKJMS433A_13	10.92	0.19	0.4275	0.0079	0.93	2.339	0.043	0.1857	0.0012	2516	17	2294	36	2705	11	0.3	
17AKJMS433A_19.2	13.53	0.09	0.5301	0.0038	0.59	1.886	0.014	0.1856	0.0012	2717	6	2741	16	2705	10	0.3	
17AKJMS433A_2.1	13.41	0.11	0.5225	0.0044	0.77	1.914	0.016	0.1862	0.0014	2708	8	2709	19	2706	12	0.4	
17AKJMS433A_8	12.03	0.16	0.4723	0.0066	0.89	2.117	0.030	0.1862	0.0012	2609	12	2491	29	2707	11	0.4	
17AKJMS433A_2.2	13.32	0.12	0.5195	0.0048	0.61	1.925	0.018	0.1861	0.0015	2701	9	2696	20	2708	13	0.5	
17AKJMS433A_5	13.09	0.13	0.5114	0.0047	0.56	1.955	0.018	0.1866	0.0018	2686	10	2664	20	2711	16	0.9	
17AKJMS433A_22	14.31	0.17	0.5606	0.0056	0.59	1.784	0.018	0.1868	0.0019	2769	11	2868	23	2714	16	0.5	

Table A.4: LA-ICP-MS U-Pb data from analysis of zircons from sample 17AKJMS457, bulk ore sample, Dogpaw deposit.

Analysis Name	***207Pb/ 235U***	***2S***	***206Pb/ 238U***	***2S***	***ρ***	***238U/ 206Pb***	***2S***	***207Pb/ 206Pb***	***2S***	***207Pb/ 235U Age***	***2S***	***206Pb/ 238U Age***	***2S***	***207Pb/ 206Pb Age***	***2S***	***Appx. Th/U***	***Rejected***
17AKJMS457																	
17AKJMS457_13.1	13.14	0.09	0.5237	0.0042	0.68	1.909	0.015	0.1825	0.0011	2691	6	2714	18	2675	10	1.6	x
17AKJMS457_10	12.40	0.10	0.4950	0.0040	0.72	2.020	0.016	0.1828	0.0010	2637	8	2592	17	2677	9	1.1	x
17AKJMS457_1	12.79	0.12	0.5061	0.0045	0.78	1.976	0.018	0.1836	0.0011	2664	9	2639	19	2684	10	1.7	
17AKJMS457_3	13.25	0.11	0.5246	0.0040	0.72	1.906	0.015	0.1841	0.0011	2699	8	2718	17	2690	10	1.3	

17AKJMS457_4	13.09	0.11	0.5141	0.0042	0.62	1.945	0.016	0.1852	0.0011	2687	8	2673	18	2701	10	1.5	
17AKJMS457_36	15.39	0.19	0.5997	0.0057	0.76	1.668	0.016	0.1859	0.0015	2841	11	3027	23	2703	13	0.3	
17AKJMS457_20	13.40	0.15	0.5219	0.0048	0.84	1.916	0.018	0.1859	0.0010	2707	10	2712	20	2704	9	0.7	
17AKJMS457_33	13.56	0.11	0.5233	0.0040	0.67	1.911	0.015	0.1863	0.0012	2718	8	2712	17	2710	11	0.4	
17AKJMS457_22	13.67	0.09	0.5295	0.0037	0.63	1.889	0.013	0.1864	0.0011	2727	6	2739	15	2712	10	0.9	
17AKJMS457_26	14.27	0.10	0.5506	0.0038	0.69	1.816	0.013	0.1871	0.0012	2767	7	2827	16	2715	10	0.5	
17AKJMS457_21	14.07	0.13	0.5453	0.0048	0.77	1.834	0.016	0.1869	0.0011	2755	9	2804	20	2716	10	0.7	
17AKJMS457_5	13.49	0.10	0.5245	0.0038	0.72	1.907	0.014	0.1870	0.0011	2714	7	2721	16	2717	10	1.3	
17AKJMS457_19	14.03	0.11	0.5415	0.0040	0.27	1.847	0.014	0.1875	0.0011	2751	8	2789	17	2718	10	0.8	
17AKJMS457_18	13.78	0.10	0.5321	0.0040	0.71	1.879	0.014	0.1874	0.0011	2735	7	2751	17	2719	9	0.9	
17AKJMS457_8	13.58	0.10	0.5221	0.0042	0.70	1.915	0.015	0.1878	0.0012	2720	7	2709	18	2721	11	1.8	
17AKJMS457_9	13.63	0.08	0.5283	0.0038	0.61	1.893	0.014	0.1878	0.0011	2724	6	2734	16	2723	10	1.0	
17AKJMS457_24	14.02	0.09	0.5392	0.0037	0.72	1.855	0.013	0.1881	0.0010	2751	6	2781	15	2725	8	0.8	
17AKJMS457_2	13.71	0.12	0.5304	0.0046	0.58	1.885	0.016	0.1881	0.0016	2729	8	2742	19	2725	14	0.7	
17AKJMS457_29	14.25	0.15	0.5482	0.0056	0.77	1.824	0.019	0.1884	0.0013	2767	10	2816	23	2726	12	0.4	
17AKJMS457_27	13.92	0.11	0.5362	0.0042	0.62	1.865	0.015	0.1884	0.0013	2744	8	2767	18	2728	12	0.6	
17AKJMS457_17	13.78	0.11	0.5306	0.0039	0.67	1.885	0.014	0.1886	0.0011	2735	7	2745	17	2730	10	0.6	
17AKJMS457_35	13.91	0.21	0.5289	0.0067	0.71	1.891	0.024	0.1893	0.0022	2742	14	2741	29	2734	19	0.2	
17AKJMS457_32	13.73	0.09	0.5249	0.0036	0.69	1.905	0.013	0.1892	0.0011	2731	6	2719	15	2735	9	0.5	
17AKJMS457_13.2	13.70	0.12	0.5267	0.0045	0.69	1.899	0.016	0.1896	0.0013	2729	9	2727	19	2736	12	1.5	
17AKJMS457_7	13.03	0.13	0.4962	0.0044	0.79	2.015	0.018	0.1897	0.0011	2682	9	2598	19	2738	10	1.0	
17AKJMS457_6	10.03	0.10	0.4199	0.0032	0.78	2.382	0.018	0.1738	0.0011	2437	9	2261	14	2593	10	1.6	x
17AKJMS457_11	10.44	0.10	0.4104	0.0041	0.84	2.437	0.024	0.1856	0.0011	2473	9	2216	19	2704	10	0.4	x
17AKJMS457_14	7.84	0.08	0.3737	0.0033	0.83	2.676	0.024	0.1521	0.0009	2211	9	2046	15	2369	10	1.9	x
17AKJMS457_16	5.30	0.06	0.3229	0.0033	0.58	3.097	0.032	0.1184	0.0011	1867	10	1805	17	1930	16	0.2	x
17AKJMS457_28	5.60	0.35	0.2780	0.0130	0.99	3.597	0.168	0.1422	0.0023	1889	54	1577	66	2246	28	0.7	x

Table A.5: LA-ICP-MS U-Pb data from analysis of secondary DD91

Analysis Name	*207Pb/ 235U*	*2S*	*206Pb/ 238U*	*2S*	*ρ*	*238U/ 206Pb*	*2S*	*207Pb/ 206Pb*	*2S*	*207Pb/ 235U Age*	*2S*	*206Pb/ 238U Age*	*2S*	*207Pb/ 206Pb Age*	*2S*
DD91_D															
DD91_D_1	12.92	0.11	0.519	0.004	0.42	1.925	0.014827	0.1826	0.0014	2674.5	8.3	2696	17	2674	12
DD91_D_2	13.26	0.1	0.527	0.004	0.63	1.896	0.014386	0.1826	0.0013	2697.2	7.3	2729	17	2678	11
DD91_D_3	13.33	0.1	0.529	0.0042	0.71	1.891	0.015014	0.1814	0.001	2703	7.2	2736	18	2663.6	9.3
DD91_D_4	13.34	0.091	0.521	0.0036	0.61	1.921	0.013288	0.1825	0.0012	2704.7	6.4	2701	15	2674	11
DD91_D_6	13.32	0.095	0.519	0.0037	0.6	1.925	0.013715	0.1825	0.0012	2702.2	6.7	2696	16	2676	11
DD91_D_7	13.36	0.092	0.523	0.0038	0.65	1.913	0.013903	0.1821	0.0011	2705.7	6.7	2710	16	2672.7	9.7
DD91_D_9	13.25	0.1	0.52	0.0036	0.46	1.925	0.013339	0.1828	0.0015	2697.3	7.3	2696	15	2676	13
DD91_D_8	13.53	0.11	0.533	0.0041	0.63	1.875	0.014421	0.1818	0.0012	2716.9	7.5	2756	17	2668	11
DD91_D_10	13.31	0.12	0.522	0.0043	0	1.915	0.015769	0.1868	0.004	2700.3	8.7	2708	18	2695	15
DD91_D_11	12.85	0.12	0.514	0.0045	0.54	1.947	0.017066	0.1829	0.0017	2669.4	9.1	2671	19	2677	15
DD91_D_13	13.09	0.13	0.52	0.0052	0.56	1.924	0.019253	0.1848	0.0018	2686.2	9.4	2696	22	2697	16
DD91_D_12	13.25	0.12	0.527	0.0045	0.55	1.898	0.016215	0.1846	0.0015	2697.1	8.8	2727	19	2695	14
DD91_D_15	13.05	0.11	0.52	0.0042	0.67	1.924	0.015545	0.1834	0.0013	2683.6	8.1	2697	18	2682	11
DD91_D_16	13.32	0.13	0.528	0.0048	0.63	1.896	0.01725	0.1831	0.0015	2703.8	8.7	2732	20	2681	13
DD91_D_17	13.19	0.13	0.518	0.004	0.41	1.93	0.014902	0.1844	0.0017	2692.6	9	2691	17	2697	15
DD91_D_18	13.40	0.12	0.527	0.0042	0.68	1.896	0.0151	0.1835	0.0013	2708.8	8.4	2733	17	2683	12
DD91_D_14	13.74	0.11	0.546	0.0041	0.71	1.832	0.013763	0.1838	0.0011	2732.4	7.8	2807	17	2685	10
DD91_D_5	13.16	0.15	0.521	0.0049	0.52	1.919	0.018038	0.1837	0.0019	2692	11	2703	21	2684	17
DD91_D_22	13.58	0.13	0.538	0.0054	0.67	1.858	0.01865	0.1828	0.0014	2719.5	9	2774	23	2676	13
DD91_D_21	13.38	0.14	0.525	0.0049	0.52	1.907	0.017812	0.1836	0.0019	2705	10	2721	21	2688	17
DD91_D_20	13.73	0.12	0.542	0.0041	0.64	1.846	0.013972	0.1834	0.0013	2730.6	8	2790	17	2683	12
DD91_D_24	13.47	0.11	0.538	0.0043	0.74	1.859	0.014862	0.1825	0.001	2713.8	7.8	2774	18	2674.4	9.4
DD91_D_25	14.07	0.18	0.562	0.007	0.78	1.78	0.022187	0.1829	0.0013	2755	12	2874	29	2678	12

DD91_D_23	12.77	0.15	0.506	0.0056	0.6	1.976	0.021855	0.1835	0.0017	2662	11	2641	24	2681	16
DD91_D_26	13.74	0.14	0.546	0.0047	0.54	1.832	0.015771	0.183	0.0018	2730.2	9.6	2807	19	2676	16
DD91_D_28	13.30	0.11	0.529	0.0039	0.52	1.889	0.013915	0.1823	0.0015	2700.2	7.7	2740	16	2673	14
DD91_D_27	13.45	0.13	0.53	0.0049	0.65	1.888	0.017464	0.1832	0.0014	2712.4	9.2	2739	21	2680	13
DD91_D_29	13.24	0.098	0.521	0.0038	0.59	1.919	0.013999	0.1826	0.0013	2696.5	7.1	2703	16	2674	12
DD91_D_51	13.45	0.11	0.529	0.0044	0.54	1.89	0.015717	0.1829	0.0015	2711.6	7.9	2737	18	2677	13

Table A.6: LA-ICP-MS U-Pb data from analysis of secondary 91500

Analysis Name	***207Pb/ 235U***	***2S***	***206Pb/ 238U***	***2S***	***ρ***	***238U/ 206Pb***	***2S***	***207Pb/ 206Pb***	***2S***	***207Pb/ 235U Age***	***2S***	***206Pb/ 238U Age***	***2S***	***207Pb/ 206Pb Age***	***2S***
DD91_D															
91500_1	1.857	0.05	0.181	0.0025	0.15	5.519	0.076142	0.0764	0.0022	1064	18	1073	14	1084	59
91500_5	1.872	0.052	0.177	0.0026	0.13	5.663	0.083367	0.0772	0.0023	1075	19	1048	14	1108	61
91500_4	1.839	0.05	0.178	0.0024	0.13	5.609	0.075493	0.0748	0.0024	1058	18	1057	13	1052	64
91500_2	1.844	0.055	0.178	0.0027	0	5.612	0.085025	0.0755	0.0025	1060	20	1057	15	1062	70
91500_6	1.808	0.04	0.18	0.0023	0.34	5.559	0.071067	0.0735	0.0016	1049	15	1066	12	1018	44
91500_9	1.815	0.045	0.176	0.002	0.21	5.698	0.064935	0.0747	0.0018	1051	16	1042	11	1035	51
91500_10	1.809	0.055	0.176	0.0025	0.11	5.672	0.080433	0.0748	0.0024	1042	20	1046	14	1013	68
91500_3	1.851	0.042	0.178	0.0024	0.27	5.615	0.075663	0.0762	0.0018	1061	15	1059	13	1089	46
91500_7	1.837	0.046	0.181	0.0029	0.02	5.519	0.088325	0.0739	0.002	1056	17	1073	16	1043	57
91500_8	1.851	0.056	0.177	0.0027	0.14	5.647	0.086085	0.0753	0.0023	1065	20	1053	14	1084	61
91500_11	1.863	0.051	0.18	0.0028	0.18	5.549	0.086228	0.0757	0.0023	1066	18	1067	15	1069	61
91500_13	1.936	0.052	0.182	0.0029	0.09	5.495	0.08755	0.0761	0.0023	1092	18	1077	16	1082	58

Appendix B: Au Assay Data

Table B.1: Au assay results from channel samples collected from trenches at the Dogpaw deposit. Samples were analyzed at the Geosceince Laboratories (Geo Labs) in Sudbury Ontario via Lead Fire Assay with ICP-MS finish (IMP-101) with a detection limit of 1.6 ppb for Au. The upper limit for IMP-101 is 5000 ppb and so samples that yielded values above this limit were re-submitted for Lead Fire-Assay with Gravimetric Finish (GFA-PBG)

#	Sample	Easting (m)	Northing (m)	Au (ppm)
Trench #1				
1	16AKJCS001	436403	5464777	0.002
2	16AKJCS002	436403	5464777	0.306
3	16AKJCS003	436403	5464777	6.582
4	16AKJCS004	436403	5464777	4.673
5	16AKJCS005	436403	5464777	0.005
6	16AKJCS006	436412	5464782	0.006
7	16AKJCS007	436410	5464787	4.662
8	16AKJCS008	436412	5464782	1.262
9	16AKJCS009	436411	5464787	13.5
10	16AKJCS010	436412	5464782	0.007
11	16AKJCS011	436416	5464797	11.45
12	16AKJCS012	436416	5464800	0.197
13	16AKJCS013	436403	5464777	0.854
14	16AKJCS014	436403	5464777	1.323
15	16AKJCS015	436403	5464777	2.363
16	16AKJCS016	436403	5464777	0.016
17	16AKJCS017	436403	5464777	0.064
18	16AKJCS018	436433	5464820	13.85
19	16AKJCS019	436433	5464820	2.263
20	16AKJCS020	436433	5464820	0.023
21	16AKJCS021	436403	5464777	9.737
22	16AKJCS022	436403	5464777	0.39

#	Sample	Easting (m)	Northing (m)	Au (ppm)
Trench #2				
23	16AKJCS023	436509	5464838	0.006
24	16AKJCS024	436509	5464838	0.019
25	16AKJCS025	436509	5464838	0.099
26	16AKJCS026	436509	5464838	0.002
27	16AKJCS027	436509	5464838	0.004
28	16AKJCS028	436509	5464838	0.009
29	16AKJCS029	436509	5464838	1.072
30	16AKJCS030	436509	5464838	0.004

31	16AKJCS031	436509	5464838	0.143
32	16AKJCS032	436509	5464838	1.741
33	16AKJCS033	436509	5464838	0.022
34	16AKJCS034	436509	5464838	0.024
35	16AKJCS035	436509	5464838	0.001
36	16AKJCS036	436509	5464838	3.591

#	Sample	Easting (m)	Northing (m)	Au (ppm)
Trench #5				
37	16AKJCS041	436867	5465129	0.015
38	16AKJCS042	436867	5465129	0.004
39	16AKJCS043	436867	5465129	0.003
40	16AKJCS044	436867	5465129	0.014
41	16AKJCS045	436867	5465129	22.42
42	16AKJCS046	436867	5465129	0.017
43	16AKJCS047	436867	5465129	2.738
44	16AKJCS048	436867	5465129	3.92

Appendix C: Deposit History

The following sub-sections summarize available historic information on the structural geology, gold mineralization and alteration at the Dogpaw, Dubenski, Cameron Lake deposit and select adjacent gold occurrences.

The Dogpaw Deposit

The following section summarizes the deposit history and information concerning the mineralization at the Dogpaw deposit detailed by Ball (2014) and Drabble et al., (2015). The deposit is designated MDI52F05SW00012, Mineral Deposit Inventory (MDI) for Ontario, by the Ministry of Energy, Northern Development and Mines (MNDM).

The Dogpaw deposit has experienced over a century of exploration and development, beginning with the discovery of gold in the area by a prospector named Dalby in 1900 (Ball, 2014). The deposit property falls within claim blocks K9991 and K9992 and ownership has exchanged hands several times. Drilling at the Dogpaw deposit is reported to have started in 1944 and since has resulted in 235 holes totaling over 19 kilometers of core (Drabble et al., 2015). In 1996 an open pit excavation produced a 500 imperial ton bulk sample from the property with a grade averaging 6.53g/t of gold after dilution (Ball, 2014). The site of the excavation is at UTM coordinates [436443E 5464918N] and the stripped exposures around the pit are of good quality. Between the 1980's and 2011 a number of mechanically stripped exposures were excavated at the Dogpaw deposit (Ball, 2014). Some of these trenches expose mineralization at surface and are now in varying levels of conditions.

Several veins of varying gold grade are reported at the Dogpaw deposit. A detailed study on the mineralization is reported as lacking however gold mineralization is noted to be strongly associated with pyrite and silica replacement of gabbro and vein breccia (Ball, 2014). While previous to this study the structural geology at the Dogpaw deposit was not constrained, a number of important structural features are reported that may have a control on gold mineralization. Gold bearing veins are reported to be hosted in minor structures, primarily in the gabbro layer of the Kakagi sill (Ball, 2014). The main structure at the property, the Dalby Bay shear zone, is reported as unmineralized and has deformed all lithologies (Ball, 2014).

The Dubenski Deposit

The following sections summarizes the deposit history and information concerning the mineralization at the Dubenski deposit detailed by Ball (2014) and Drabble et al., (2015). The deposit is designated MDI52F05SW00013 by the MMND.

The Dubenski deposit was discovered by A. Gauthier in 1936 following prospecting in the area (Ball, 2014). Relative to the Dogpaw deposit, the Dubenski deposit has received significant industry attention since it's discovery, however due to sporadic ownership of the property, historic data is largely missing. Drilling at the Dubenski deposit is reported to have started in 1936 and ended in 2010 with a total of 268 holes drilled yielding over 29 kilometers of core (Drabble et al., 2015). There are well over a dozen mechanically stripped exposures at the Dubenski deposit, however the majority are overgrown, and few are of quality for detailed mapping. A shaft was dug to a depth of 27 meters in 1946 followed by a second shaft in 1950 (Ball, 2014). Two small shafts were found on-site, the approximate locations are at UTM coordinates [438420E 5464262N] and [438328E 5464282N]. An extensive drilling program was

conducted by Houston Lake Mining Inc between 2008 and 2010, however the final and most extensive phase of drilling is not documented (Ball, 2014).

Gold mineralization at the Dubenski deposit is reported as poorly documented (Ball, 2014). Previous workers have suggested an early strata-bound origin, or that gold introduction was related to a later phase of deformation (Dunbar and Morton, 2008). High-grade zones are associated with disseminated pyrite and significant silicification of the hosting felsic to intermediate tuff (Ball, 2014). Gold is also associated with lenses or zones of pyrite (Dunbar and Morton, 2008). Unlike the Dogpaw deposit, gold mineralization at the Dubenski deposit is reported to be hosted in the major structure at the deposit, the Flint Lake shear zone, a structure that has been compared to the Cameron Lake shear zone which hosts the Cameron Lake deposit (Ball, 2014). There is an apparent strong structural control on gold, with gold reported as 'flakes' or disseminated along foliation planes (Dunbar and Morton, 2008). Dunbar and Morton (2008) also refer to the "Dubenski Shear Zones" as a main gold hosting structure, and it is unclear if this is referring to the Flint Lake shear zone by another name. The geology at the deposit is often reported as complicated attributed to a complex deformation history (Tetclock et al., 2016). This has likely hampered efforts in delineating mineralization at depth during historic drilling programs. Mineralization is exposed at surface at trenched exposures.

The Cameron Lake Deposit

Relative to other known gold deposits in the Rowan-Kakagi greenstone belt, the Cameron Lake deposit is the most advanced and explored. The following sections summarizes the deposit history and information concerning the mineralization at the Cameron Lake deposit detailed by Ball (2014) and Drabble et al., (2015). The most recent model for gold mineralization, detailed

mapping and sampling at the Cameron Lake deposit is detailed in Tetlock et al., (2016). The deposit is designated MDI52F05SE0008 by the MNDM.

The Cameron Lake deposit has a relatively short yet more detailed history compared to the Dogpaw and Dubenski deposits. The deposit was first discovered in 1960 by Noranada Exploration Company Limited (Ball, 2014). Since discovery the area has been mapped, trenched and drilled extensively. A total of 928 holes were drilled since 1960, yielding over 113 kilometers of core (Ball, 2014). Underground works are found at the Cameron Lake deposit. In 1986 an underground exploration program was conducted by Nuinsco but the deposit was never developed into a producing asset (Ball, 2014). The underground workings are approximately located at UTM coordinates [447086E 5460129N] and several trenches that expose gold mineralization at surface are found at UTM coordinates [447200E 5459900N].

Relative to the Dogpaw and Dubenski deposit, the structural geology, mineralization and alteration has been well documented at the Cameron Lake deposit. The deposit is hosted in a suspected splay of the regional-scale Pipestone-Cameron fault zone, referred to as the Cameron Lake shear zone. The deposit is believed to be lithological controlled, with a zone of alteration, deformation and mineralization ‘sandwiched’ between a variably deformed and altered mafic hanging wall and gabbro footwall (Tetlock et al., 2016). The Cameron Lake shear zone is comprised of several deformation zones that anastomose around relatively massive and unaltered, fine-grained mafic blocks, some of which preserve primary igneous structures, such as pillows and ash beds. Drilling has confirmed that these relatively massive and barren rocks extend at depth and likely account for the drop in gold grades across the hosting structure (Tetlock et al., 2016). There is a strong association between gold and pyrite, with high-grade

gold values found with the highest pyrite concentrations (Ball, 2014). Gold is also associated with a network of quart-veins and vein breccia and a proximal potassic alteration (Tetlock et al., 2016). Feldspar porphyry dykes are also found within the Cameron Lake shear zone.

The Angel Hill Occurrence

The Angel Hill occurrence is located approximately one-kilometer south-west of the Dogpaw deposit property. The following sections summarizes the deposit history and information concerning the mineralization at the Dubenski deposit detailed by Ball (2014) and Drabble et al., (2015). The most recent study on the occurrence is by Secord (2011) with a M.Sc. study on the geochemistry and gold mineralization at the deposit. A report by Cutting and Anthony (2005) summarizes the most recent exploration work on the gold occurrence. Both Secord (2011) and Cutting and Anthony (2005) provide the most recent detailed mapping of the local geology and gold hosting structures. The deposit is designated MDI52F05SW00140 by the MNDM.

The Angel Hill occurrence is one of several gold occurrences often referred to as the west Cedartree Lake gold properties or projects. Prospecting and sampling were carried out on a number of occurrences in the area in the 1940's by Sylvanite Gold Mines Limited (Cutting and Anthony, 2005). Houston Lake Mining conducted trenching, channel sampling and drilling in the early 2000's with a total of 27 holes yielding approximately 1.85 kilometers of core (Ball, 2014).

The Angel Hill gold occurrence is reported as structurally hosted in a network of narrow, brittle-ductile shear zones, collectively referred to as the Angel Hill gold zone (AHGZ), between a basal ultramafic layer and gabbroic layer of the Kakagi sill (Cutting and Anthony, 2005). The

AHGZ is marked by a distal serpentine and chlorite alteration and a proximal silica-carbonate-sericite alteration (Cutting and Anthony, 2005) (Ball, 2014). Felsic porphyry dykes are reported as spatially related to the AHGZ, are found along trend of gold hosting structures and are variably deformed (Cutting and Anthony, 2005). They are reported as deformed by the main deformation zone and in some cases boudinaged (Secord, 2011). Visible gold is reported in quartz veins and as free gold in the AHGZ and is associated with pyrite, chalcopyrite, galena and molybdenite (Ball, 2014). Following detailed mapping and oxygen and sulfur isotope analysis at the occurrence Secord (2011) concluded that the gold mineralization at the AHGZ was the result of multiple episodes of fluid influx, either magmatically or metamorphically sourced, over a protracted deformation history.